The International Journal of Advanced Manufacturing Technology (2018) 98:1925–1975
https://doi.org/10.1007/s00170-018-2314-1

ORIGINAL ARTICLE

Influences of tool structure, tool material and tool wear on machined surface integrity during turning and milling of titanium and nickel alloys: a review

Bing Wang [1,2] · Zhanqiang Liu [2,3]

Received: 13 February 2018 / Accepted: 5 June 2018 / Published online: 28 June 2018

Abstract
Titanium and nickel alloys have been used widely due to their admirable physical and mechanical properties, which also result in poor machinability for these alloys. Improvement of surface integrity of titanium and nickel alloys is always a challengeable subject in the area of manufacture. Besides the cutting parameters and cutting environments, the structure and material of cutting tools are also the most basic factors that govern the machined surface integrity. This review paper provides an overview of the machined surface integrity of titanium and nickel alloys with reference to the influences of tool structure, tool material, as well as tool wear. Surface integrity mainly covers geometrical characteristics, microstructure alterations and mechanical properties of the machined surface. Influences of cutting tool parameters on above characteristics of machined surface integrity are reviewed respectively, and there are many different types of surface integrity problems reported in the literatures. However, the current research on the effects of tool parameters on machined surface integrity mainly depends on practical experiments or empirical data, a comprehensive and systematic modeling approach considering the process physics and practical application is still lacking. It is concluded that further research for the influence of tool parameters on machined surface integrity should consider the requirements of service performance (e.g. fatigue life) for machined components. It is vital important to establish the mapping relationships among the cutting tool parameters, machined surface integrity, and the service performance of machined components.

Keywords Machining · Surface integrity · Tool structure and material · Tool wear · Titanium and nickel alloys

1 Introduction

Titanium and nickel alloys are widely used as structural materials due to their high strength-to-weight ratio (especially for titanium alloys), high fracture toughness and fatigue strength, superior corrosion and creep resistance, and ability to operate at high temperatures, etc. [1–4]. These admirable properties make titanium and nickel alloys be extensively used in such fields as aerospace, automotive, power stations, petrochemical, biomedical, marine, military and nuclear sectors [5–8]. Based on the forecast of Airbus Global Market, over 29,000 commercial airplanes are demanded all over the world from the year of 2013 to 2032 (http://www.aircraft.airbus.com/market/global-market-forecast-2017-2036/), which also demonstrates the huge demand for titanium and nickel alloys.

A typical turbofan engine primarily comprises of such four major components as fan, compressor, combustor and turbine as shown in Fig. 1 [9], in which extensive use of titanium and nickel alloys in the engine can be noted. Because titanium alloys can maintain high creep and oxidation resistance at temperatures under 400 °C, they are mainly used for the manufacture of fan and compressor within the turbofan engine. Nickel alloys have the ability to retain most of their strength

✉ Zhanqiang Liu
melius@sdu.edu.cn

Bing Wang
sduwangbing@gmail.com

[1] School of Materials Science and Engineering, Shandong University, Jinan 250061, People's Republic of China

[2] School of Mechanical Engineering, Key Laboratory of High Efficiency and Clean Mechanical Manufacture of MOE, Shandong University, Jinan 250061, People's Republic of China

[3] Key National Demonstration Center for Experimental Mechanical Engineering Education, Jinan 250061, People's Republic of China

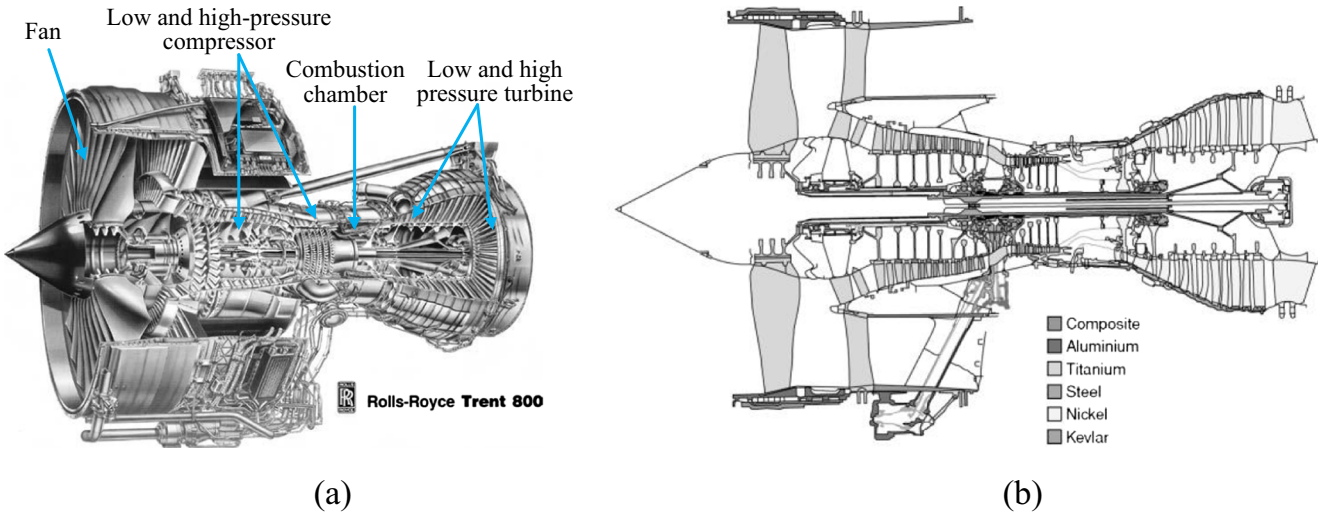

Fig. 1 Cross section of Rolls-Royce Trent 800 turbofan engine (**a**) main structure; (**b**) illustration of material usage in the Trent 800 engine

even after long exposures to extremely high temperatures up to 600 °C, so they are mainly used in the hot sections of critical components in turbofan engine including combustor and turbine. About 50% by weight of an aero-engine is made up of nickel alloys [10–12]. Most of the turbofan engine components need to be machined to remove excess material (by processes such as turning, milling, drilling and grinding, etc.) and achieve final dimension in addition to surface finish before they are put into service.

With the objectives to possess high service performance and reach high reliability levels for a product, improving the machined surface integrity is one of the most relevant factors especially for critical structural components in aerospace industry. The evaluation on surface integrity covers geometrical characteristics, microstructure alteration and mechanical properties of the machined surface. The geometrical and microstructural characteristics of the machined surface are also called as topological parameters and metallurgical states, respectively. The geometrical characteristics of machined surface include geometrical morphology, surface roughness and surface defects, etc. The microstructure alterations of machined surface consist of plastic deformation layer, grain size and texture, phase transformation, etc. The mechanical properties of machined surface mainly indicate the state of residual stress and micro hardness.

Despite the increased demand of titanium and nickel alloys in engineering fields, there are difficulties to achieve good machined surface integrity due to their low machinability rating [13]. Because titanium and nickel alloys maintain high strength and hardness at elevated temperatures, machining is difficult to perform on them. In addition, the physical properties of these alloys such as low thermal conductivity, high work hardening, and high chemical reactivity aggravate their poor machinability rating.

Large amounts of literature have been reported related to machining of titanium and nickel alloys such as rapid tool wear and undesirable machined surface quality [14–17]. The low thermal conductivity of such alloys is prone to cause increased temperatures at the tool cutting edge and results in adhesion of workpiece material to the cutting edge. Then these factors lead to accelerated tool wear during machining process. In addition, severe localized heat, high stresses and temperature gradients within the cutting zone are prone to cause undesirable microstructure alterations of machined surface and subsurface. For example, the white layer formation and surface damage may cause detrimental effects on the performance of the machined part. The undesirable surface defects and tensile residual stresses tend to cause the stress corrosion cracking, failure due to fatigue and creep on the machined surface [18]. Due to significant difficulty associated with machining, these unfavorable alterations are particularly of more concern for titanium and nickel alloys. It is very important to obtain superior surface quality including geometrical, microstructural and physical characteristics of machined surface and subsurface to enhance the resistance to fatigue and creep failure for components made up of titanium and nickel alloys.

Apart from the cutting parameters (cutting speed, feed rate and depth of cut, etc.) and cutting environments (dry cutting, wet cutting, and cryogenic cutting, etc.), the structure and material of cutting tools have been recognized as one of the most basic factors that govern the machined surface integrity [19–22]. One cannot achieve good surface integrity without considering appropriate tooling (including material and structure) requirements. Selection of cutting tool with good machining performance has been always a big challenge to manufacturers. The application of advanced processing methods such as minimum quantity lubrication, high pressure cooling system and subzero cooling system which aims to improve the machinability of titanium and nickel alloys have been

emerged and gradually applied in recent years. Nevertheless, the traditional machining modes, especially for turning and milling, are still widely used due to their wide applicability. Several review literatures [5, 7, 12, 17] can be tracked related to the machining induced surface integrity of titanium or nickel alloys considering the influences of cutting parameters and cutting environments. While the research about the influences of tool material and tool structure on the machined surface integrity are still lacking and have not been reviewed intensively. It is highly desirable to develop surface integrity data for general guidelines to be employed or considered for the manufacture of critical components.

The paper aims to present an overview of the machined surface integrity of titanium and nickel alloys with reference to the influences of different cutting tool structures and materials. The paper mainly illustrates the state of the art research work performed for turning and milling applications by utilizing different cutting tools. These two kinds of cutting methods are the most widely used processes in manufacture. The review can also provide instruction for other cutting modes such as drilling, grinding, boring, reaming and broaching, etc. This review starts with the illustration of tool structures and tool materials in turning and milling processes. Then the influences of cutting tool structure and material on the machined surface integrity of titanium and nickel alloys are reviewed. These researches cover the experimental, theoretical and numerical investigations in the field of turning and milling processes. After that, the influence of cutting tool wear on the machined surface integrity is reviewed. Finally, the existing research limitations and the latest ideas are presented. The relationships between machined surface quality and its influence factors as well as the evaluation parameters are summarized in Fig. 2, in which the review scope of this paper is emphasized by the dashed line area.

2 Workpiece materials

2.1 Titanium alloys

Titanium alloys have been widely used due to their superior mechanical properties and improvements of machinability. The good bio-compatibility in addition to the excellent corrosion and creep resistance for titanium alloys have also made them suitable for bio-medical applications [18, 23–26]. Based on different phase compositions, titanium alloys are normally categorized into such four main types as α-titanium alloys, near α-titanium alloys, $\alpha+\beta$ alloys, and β alloys [23]. The phase diagram for titanium alloys is presented in Fig. 3 [2]. The α-titanium alloys mainly contain α-phase which has close-packed hexagonal microstructure at ambient steady state. The alloy elements that increase the transformation temperature from α to β phase are known as α-phase stabilizers. These elements include oxygen, nitrogen, carbon, boron and aluminum, etc. [23]. The α-alloys exhibit high hardness and excellent creep resistance, which make them be widely used as structural components demanded with good high temperature creep resistance. Near α-alloys act more like α-alloys but they contain small quantities of β-phase less than 10% in volume generally. Typical examples of near α-alloys include Ti6.5Al2Zr1Mo1V, Ti8Al1Mo1V and Ti6Al5Zr0.5Mo0.25Si, etc.

The $\alpha+\beta$ dual phase titanium alloys contain both α and β stabilizers with high proportions. The β-phase has body-centered cubic structure, and the alloying elements act as β-stabilizers include molybdenum, vanadium, niobium, tantalum, iron, silicon, etc. [23]. $\alpha+\beta$ titanium alloys possess medium strength and good hardenability. The volume fractions of α and β phases in addition to the mass fractions of alloying elements in both phases can be adjusted through different heat treatments. This kind of titanium alloy is commonly used for high strength applications with working temperature range of 350–400 °C in industry. The commonly used $\alpha+\beta$ titanium alloys include Ti6Al4V, Ti2Al1.5Mn, Ti4Al1.5Mn, Ti6Al2.5Mo1.5Cr0.5Fe0.3Si, Ti6Al7Nb, among which Ti6Al4V is the most widely used one [27–30]. The β titanium alloys have enough β stabilized alloying elements, and this kind alloy exhibits all β phase under ambient temperature. The β titanium alloys are denser in nature and present high strength at low operating temperatures [2]. The tensile strength of β titanium alloys at ambient temperature can reach 1300–1400 MPa through aging treatment. The commonly used β titanium alloys include Ti5Mo5V8Cr3Al and Ti15Mo2.7Nb3Al0.25Si, and they are mainly used as structural components in aerospace industry.

2.2 Nickel alloys

Nickel alloys have also been extensively used in various industry fields due to its admirable physical and mechanical properties. Nickel alloys belong to the most widely used heat resistant alloys (also called as super alloys), which are mainly divided into such subcategories as nickel base, iron base and cobalt base alloys [12]. Nickel base alloys consist of nickel as the main component with at least 50% content, and Inconel 718 is the most popular nickel base alloy [31–34].

Figure 4 provides a perspective for the development of nickel alloys since their first appearance in the 1940s [9]. Over the development of more than half one century, a concerted period of alloy and process development has enabled the performance of super alloys to be improved dramatically. It can be seen from Fig. 4 that the development history for nickel alloys is wrought alloy, conventionally cast alloy, directionally solidified alloy, and single crystal alloy. The mechanical properties and high temperature resistance of such above four kinds of nickel alloys promote progressively. Correspondingly, the machinability for these alloys becomes poorer.

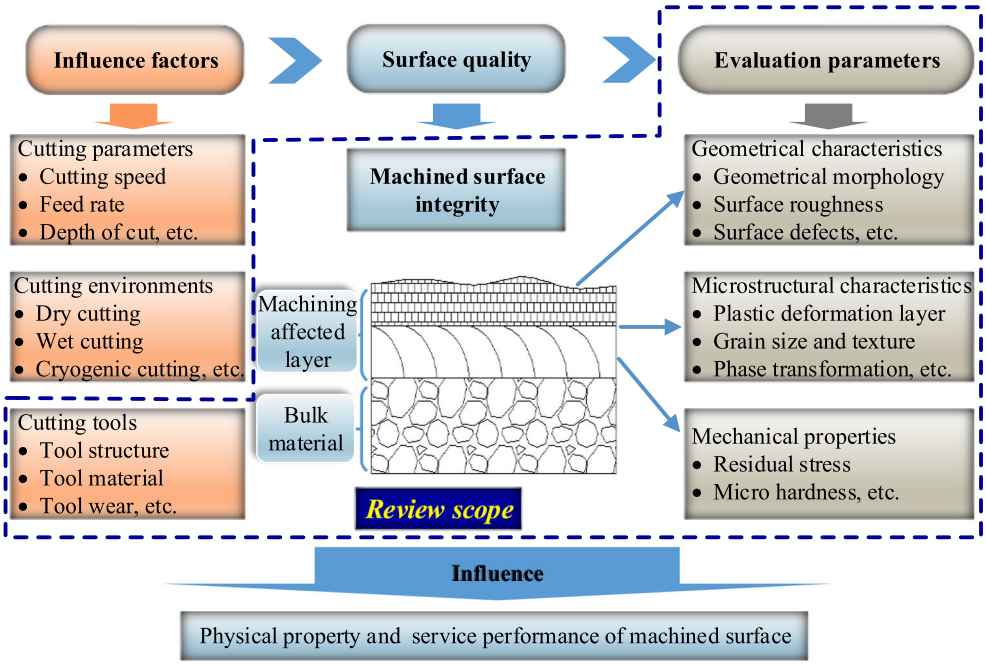

Fig. 2 The review scope of this paper

It is well known that the number of alloying elements is generally greater than ten for nickel alloys and they are among the most complexed engineered materials. Although a wide variety of alloying elements are added, some broad rules can be tracked. Figure 5 shows the categories of important alloying elements in the constitution of nickel alloys and their relative positions in the periodic table [35]. It can be seen that most of the alloying elements in the nickel alloys are located in the d block of transition metals. Nearly all nickel alloys contain significant amounts of chromium, cobalt, aluminum and titanium, as well as small amounts of boron, zirconium and carbon. Other elements are also added for partial nickel alloys, including rhenium, tungsten, tantalum and hafnium from the 5d block of transition metals, and ruthenium, molybdenum, niobium and zirconium from the 4d block [35]. The behavior of each alloying element and its influence on the phase stability depends strongly upon its position within the periodic table as shown in Fig. 5.

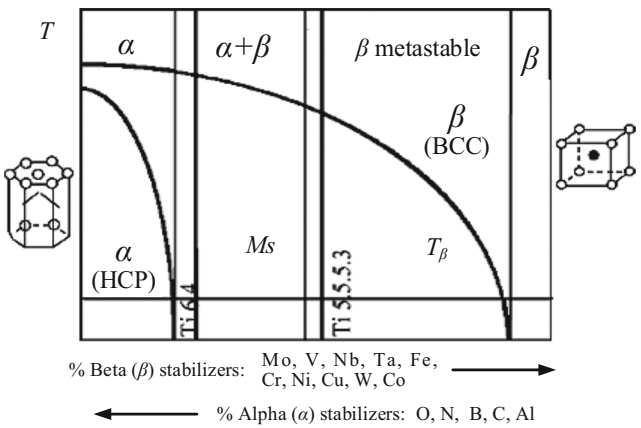

Fig. 3 Phase diagram of titanium alloys [2]

Different alloying elements have their own contributions in constituting the phases and affecting the properties of various grades of nickel alloys [9]. The values located at the top left corner of each square box in Fig. 5 indicate the percent difference in atomic diameter from Ni for the located elements. Taking the two elements of metallic element niobium (i.e. Nb) and non-metallic element carbon (i.e. C) for example, the atomic radius (or called as metallic radius for metallic elements) of Ni is 124.6 pm, while those of elements Nb and C are 147 pm and 91 pm, respectively. In result, the percent difference in atomic diameter between Nb and Ni can be calculated as $(147–124.6)/124.6 \times 100\% = 18\%$, while that between C and Ni can be calculated as $(91–124.6)/124.6 \times 100\% = -27\%$.

A first group of alloying elements includes iron, cobalt, chromium, ruthenium, molybdenum, rhenium and tungsten, which prefer to constitute and stabilize the phase of austenitic γ. These elements have atomic radii approximate equal to that of nickel. A second group of alloying elements including aluminum, titanium, niobium and tantalum, have greater atomic radii and promote the formation of ordered phases such as the compound $Ni_3(Al, Ta, Ti)$, which is known as γ' phase. A third group of elements including boron, carbon and zirconium tend to assemble on the grain boundaries of the γ phase, due to their much different atomic sizes compared with nickel. The phases of carbide and boride are also promoted to be formed with the third group of elements.

The microstructure of a typical nickel alloy consists of such different phases as following [36].

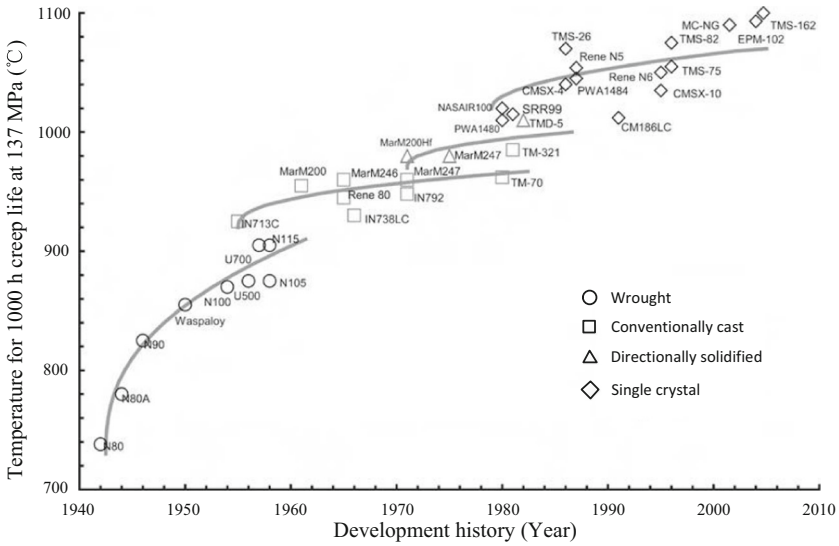

Fig. 4 Evolution of nickel alloys since their first appearance in the 1940s

(1) The gamma phase denoted by γ. It exhibits the face-centered cubic structure and forms a continuous matrix phase, in which the other phases reside. This phase contains significant concentrations of such elements as cobalt, chromium, molybdenum, ruthenium and rhenium, etc.
(2) The gamma prime phase denoted by γ'. It forms as a precipitate phase coherent with the matrix of γ phase, and it is rich in such elements as aluminum, titanium and tantalum. In some nickel-iron super alloys which is rich in niobium, another ordered phase γ'' is preferred to be formed instead of γ'.
(3) Carbides and borides. Carbon, often present at concentrations up to 0.2 wt.%, combines with reactive elements such as titanium, tantalum, chromium, molybdenum, tungsten, niobium, and hafnium to form carbides. The elements of chromium and molybdenum promote the formation of borides. Both carbides and borides prefer to reside on the γ-grain boundaries.
(4) Other phases such as the topologically close-packed (TCP) phases μ, σ and Laves can also be found in certain nickel alloys, particularly in the service aged condition. However, the formation of these compounds has negative influence on the material property and should be avoided to form.

3 Tool structure, tool material and tool wear

The structure and material of cutting tools are important factors that govern the machined surface integrity. Selection of appropriate cutting tools is the basis to achieve good surface integrity. There are different geometrical parameters to

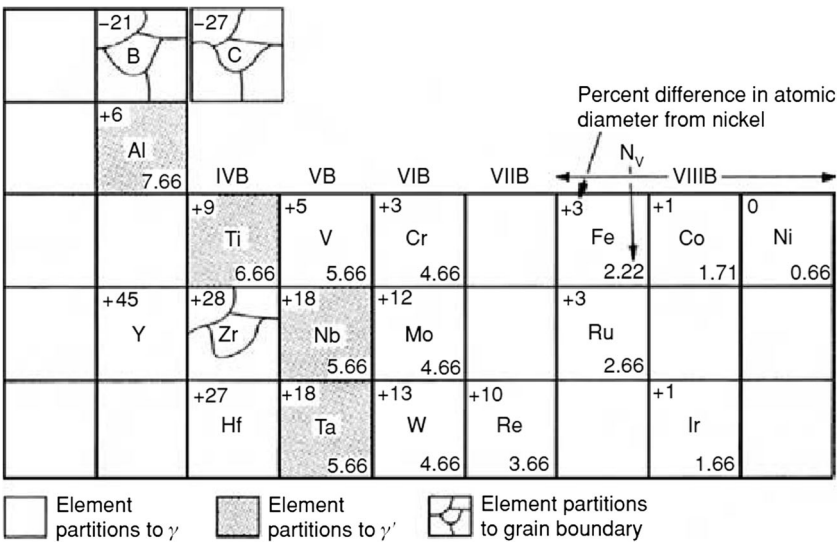

Fig. 5 Categories of important alloying elements in constitution of nickel alloys and their relative positions in the periodic table

characterize the cutting tool structure for different kinds of cutting tools including turning and milling tools. There are also varied cutting tool materials to select for machining of the same workpiece material.

3.1 Tool structure

3.1.1 Turning

Turning is the most widely used machining process to fabricate the rotatory components. The main parameters to describe the turning tool structure mainly include tool angles and cutting edge parameters. The main turning tool angles include the rake angle, the clearance angle, the cutting edge angle, the minor cutting edge angle, and the inclination angle, etc. The cutting edge of turning tool can be characterized by the tool nose radius, the cutting edge radius, in addition to the cutting edge shape [37]. Different cutting edges are prepared to improve the tool cutting performance such as chamfered edge, honed edge, and wiper, etc. The variation of such above geometrical parameters for turning tools affects the material deformation and removal behavior within the cutting zone including the chip and the machined surface.

3.1.2 Milling

Milling is a commonly used machining process to achieve finished flat and curved surfaces. For milling tool with small diameter (generally smaller than 25 mm), the solid milling tool is used, while the milling inserts combined with milling tool holder are used for the milling tools with large diameter. The geometrical parameters to characterize the milling insert are similar with the turning one. The solid milling tool mainly includes flat end milling tool and ball-end milling cutter.

The basic geometry of flat end milling tool includes external shape dimensions and geometrical parameters of side edge and end edge. Besides the tool diameter, tool length and tool flute length, the helical angle and cutting edge angles are the main geometrical parameters that influence the milling process [38]. The cutting edge angle can be subdivided into the side edge angles and the end edge angles. Compared with the flat end milling tools, the ball end milling tools have another important geometrical parameter of ball nose radius. The number of tool flutes and the pitch between adjacent flutes also affect the milling process through changing the dynamic behavior of milling tools for both flat and ball end milling tools.

3.2 Tool material

Cutting tool material is one of the most basic factors that influence the machined surface integrity especially for the difficult-to-machine materials including titanium and nickel alloys [12]. A machining process cannot be conducted efficiently if inappropriate cutting tool material is selected, which is apt to result in poor machined surface quality. Low machinability rating of titanium and nickel alloys causes the high mechanical and thermal stresses within the cutting zone, which then causes severe plastic deformation on machined surface and undesirable tool wear. In addition, the high chemical reactivity of titanium accelerates the tool wear rate and deteriorates the machined surface further consequently. The cutting tool materials should exhibit excellent physical and mechanical properties to withstand elevated temperatures and high stresses during machining of titanium and nickel alloys. It is concluded from previous literature [39] that the cutting tool materials should possess the characteristics of high hot hardness, high thermal shock resistance, low chemical affinity, excellent oxidation resistance, and high fracture toughness to guarantee the machined surface integrity with excellent tool life. A cutting tool should keep the five characteristics in correct balance to perform cutting process economically and efficiently.

Figure 6 presents the properties of different cutting tool materials at hardness and toughness scales (http://www.mitsubishicarbide.net/contents/mmus/enus/html/product/technical_information/information/sessaku.html). The cutting tool materials cover high speed steel (HSS), cemented carbide, coated cemented carbide, ceramics, cubic boron nitride (CBN), diamond, and etc., among which HSS is the toughest material and diamond is the hardest material. High fracture toughness is required for cutting tools to avoid chipping, shocks, vibrations, misalignments, and runouts, while high hardness is needed to improve the tool wear resistance and guarantee the ability to machine workpiece materials with high hardness [40].

HSSs are complex iron-base alloys of tungsten, molybdenum, chromium, vanadium, cobalt or combinations, which belong to strong carbide forming elements [41]. Although HSSs possess the highest toughness, they are not preferred for turning and milling of difficult-to-machine materials such as titanium and nickel alloys due to their relative low hardness. However, they are recommended to be used in some complex shaped tools like drilling application for titanium alloys, because HSS has high bending strength than other tool materials and HSS tool materials are easier to be processed for drilling applications.

Cemented carbide is fabricated through powder metallurgy technology with hard metal carbides (WC, TiC, etc.) and bonding metals such as Co, Ni or Mo, etc. Cemented carbide tools have been widely used due to their combined superior properties of high strength and hardness, high toughness, excellent wear and heat resistance [42–44]. The emergence of new kind cemented carbides such as micro-grain cemented carbide and cermet has improved the cutting performance further. Coatings are also utilized to improve machining performance of carbide tools. Higher hardness of coating increases resistance towards tool wear due to abrasion, adhesion,

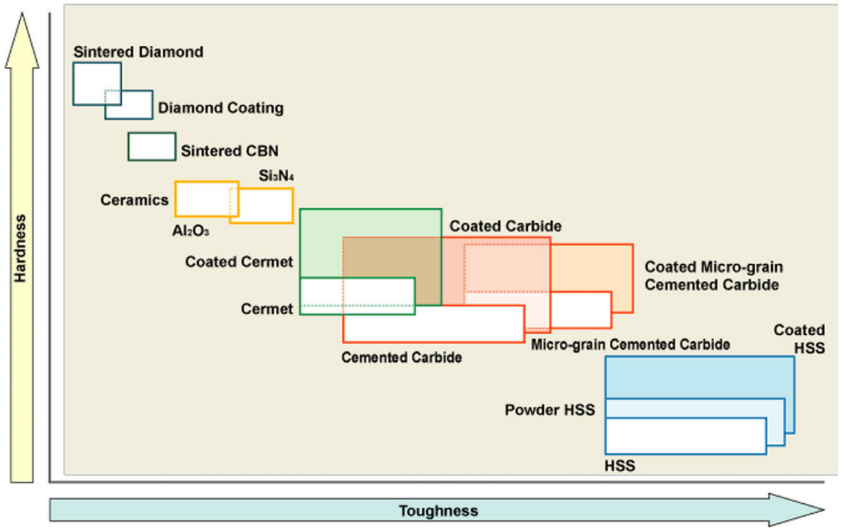

Fig. 6 The properties of hardness and toughness for different cutting tool materials

diffusion, and oxidation wear [14, 45, 46]. The tool coating can also decrease the friction coefficient which is beneficial to lower the cutting temperature by easier chip flow through tool rake face [45]. Previous researches have demonstrated that the thin tool coating can make a noteworthy promotion in machining performance, tool life, and productivity [47–49]. Based on the preparation technology, the tool coating can be divided into physical vapor deposition (PVD) coating and chemical vapor deposition (CVD) coatings. The coating materials include TiC, TiN, Al_2O_3, TiCN, TiAlN, TiAlN, etc. The coating tools also develop from single layer to multiple layers, ultrathin and nano layers to enhance machining performance [12].

Ceramic materials have unique physical and mechanical properties especially at high temperature, such as high hot hardness, high wear resistance, relatively low chemical reactivity with steels and many other materials [50]. Consequently, ceramic cutting tools exhibit superior machining performance especially for machining of super hard materials that are hard to be performed with traditional tool materials. In addition, the optimum cutting speed of ceramic cutting tools is three to ten times larger than that of ordinary cemented carbide tools with the same geometrical parameters, which can improve the processing efficiency dramatically. However, literatures [12, 51] suggest that titanium alloys are not recommended to be machined with ceramic tools because of high chemical affinity between ceramic tools and workpiece material, but nickel alloys have been proved to be machined efficiently with ceramic cutting tools [52].

Beside ceramic inserts, solid ceramic cutting tools have also been developed with the advancement of ceramic sintering and ceramic grinding techniques [38, 53, 54]. Kennametal has introduced new SiAlON KYS40 ceramic grade for rough milling of nickel alloys [55]. Through comparison of suggested cutting speed between solid ceramic tools against carbide tools for machining of nickel alloys, it is indicated that the solid ceramic tools are capable to operate at cutting speed 20 times higher than ordinary carbide tools and provide longer tool life simultaneously [55].

Diamond and CBN are the top two hardest tool materials at present. Diamond-coated and polycrystalline diamond (PCD) tools have been used successfully for machining of titanium alloys, while it does not recommend to perform nickel alloys machining with PCD tools due to chemical reaction between diamond and nickel leading to accelerated tool wear and damage [56]. Although CBN tools can be used for machining of both titanium and nickel alloys, they are still limited to be used in finishing operations due to the high preparation cost.

3.3 Tool wear

Some specific researches on tool wear mechanisms and tool failure modes during machining titanium and nickel alloys have been conducted [15, 57–59]. Cutting tools experience severe thermal and mechanical shocks during machining process. The high cutting stresses and high temperatures are generated at and/or close to the cutting edge to affect the tool wear rate and tool life greatly. Consequently, the tool wear behavior plays an important role on machined surface formation and affects the machined surface integrity greatly.

The main difference between turning and milling is that turning is continuous machining mode while milling is intermittent one, which results in variations of tool wear behavior and corresponding tool wear mechanism. For turning of titanium and nickel alloys, high temperature is the main factor that induces the tool wear due to thermal accumulation close to the cutting edge [57]. Consequently, flank wear, crater wear, chipping or notching caused by thermal shocks are the prominent tool failure modes. Comparatively, the combination of high thermal, high mechanical and cyclical stresses, as well as adhesion of the work material onto the tool faces are the main factors that induces the tool wear during milling process of

titanium and nickel alloys. In result, notching, chipping and catastrophic failure are the prominent tool failure modes.

Moreover, the different tool materials exhibit varied tool wear behavior and wear mechanisms during machining of titanium and nickel alloys due to their different mechanical and thermal properties. For the tool materials with low hardness such as high speed steels, rapid loss of their hardness at elevated cutting temperatures above 600 °C tends to cause severe plastic deformation of tool material. For the tool materials with moderate hardness and toughness such as cemented carbide and coating tools, the rake and flank surface wear resulted from dissolution-diffusion and attrition are the prominent tool failure modes during machining of titanium and nickel alloys. Moreover, the high chemical activities for titanium alloys also aggravate the tool crater wear. Due to high brittleness accompanied with high hardness for ceramic tools, notch wear and chipping are the main tool wear mechanisms.

4 Research and analysis methods of machined surface integrity

Machined surface integrity can be evaluated by a group of parameters to describe the geometrical characteristics, microstructure alterations, and mechanical properties of machined surface as summarized in Fig. 2. There are different research and analysis methods about machined surface integrity based on different characteristic parameters of machined surface, and the methods can be divided into experimental investigation, empirical modeling, analytical modeling and numerical analysis mainly based on finite element method (FEM).

4.1 Experimental investigation of machined surface integrity

Experiments have been the primary method to investigate the machined surface integrity including the geometrical characteristics, microstructure alterations, and mechanical properties of machined surface. Although the costs of research and time-consuming are always high for experiments, the experimental results can provide direct answers for what demanded. There are many accessible literatures [5, 7, 12] conducting experiments to investigate the machined surface roughness, surface defects, machining affected layer, white layer formation, residual stress and micro hardness distribution, etc. The influences of input variables (including cutting parameters, cutting tool parameters, and cutting environments, etc.) on the machined surface integrity can be obtained. In addition to the direct outputs of experimental research, the experiments can be used to validate the results of analytic models and numerical analyses. Empirical fitting or extrapolation based on limited experimental results can also provide effective instruction for practical application.

The geometrical characteristics of machined surface are usually measured or observed with the aid of profilometer, optical microscope (OM) or scanning electron microscopy (SEM) which includes backscattered electron microscopy (BSE) and secondary electron (SE) modes. Surface profilometer, OMs including super-depth microscope, white-light interferometry and laser scanning confocal microscope are commonly used to achieve three dimensional (3D) images of the machined surface [60]. These instruments can provide detailed information about the topological parameters of the machined surface including the geometrical morphology, surface roughness as well as surface defects. Measurement of surface profile or observation of surface morphology does not need any further processing on the machined surface.

In-depth analysis of microstructure alterations of machined surface and subsurface have been carried out with the help of advanced micro-examination techniques such as high magnification OM, SEM, energy dispersive spectroscopy (EDS), X-ray diffraction (XRD), electron backscatter diffraction (EBSD) and transmission electron microscopy (TEM), etc. [5]. Among above advanced techniques, OM and SEM are the most convenient operated and have been the most widely used methods, while EBSD and TEM have higher magnification and can observe the microstructures with smaller scales. The techniques of EDS and XRD are always used to examine the elements and phase compositions. The specimen preparation for in-depth observation generally needs the procedures of sample cutting, inlay, grinding and polishing, followed by metallographic etching in the end [61]. Then the microstructure alterations (including the plastic deformation degree and depth, white layer formation, evolution of grain size and grain orientation, recrystallization, phase transformation, etc.) can be analyzed with above micro-examination techniques.

Mechanical properties including residual stress and micro hardness also present gradient distribution characteristics along the in-depth direction from machined surface to bulk material. Measurements of residual stress within machined subsurface can be conducted with destructive or nondestructive test methods [5]. The residual stress measured with destructive test method is calculated indirectly through measurement of material macro or micro deformation after residual stress release within the tested area. The commonly used destructive test method of residual stress mainly include hole drilling method [62], ring core method [63], contour method [64], etc. The nondestructive test method of residual stress mainly include X-ray diffraction method [65], synchrotron X-ray diffraction method [66], neutron diffraction method [64], ultrasonic method [67], in addition to electromagnetic method [68], etc. X-ray diffraction is the most widely used nondestructive test method due to the advantages of easy operation and relative higher measurement accuracy. With the help of electrochemical polishing, the in-depth profiles of residual stress within machined subsurface can be depicted. The

micro hardness of machined surface can be measured with the aid of micro hardness tester. The characteristic parameters of work hardening for machined surface mainly include the micro hardness values within machined subsurface and the depth of hardening layer. The in-depth profiles of micro hardness for machined subsurface can be measured after treatment of specimen with the same procedures as in-depth microstructure observation while etching may be not necessary.

4.2 Empirical modeling of machined surface integrity

Empirical models of machined surface integrity are established based on mathematical statistic analysis of experimental results of characteristic parameters for machined surface. The empirical models are generally developed according to minimum error principles, and aim to express the relationships between dependent variables (i.e. the parameters to characterize machined surface integrity) and independent variables (i.e. cutting parameters, tool parameters, and the other parameters that influence the machining process) [69]. Actually, the research on machined surface integrity based on empirical models is the extension of experimental investigation. The most widely used expression form for empirical is polynomial equation fitted based on least square method. Empirical models are obtained with limited experimental results and can be extrapolated to predict the machined surface roughness in a relative larger range of independent variables. The reliability and accuracy of empirical models depend on the appropriate expression functions and experimental sample size, in addition to the dependent experimental techniques.

Some research has established empirical models to predict different characteristic parameters of machined surface integrity including geometrical parameters [70, 71], microstructure alterations [72] and mechanical properties [73–75]. The effects of cutting parameters such as cutting speed, feed rate and depth of cut, tool parameters such as tool nose radius on the machined surface integrity have been investigated. Joshi et al. [71] established the empirical model of machined surface roughness R_a corresponding to the cutting parameters for nickel alloy UDIMET 720 expressed by Eq. (1). In the same way, they developed the empirical models of residual stress σ_m parallel with the milling direction, residual stress σ_n normal to milling direction, in addition to shear residual stress 剪$_{mn}$ as expressed by Eqs. (2)–(4), respectively. Similarly, Sridhar et al. [73] proposed the empirical model of residual stress for titanium alloy Ti-834 corresponding to the cutting parameters of cutting speed, feed rate and depth of cut in the same pattern as Eq. (1).

$$R_a = a_1 + a_2V_c + a_3f + a_4a_p + a_5V_cf + a_6fa_p + a_7V_ca_p + a_8V_cfa_p \quad (1)$$

$$\sigma_m = b_1 + b_2V_c + b_3f + b_4a_p + b_5V_cf + b_6fa_p + b_7V_ca_p + b_8V_cfa_p \quad (2)$$

$$\sigma_n = c_1 + c_2V_c + c_3f + c_4a_p + c_5V_cf + c_6fa_p + c_7V_ca_p + c_8V_cfa_p \quad (3)$$

$$\tau_{mn} = d_1 + d_2V_c + d_3f + d_4a_p + d_5V_cf + d_6fa_p + d_7V_ca_p + d_8V_cfa_p \quad (4)$$

where a_i, b_i, c_i, d_i ($i = 1, 2, 3\ldots$) are the polynomial coefficients to be fitted, V_c is the cutting speed, f is the feed rate, a_p is the depth pf cut.

Shi et al. [72] expressed the white layer thickness formed during turning process as a linear equation with square root transformation considering the influences of cutting speed, feed rate, tool rake angle, tool nose radius, tool flank wear, tool thermal conductivity, as well as coolant condition.

An important way for understanding machined surface integrity is to research the microstructure alterations under different cutting conditions, and to establish the relationship between microstructure alterations (including grain sizes with phase fractions) and other surface integrity parameters such as micro hardness and residual stress. Arisoy et al. [76] investigated the effects of workpiece material microstructure on the micro hardness distribution of machined subsurface for Inconel 100, and established the empirical model of micro hardness as expressed by Eq. (5).

$$HV = e_0 + e_1\left(g_1^{m_1}h_1^{n_1}\right) + e_2\left(g_2^{m_2}h_2^{n_2}\right) + e_3\left(g_3^{m_3}h_3^{n_3}\right) + e_4\left(g_{avg}^{m_4}\right) \quad (5)$$

where HV is the micro hardness, e_i ($i = 0, 1, 2\ldots$) are the polynomial coefficients to be fitted, m_i, n_i ($i = 0, 1, 2\ldots$) are the exponents of empirical model. g_{avg}, g_1, g_2, g_3 are the γ-matrix, primary, secondary and tertiary γ' grain sizes, respectively. h_1, h_2, h_3 are corresponding volume fractions of γ' grains. The above model parameters were obtained through genetic algorithm based on measurements of different grain sizes and corresponding fractions.

Capello [77] proposed a regression model of residual stress σ expressed by Eq. (6) considering the influences of such independent variables as feed rate f, tool nose radius r, and entrance angle (χ) for different workpiece materials.

$$\sigma = 1000\log\left(k_1f^{k_2}r^{k_3}\right) - k_4\chi \quad (6)$$

where k_i ($i = 1, 2, 3\ldots$) are coefficients of empirical model for residual stress.

Moreover, through analyzing the characteristics of residual stress profiles within machined subsurface, Ulutan et al. [78] and Yang et al. [74] developed the empirical models of residual stress based on sinusoidal decay function for nickel alloys

GTD-111, Inconel 100, and titanium alloy Ti6Al4V, respectively. The empirical model of residual stress σ is expressed with Eq. (7) and the coefficients were fitted by Particle Swarm Optimization (PSO) method.

$$\sigma = C_0 e^{-\frac{\zeta\omega_d x}{\sqrt{1-\zeta^2}}}\cos(\omega_d x + \varphi) \tag{7}$$

where C_0 is the amplitude constant, x is the distance to the machined surface, ω_d is the damped frequency, ζ is the damping coefficient, φ is the phase angle. Yang et al. [74] found that the coefficients of C_0, ω_d, ζ and φ depended on the cutting parameters of cutting speed and feed rate in milling process of Ti6Al4V.

Pawade et al. [79], Ren and Liu [61] carried out turning experiments of Inconel 718 to establish empirical prediction models of the yield strength and strain of the workpiece material within machined subsurface as expressed by Eqs. (8) and (9). The authors found that the yield strength and strain of workpiece material depended on the micro hardness and material hardening coefficient. It is indicated that the material yield strength has linear relationship with the micro hardness while the strain has logarithmic relationship with it. Through measurement of micro hardness along the direction from machined surface to bulk material, the corresponding yield strength and strain within machining affected layer can be obtained.

$$\sigma_y = 0.801\left\{\frac{HV}{2.9}[1-(m-2)]\left[\frac{12.5(m-2)}{1-(m-2)}\right]^{m-2}\right\} \tag{8}$$

$$\varepsilon = \frac{\ln\sigma_y - \ln C}{n} \tag{9}$$

where σ_y and ε are the yield strength and the strain of workpiece material within machined subsurface, respectively. The parameter m is Meyer's index and it depends on the hardening coefficient of workpiece material [79]. C is the yielding-to-tensile ratio of workpiece material.

4.3 Analytical modeling of machined surface integrity

Analytical modeling of machined surface integrity depends on analytical models of cutting process including the kinematic and energy equations of cutting system, models of cutting force, cutting temperature, material deformation strain and strain rate within cutting zone, etc. Because of large number of variables involved in cutting process, analytical modeling of machined surface integrity is faced with more challenges than other research methods and it is always regarded as the most difficult one to perform [5]. Nevertheless, analytical modeling of machined surface integrity is beneficial to understand the machining process from the viewpoint of physical nature other than superficial phenomenon, so it has remarkable advantages than other research methods. Accurate description of initial conditions and boundary conditions, in addition to appropriate assumptions of cutting process are foundations to achieve reliable analytical models.

Through analysis of relative motion of milling tool and workpiece during end milling process, Yang and Liu [80] established an analytical model as expressed by Eq. (10) to predict the machined surface topography of end milling surface, based on which the surface generation mechanism in peripheral milling with variable pitch end milling tools was revealed. The model considered the influences of cutting parameters and several sources of machining errors such as the tilting, run out and deflection of cutting tool. The authors found that the helix angle of end milling tool and the feed rate were the main factors influencing surface topography through sensitivity analysis. The analytical model of surface topography prediction as Eq. (10) describes the path of a point on one tool flute (e.g. flute *i)* and the j^{th} level with respect to the workpiece in a Cartesian coordinate (x, y, z) at a given cutting instant t. Through a set of peripheral milling experiments for Ti6Al4V, it was confirmed that the proposed model could predict the machined surface morphology with enough precision [80].

$$\begin{aligned} x(i,z_j,t) &= r\cos\left(wt+\varphi_{pi}-z_j\tan\beta_i/r\right) \\ y(i,z_j,t) &= r\sin\left(wt+\varphi_{pi}-z_j\tan\beta_i/r\right)+ft \end{aligned} \tag{10}$$

where r is the tool radius, w and f are the tool angular velocity and the feed rate, respectively. β_i is the helix angle of cutting edge i, φ_{pi} is the pitch angle between cutting edge i and cutting edge i + 1.

Cutting tool structure is one of the basic factors that influence the geometrical parameters of machined surface. Analytical modeling of machined surface topography related to different cutting edge geometry can provide instruction for design and selection of cutting tools. Zhang and Liu [81] established an analytical model of machined surface topographies in finish turning with conventional and wiper inserts during turning process as expressed by Eq. (11).

$$\begin{bmatrix} x \\ y \\ z \\ 1 \end{bmatrix} = T_{wt}T_{tv}\begin{bmatrix} u_v \\ v_v \\ w_v \\ 1 \end{bmatrix} = \begin{bmatrix} 1 & 0 & 0 & 2\pi R'\cdot\Delta t\cdot n/60 \\ 0 & 1 & 0 & 0 \\ 0 & 0 & 1 & L-nf/60 \\ 0 & 0 & 0 & 1 \end{bmatrix}\begin{bmatrix} 1 & 0 & 0 & 0 \\ 0 & 1 & 0 & r_1 \\ 0 & 0 & 1 & 0 \\ 0 & 0 & 0 & 1 \end{bmatrix}\begin{bmatrix} u_v \\ v_v \\ w_v \\ 1 \end{bmatrix} \tag{11}$$

where $[x\ y\ z]^{\mathrm{T}}$ is the path of an arbitrary point in the workpiece coordinate system, based on which the machined surface topography can be generated. L is the cutting length, R' is the workpiece radius, n is the spindle rotation speed. T_{wt} and T_{tv} are transformation matrixes from cutting tool coordinate system to workpiece coordinate system. $[u_v\ v_v\ w_v]^{\mathrm{T}}$ is the path of a point in the

cutting tool coordinate system with an angle θ relative to the cutting direction expressed by Eq. (12).

$$\begin{bmatrix} u_v \\ v_v \\ w_v \end{bmatrix} = \begin{cases} \begin{bmatrix} 0 \\ -r_1\cos\theta \\ -r_1\sin\theta \end{bmatrix} & (\theta > 0) \\ \begin{bmatrix} 0 \\ r_2(1-\cos\theta)-r_1 \\ -r_2\sin\theta \end{bmatrix} & (-\alpha \le \theta \le 0) \\ \begin{bmatrix} 0 \\ r_2[1+\sin\theta/\sin(\delta-\theta)]-r_1 \\ r_2\cos\theta/\sin(\delta-\theta) \end{bmatrix} & (\theta < -\alpha) \end{cases} \tag{12}$$

where δ refers to the wiper angle, r_1 and r_2 represent the tool nose radius and wiper radius of the cutting inserts, respectively.

Zhang and Liu [81] validated the reliability of their proposed model in Eq. (11) with the turning experiments of Ti6Al4V and proved the agreement of machined surface topographies between predicted results and experimental measurements.

Some research has also been conducted to seek the analytical modeling of mechanical properties of machined surface. Ulutan et al. [82] proposed an analytical prediction model of residual stress as expressed by Eq. (13) based on elasto-plastic analysis of machined subsurface, and their model could be suitable to different workpiece materials including titanium and nickel alloys. The model established by Ulutan et al. [82] considered the combined effects of body forces, hydrostatic pressure, normal compressive pressure, tensile surface traction, in addition to tangential traction on the machined surface. The prediction accuracy was also proved through comparison of analytical and experimental results of residual stress within machined subsurface for bearing steel 100Cr6.

$$\begin{aligned} \sigma_{xx}^{el} &= \sigma_{xx}^{mech} + \sigma_{xx}^{therm} \\ \sigma_{zz}^{el} &= \sigma_{zz}^{mech} + \sigma_{zz}^{therm} \\ \sigma_{xz}^{el} &= \sigma_{xz}^{mech} + \sigma_{xz}^{therm} \\ \sigma_{yy}^{el} &= \nu\left(\sigma_{xx}^{el} + \sigma_{zz}^{el}\right) - \alpha ET \\ \sigma_{ij}^{mech} &= f(z, x, f_r, f_t) \\ \sigma_{ij}^{therm} &= f(z, x, \alpha, T, E, \nu, G) \end{aligned} \tag{13}$$

where x and y are the distances parallel and vertical to the cutting speed direction, respectively. z is the depth of investigated location. f_r is the radial cutting force, f_t is the tangential cutting force, T is the temperature, E is the Young's Modulus of workpiece material, ν is the Poisson Ratio, α is the thermal expansion coefficient of workpiece material, G is the array of plain strain Green's function values.

Wu and Matsumoto [83] carried out analytical research on residual stress distribution within machined surface based on the assumption that the loading history of any point on the machined surface was identical. They proposed that compressive loading resulted in tensile residual stress, while compressive residual stress was formed under tensile loading. Liu and Barash [84] established prediction model of residual stress on machined surface based on slip line field theory, and they used the model to analyze the influence of tool wear on residual stress distribution effectively. Liang and Su [85] also established similar analytical model of residual stress to investigate the effects of cutting parameters and material properties on residual stress profiles within machined subsurface.

4.4 FEM-based analysis of machined surface integrity

Some important characteristics of machined surface integrity can be researched based on FEM analysis including microstructure alterations, micro harness, and residual stress distribution within machining affected layer. Selection of appropriate material models including material constitutive model and fracture criterion, as well as chip separation criterion is the prerequisite to get accurate results compared to the practical situation [6]. Because cutting process is a typical elasto-viscoplastic material deformation process, FEM-based simulation techniques can provide fairly accurate results to understand the physical phenomena occurring on machined surface [5]. FEM-based analysis of machined surface integrity can reduce the research cost due to much less experimental work needed to be conducted. Only several groups of experiments are needed to validate the reliability of FEM models. FEM-based analysis provides the possibility to predict different characteristics of machined surface integrity under different cutting conditions. Nevertheless, research on surface integrity based on FEM may take excessive computational time and one main task of FEM-based analysis is to optimize the model and improve the computational efficiency.

Compared to research on chip formation mechanism with FEM-based analysis, the research on machined surface integrity should be paid more attention to. Two dimensional (2D) simulation has been widely used to analyze the distribution of strains, strain rates, temperatures, stresses and residual stresses on machined surface during machining of titanium and nickel alloys, due to its relative simpler modeling procedures and higher computational efficiency [6]. Different material models including elastic, plastic, elastic-plastic, or elastic-viscoplastic models have been used in the simulation models. Material fracture models leading to chip formation based on material damage criteria [6, 86, 87] or automatic remeshing techniques [88] are used in FEM simulation. Considering practical application of machining process like turning and milling, 3D modeling based on FEM analysis have also been performed to investigate machined surface integrity.

Ding and Shin [89] adopted coupled Eulerian-Lagrangian FEM and dislocation density-based material model to investigate grain refining behavior within cutting deformation zone during orthogonal cutting process. They proved the effectiveness of the model though analyzing the mechanical behavior of pure titanium under different loading conditions of strains, strain rates, and temperatures. Wang et al. [90] investigated the grain size and micro hardness distribution within machined

subsurface during high speed machining of Ti6Al4V with the user subroutine VUSDFLD in Abaqus/Explicit software. The models of Zener-Hollomon and Hall-Petch were used to predict the grain size d and micro hardness HV as expressed by Eqs. (14) and (15), respectively.

$$d = a_1 d_0^{h_1} \varepsilon^{n_1} \dot{\varepsilon}^{m_1} \exp(m_1 Q/R(T+273)) + c_1 \quad (14)$$

where Q is the apparent activation energy for workpiece material,R is the gas constant,d_0 is the initial grain size of workpiece material, ε、$\dot{\varepsilon}$ 、T are the strain, the strain rate and the temperature, respectively. a_1、h_1、m_1 and c_1 are material constants.

$$HV = c_0 + cd^{-0.5} \quad (15)$$

where c_0 is the initial micro hardness of workpiece material and c is material constant.

Calamaz et al. [91] proposed a modified material constitutive model for Ti6Al4V through including of strain softening item in FEM simulation, and the simulation results of material deformation behavior during machining process was improved. Ranganath et al. [92] performed FEM-based analysis to investigate the white layer formation during machining of Inconel 718 and suggested that further research was needed to obtain more accurate and reliable FEM simulation models. Arisoy et al. [76] performed 3D FEM simulations to predict the average grain size during machining of Inconel 100 by implementing modified temperature dependent flow softening based material and Johnson-Mehl-Avrami-Kolmogorov crystallization models. Their simulation prediction results on the average grain sizes, phase fractions, and resultant micro hardness presented good agreements with experimental results and revealed the reliability of their developed FEM model. With the same method, Arisoy and Özel [93] established 3D FEM model for machining of Ti6Al4V and predicted the machining induced microstructure successfully, and they also investigated the effects of tool micro-geometry, tool material as well as cutting conditions on the microstructure alterations of machined surface. Yang et al. [74] carried out 2D FEM simulation analysis for machining of Ti6Al4V to investigate the residual stress profiles within machined subsurface and established empirical model of residual stress distribution.

5 Influence of tool structure on machined surface integrity

Surface integrity is directly related to the physical property and service performance of machined components. The demand for machined surface integrity varies depending on the surface working conditions. For the finished surface in mechanical contact, the parameters of machined surface integrity that govern the wear and frictional behavior of contacting bodies should be paid more attention to. These parameters mainly involve the geometrical parameters including surface roughness and surface defects. Having the possibly smoothest surface and least surface defects are desired for such cases. However, in other cases such as biomedical field, a rougher machined surface will be preferred [94]. If the machined surface is working under alternating loading conditions, the mechanical properties (especially the residual stress distribution) of surface integrity are more important. The turbine disk and blade are typical example for such cases, where the compressive residual stress on the machined surface is desired [5].

Considering that cutting tool is one of the most basic factors that govern the machined surface integrity as mentioned above, the influence of cutting tool structure on machined surface integrity of titanium and nickel alloys is reviewed in this section. Then the influences of tool material and tool wear on machined surface integrity will be reviewed following. In every section, the variation of machined surface integrity under different cutting tools will be presented with respect to geometrical characteristics, microstructure alterations, and mechanical properties in details.

5.1 Influence of tool structure on geometrical characteristics of machined surface

Geometrical characteristics of machined surface mainly include geometrical morphology, surface roughness, and surface defects, etc. Surface roughness is widely described by arithmetic average deviation of profile (R_a) and maximum profile height (R_z). Surface defects refer to high frequency irregularities on the machined surface caused by the interaction between the cutting tool and the workpiece material. The common defects of machined surface include feed marks, grooves, pits, metal debris, smeared material and micro cracks, etc. [20, 57, 95], which are of interest as they possibly give an indication of weakness that could influence the mechanical property and fatigue performance of the machined parts.

The cutting tool structure including cutting tool angles and cutting edge shape have great influence on the geometrical characteristics of machined surface for titanium and nickel alloys. Round insert with large nose radius [20, 96–98] can improve the machined surface quality compared to square insert due to larger contact length of the tool. The chamfered and honed tools are beneficial to guarantee the strength of cutting edge and prevent the cutting edge chipping [7]. Cutting tools with chamfered edge are recommended to be used for machining of difficult to machined materials including titanium and nickel alloys due to their high edge strength.

The single-point continuous turning of Inconel 718 using round and rhomboid-shaped ceramic tools found that the round inserts produced a better surface finish than the rhomboid inserts under the same cutting conditions [99]. Arunachalam et al. [20] investigated the effects of insert

shape, cutting edge preparation and nose radius on surface finish of Inconel 718 at such identical turning conditions as the cutting speed V_c of 60 m/min, feed rate f of 0.1 mm/rev and depth of cut a_c of 0.5 mm. Their investigation as shown in Fig. 7 suggests that the coated carbide cutting inserts with round shape, honed cutting edge, negative type and large nose radius (0.8 mm) can decrease the surface roughness under dry cutting conditions [20]. Correspondingly, the surface defects can also be reduced under above cutting conditions. The larger values of surface roughness obtained with the sharp cutting edges are mainly related to the chipping of sharp cutting edge during the entry and cutting process, while it can be alleviated for the inserts with honed cutting edge leading to lower surface roughness. Significant improvement in machined surface roughness can be achieved if appropriate cutting tool geometry is selected. It has been demonstrated to produce surface roughness R_a below 0.5 μm during turning Inconel 718 at 500 m/min, which provide the evidence to use modified edges for finish machining where high finished surface quality is required [97].

The higher value of chamfer angle is proved to produce lower surface roughness and the influence of chamfer on the machined surface roughness enhances at higher cutting speeds [100]. Özel et al. [101–103] investigated the effects of uniform and variable micro-geometry of cutting edge on the machinability and machined surface integrity for Ti6Al4V (Fig. 8), which revealed that the variable micro-geometry of cutting edge produced lower cutting force under high cutting speeds, which can be expected to generate better surface quality.

The modified cutting edge with wiper has been used to improve the surface quality [104, 105]. A generalized analytical model [81] of machined surface topography considered the geometrical differences between conventional and wiper turning inserts and compared the topographies generated with these two different inserts under the same cutting parameters. It can be figured out in Fig. 9 that the peak-to-valley height on the machined surface decreases with about 50% at the same cutting parameters, although the texture of surface topography is nearly the same. The role of modified wiper on the machined surface roughness is similar with that of the large tool nose radius. The model can be extrapolated to predict the machined surface topography for machining of different workpiece materials with varied cutting tools and cutting parameters.

There is little available research about the effect of solid milling tool structure on the geometrical characteristics of machined surface. Milling tools with varied pitch or varied helix angles are adopted to improve the vibration performance during milling process, which can generate better surface quality subsequently [106–108]. End milling of Ti6Al4V was performed using AlTiN coated 4-flute end milling tool with

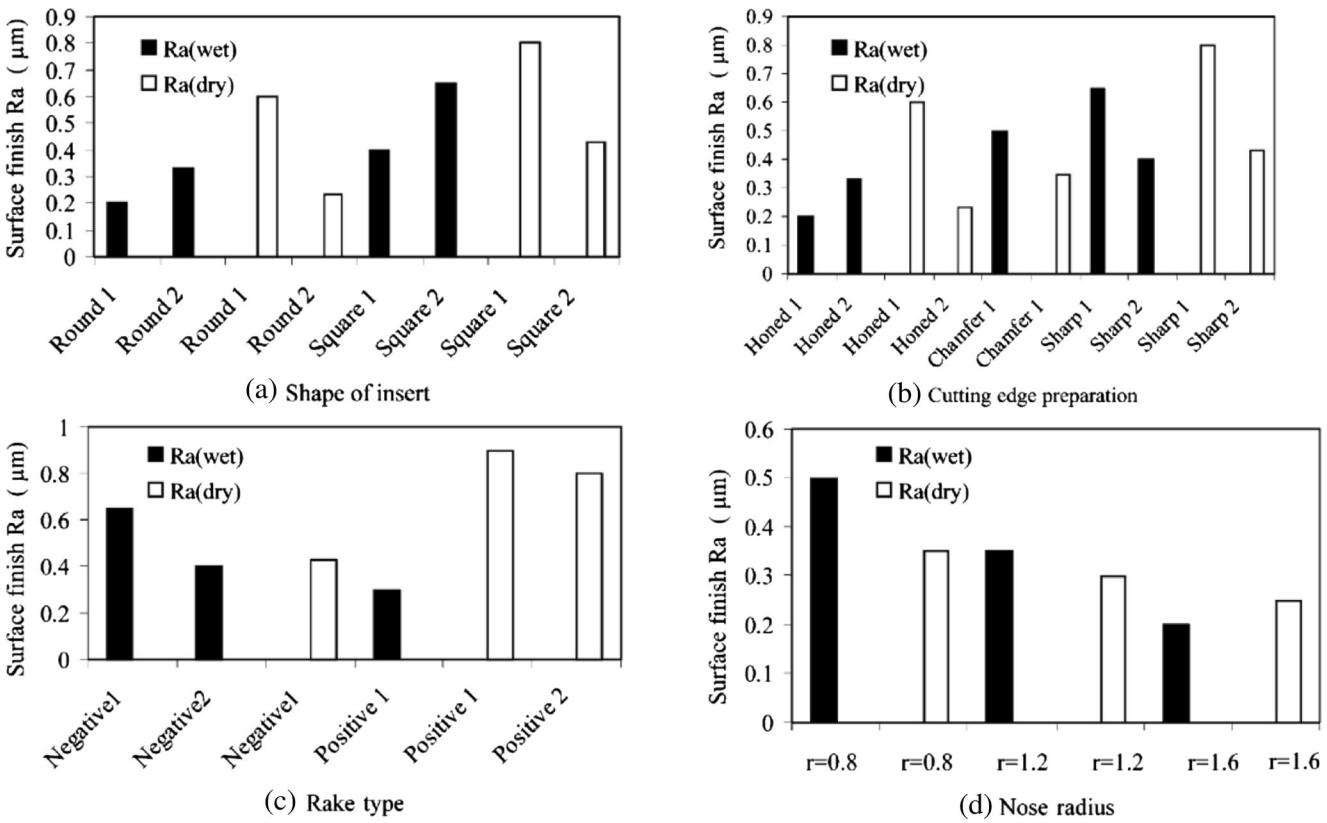

Fig. 7 Effect of insert geometrical parameters on machined surface roughness after turning of Inconel 718 at $V_c = 60$ m/min, $f = 0.1$ mm/rev and $a_p = 0.5$ mm (**a**) effect of insert shape; (**b**) effect of cutting edge preparation; (**c**) effect of rake angle; (**d**) effect of tool nose radius [20]

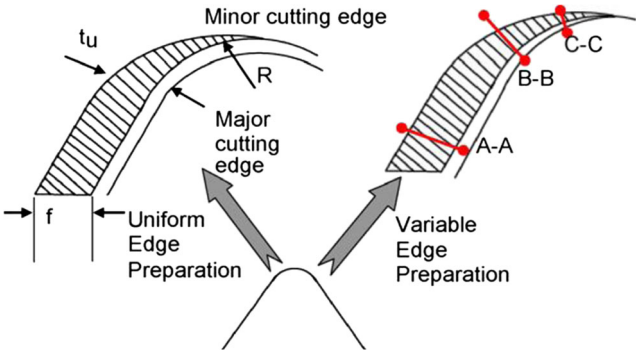

Fig. 8 Uniform and variable micro-geometry of cutting edge [101]

varied helix angles (38° and 41°) [108]. Figure 10 presents the surface defects generated with the same milling tools under different cutting parameters. It indicates that the defects of end milling surface for Ti6Al4V under low cutting speed are mainly scratch marks, plucking and dimples as shown in Fig. 10(a)–(d) due to large cutting force leading to the tearing of chip from the bulk material. With the cutting speed increasing, the chip serrated degree increases and tends to form fragmented chip due to poor thermo-physical properties of Ti6Al4V, which has been researched widely from the viewpoint of chip formation mechanism [8, 109, 110]. Then the surface defects of Ti6Al4V evolve to adhered material particles and debris of microchips as shown in Fig. 10(e)–(h).

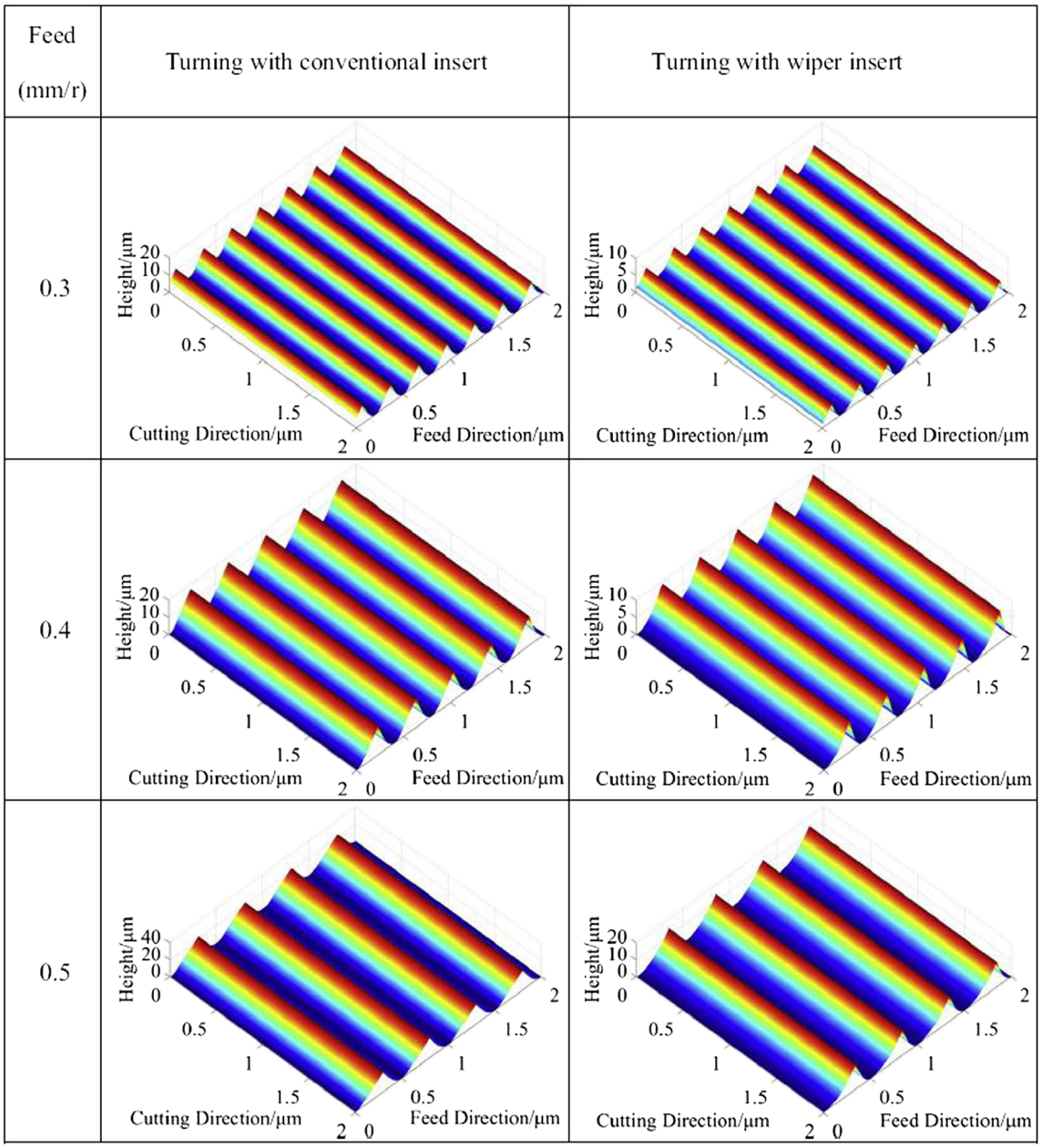

Fig. 9 Surface topography generated after turning with wiper and conventional inserts [81]

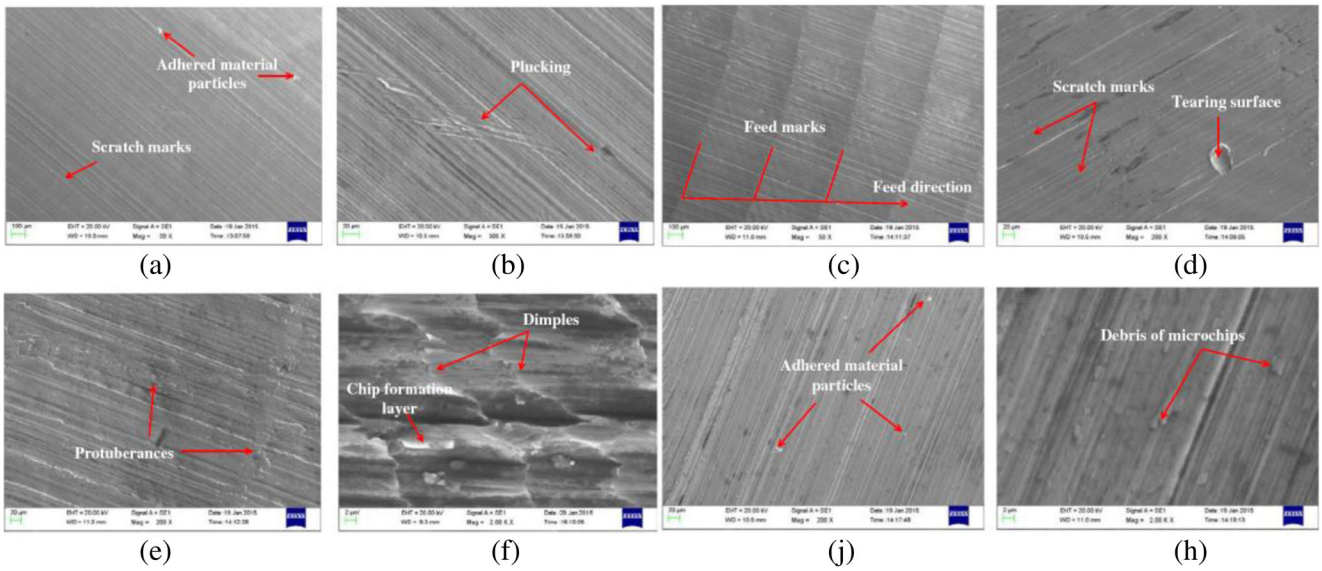

Fig. 10 Machined surface defects for Ti6Al4V generated under different milling parameters: (**a**), (**b**) $V_c = 20$ m/min, $f = 0.03$ mm/z, $a_e = 1.5$ mm; (**c**), (**d**) $V_c = 50$ m/min, $f = 0.05$ mm/z, $a_e = 2.0$ mm; (**e**), (**f**) $V_c = 80$ m/min, $f = 0.04$ mm/z, $a_e = 1.0$ mm; (**g**), (**h**) $V_c = 110$ m/min, $f = 0.02$ mm/z, $a_e = 0.5$ mm [108]

Besides the commonly modified cutting edge and varied cutting tool angles, the micro textures fabricated on the tool rake or flank face are expected to improve the friction performance of cutting tools and machined surface quality [111–113]. Arulkirubakaran and Senthilkumar [111] performed turning experiments on Ti6Al4V with coated (TiN, TiAlN) and uncoated cutting inserts with different textured patterns fabricated on the rake face. The textured patterns include linear texture with grooves parallel to the chip flow (PA.T), grooves perpendicular to chip flow (PE.T), cross-texture (CR.T) and non-texture (NT) as shown in Fig. 11. All the grooves fabricated on the tool rake face have an

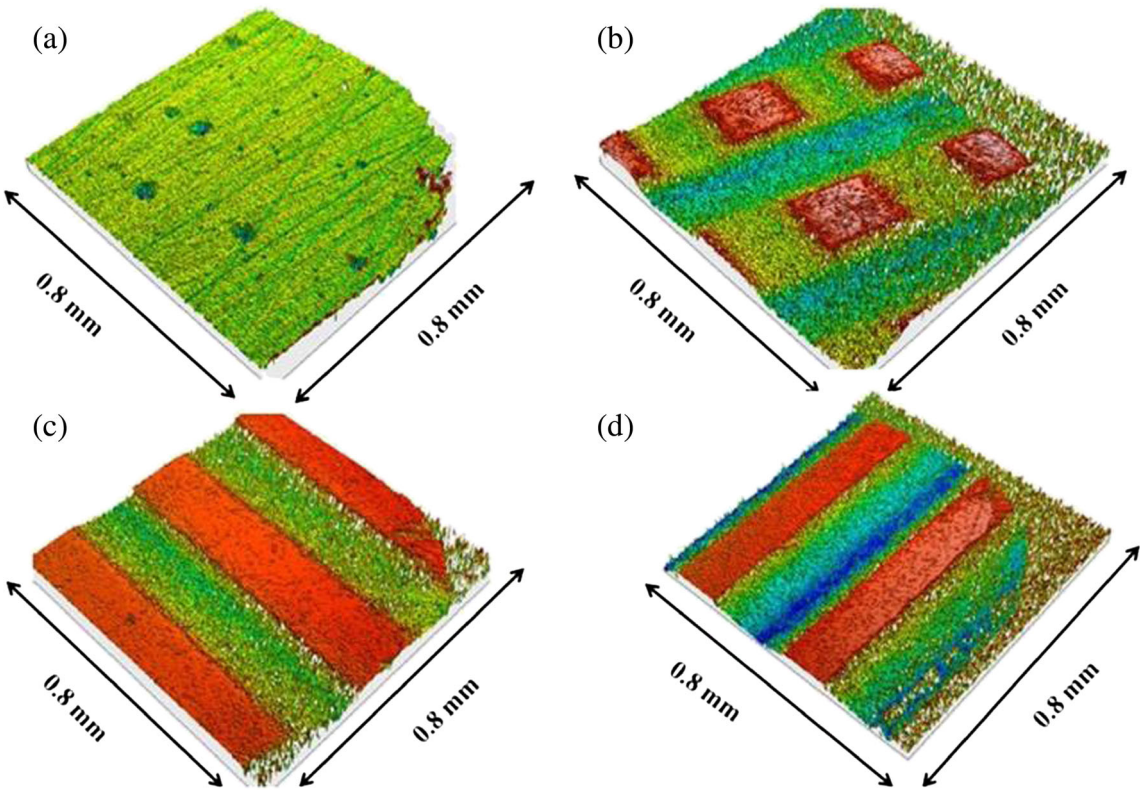

Fig. 11 Topography of textures fabricated on tool rake face (**a**) non-texture (NT); (**b**) cross-texture (CR.T); (**c**) grooves parallel to chip flow (PA.T); (**d**) grooves perpendicular to chip flow (PE.T) [111]

average size of 250 μm in width and 100 μm in depth, and all other tool geometrical parameters were kept as the same.

It was observed that the machined surface roughness of Ti6Al4V decreased with cutting speed increasing for any given tool texture pattern (Fig. 12) [111], which could be attributed to the thermal softening effect at higher cutting speed. The textured tools exhibited lower surface roughness compared to those obtained with non-textured tools at a given cutting speed, including the coated and uncoated tools. The textures fabricated on the tool rake face can decrease the tool-chip friction efficiently, which is beneficial for the chip flow, lowering the cutting force and improving the machined surface roughness. Among the cutting inserts with different texture patterns, PE.T tool presented the best cutting performance and generated the lowest machined surface roughness when other cutting parameters were the same. The combined effects of rake face texture and tool coating enhance the cutting performance further and generate better surface roughness compared to that of uncoated or non-textured tools.

The diamond tool with textures fabricated on the tool rake face having the depth of 43 nm and width of 1.8 μm was prepared by Kawasegi et al., and used in the machining of nickel phosphorus alloy [112]. Their research found that the cutting performance of textured diamond tool was enhanced by lowering the friction coefficient and cutting forces for nickel phosphorus alloy, while the machined surface quality was qualified simultaneously. It is demonstrated that the textured diamond cutting tool provides an effective way to improve the machining performance of nickel alloys. In another study for machining of nickel alloy, a novel CBN cutting tool with textured flank face was developed to be used in high speed machining of Inconel 718 [113]. It was identified that the CBN cutting tool with textured flank face could improve the cutting performance of cutting tool and prolong the tool life. The micro grooves fabricated on the flank face significantly suppressed the cutting edge chipping, which can be expected to reduce the formation of surface defects and lower the machined surface roughness.

5.2 Influence of tool structure on microstructure alterations of machined surface

It has been recognized that microstructure alterations occur in surface layer as a function of cutting parameters and cutting tool conditions in machining of several alloy systems including titanium and nickel alloys [114]. As one of the significant parameter to access the surface integrity, microstructure alteration of machined surface also plays a critical role and can tremendously affect the components performance and their service life. It is important to understand the final state of the machined surface microstructure after machining process applied with different tool structures. Microstructure alterations induced by machining processes mainly include plastic deformation layer, variation of grain size and grain orientation through recrystallization and recovery, in addition to phase transformation, etc. [5]. Accurate prediction for the effects of tool structure, especially the effect of micro-geometry (cutting edge radius, chamfer or wiper size, etc) of cutting tools on machining induced microstructure alteration is one of the great challenges that the machining workshop is facing. Modeling of microstructure alteration for Ti6Al4V and Inconel 718 has been focused on by many researchers, but the vast majority of the current literatures concentrate on thermomechanical processing rather than machining as indicated in literature [115].

In-depth analysis of microstructure alteration of machined surface and subsurface for titanium and nickel alloys has been carried out with the help of different advanced microexamination techniques. The effects of cutting edge geometry including chamfer angle and hone radius on microstructure alteration during orthogonal cutting of Inconel 718 were investigated, in which the cutting speed and uncut chip thickness were fixed at 70 m/min, and 0.1 mm, respectively [116]. The cutting edge geometrical parameters including chamfer angle and hone radius were changed at four different levels for each tool edge preparation as shown in Fig. 13.

Figure 13 indicates that increases of both chamfer angle and hone radius result in the increase of machined surface

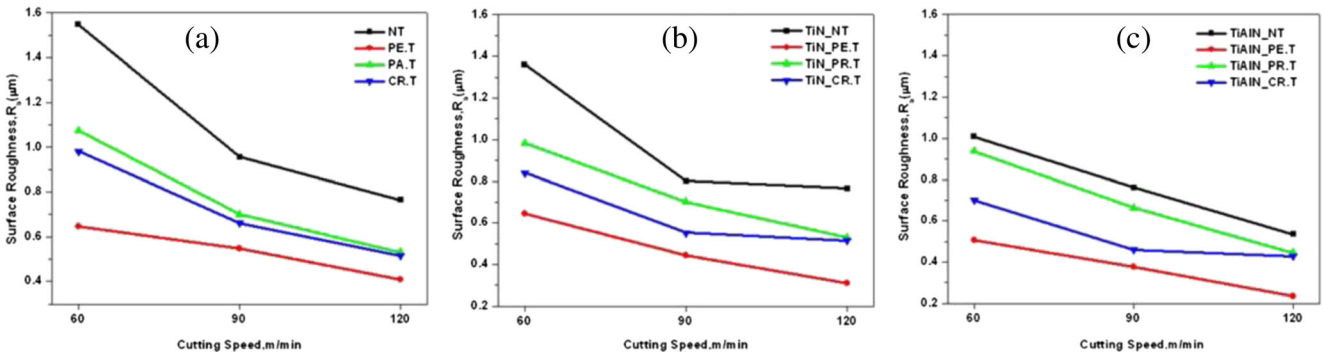

Fig. 12 Machined surface roughness of Ti6Al4V formed using cutting tools with different rake face textures (**a**) uncoated tool, (**b**) TiN coated tool, (**c**) TiAlN coated tool [111]

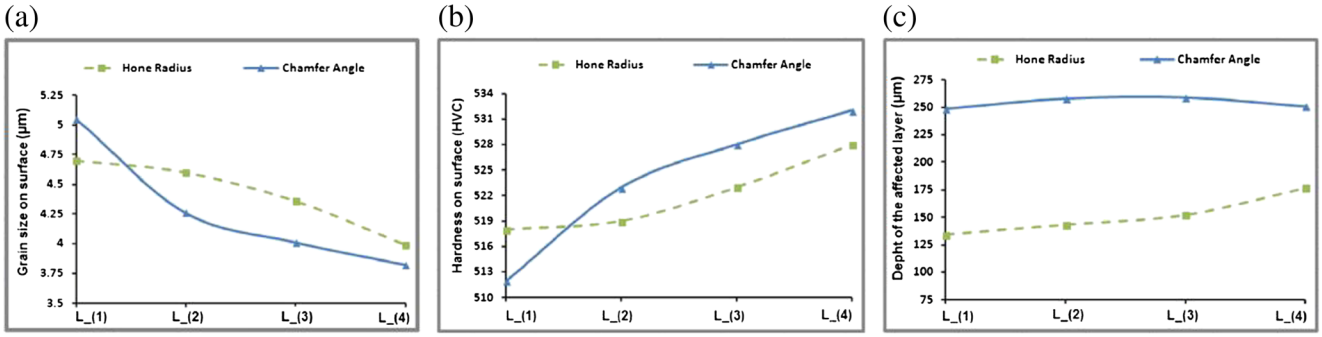

Fig. 13 Effects of cutting edge geometry on microstructure alterations of machined surface (**a**) grain size; (**b**) micro hardness; (**c**) depth of machining affected layer. The hone radius and chamfer angle for tools of L_(1), L_(2), L_(3) and L_(4) are 25 μm and 10°, 50 μm and 20°, 75 μm and 30°, 100 μm and 40°, respectively [116]

hardness (one index of mechanical properties for machined surface) and decrease of surface grain size, and this variation is more insensitive for chamfered tool than honed tool [116]. Figure 13(c) indicates that the depth of machining affected layer formed with the chamfered tool is significantly larger than that formed with the honed tool, which can be attributed to the severer plastic deformation induced by chamfered edge during machining process. It can also be seen from Fig. 13 (c) that the depth of machining affected layer is more sensitive to the tool edge type than specific geometrical parameters for each tool edge.

The research on the effects of cutting edge radius on microstructure evolution of machined surface for Inconel 100 consisting of such two main phases as γ and γ' revealed the microstructure alteration within machined subsurface [76]. Three kinds of cutting tools with the edge radii of 5 μm, 10 μm and 25 μm were researched. Figure 14 presents the microstructure of Inconel 100 subsurface including grain sizes of primary γ' (d_1) and secondary γ' (d_2) under cutting speed of 12 m/min and feed rate of 0.05 mm/rev using different cutting tools. The results showed that the uncoated WC/Co tools with edge radii of 5 mm and 25 mm generated larger primary γ' precipitates (d_1) on the machined surface, followed by the uncoated WC/Co tools with the edge radius of 10 mm. Comparatively, these trends were reversed for the sizes of secondary γ' precipitate, and the TiAlN coated tool generated the largest secondary γ' grains.

Another research performed by Arisoy and Özel [93] revealed the effect of tool edge radius on microstructure evolution of machined surface for Ti6Al4V, in which the cutting tools were the same as those in literature [76]. Under the cutting speed of 55 m/min, feed rate of 0.05 mm/rev and depth of cut of 2 mm, the grain size of machined surface generated using the sharp tool with cutting edge radius of 5 μm was the smallest. When the cutting speed increased to 90 m/min with the other cutting parameter unchanged, the grain size of the machined surface generated using the tool with cutting edge radius of 5 μm was the largest. It means that the plastic deformation behavior of the machined surface varies significantly for cutting tools with different micro-geometries under different cutting parameters.

Besides the grain size evolution, the depth of machining affected layer is another commonly used parameter to characterize the microstructure alteration induced by machining. The effects of tool nose radius on plastic deformation depth of machined surface for Inconel 718 at the cutting speed of 40 m/min and depth of cut of 0.25 mm have been researched [117]. The tool nose radius was varied from 2 mm to 6 mm and the feed rate was varied from 0.25 mm/rev to 0.5 mm/rev. It can be seen from Fig. 15 that the deformation depth of machined surface increases to over 20 μm using the cutting tool with 6 mm nose radius, while the deformation depth fluctuates at about 12 μm for all the other tool nose radii used. Arunachalam et al. [20] stated that round tools with 6 mm tool nose radius produced higher cutting forces than square tools with smaller tool nose radius during turning of Inconel 718. The deeper plastic deformation layer formed with larger tool nose radius can be attributed to the larger cutting forces leading to severer plastic deformation on the machined surface.

Microstructure alterations of end milling surface have also been focused on, among which the variation of microstructural features for Ti6Al4V machined with 4-flute and variable helix angles end milling tools were investigated (Fig. 16) [118]. The assessed microstructural features covered the grain size, phase transformation, deformation layer thickness, as well as the sensitivity of microstructure variation to milling parameters. It was suggested that the 4-flute and variable helix angles end milling tools can generate better surface quality for Ti6Al4V under high cutting speeds, for which the microstructure alterations were slighter than those generated under lower cutting speeds.

5.3 Influence of tool structure on mechanical properties of machined surface

Residual stress is referred to the stress that remains when the external force is absence [119]. Residual stress on the machined surface is generally formed by inhomogeneous plastic

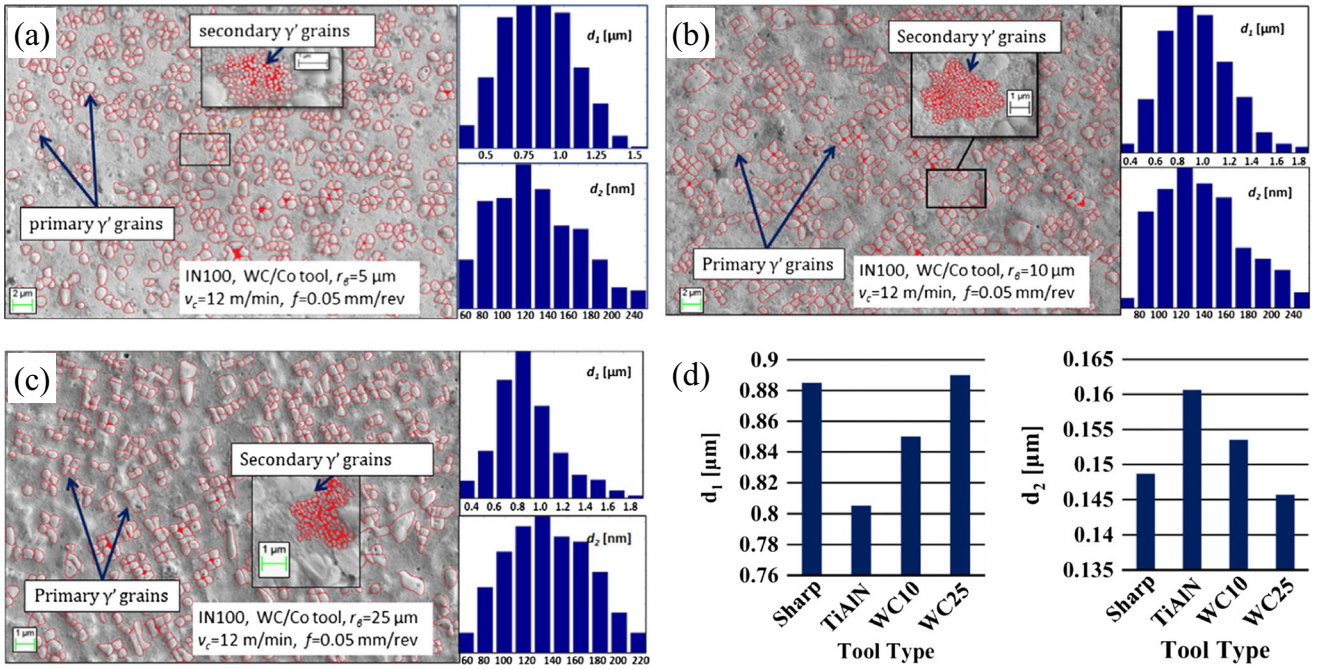

Fig. 14 Microstructure of machined subsurface for Inconel 100 including grain sizes of primary γ′ (d_1) and secondary γ′ (d_2) under V_c = 12 m/min and f = 0.05 mm/rev (**a**) sharp WC/Co tool with r_β = 5 µm; (**b**) WC/Co tool with r_β = 10 µm; (**c**) WC/Co tool with r_β = 25 µm; (**d**) effects of tool type and edge radius on primary and secondary γ′ grains [76]

deformation and/or phase transformations companied with extremely large strains, large strain rates and high temperatures [120]. Depending on different distribution characteristics of residual stress, it can be either beneficial or detrimental to the service performance and life of manufactured components. Previous research suggests that the compressive stresses are usually beneficial to the fatigue life, the creep behavior as well as stress corrosion resistance, while the effects of tensile residual stresses are usually adverse [121]. Consequently, it is of vital importance to control the residual stresses within the machining affected layer to fall in the compressive range. The distribution of residual stress is one of the most significant parameters in the manufacture of components especially in the aerospace industry where components work under the alternating mechanical and thermal loadings and fatigue failure always occur. Bellows [122] concluded that the mechanical properties of components made from Inconel 718 are more sensitive to residual stresses than to surface finish.

The research on surface integrity during machining of age hardened Inconel 718 [20] suggested that coated carbide inserts

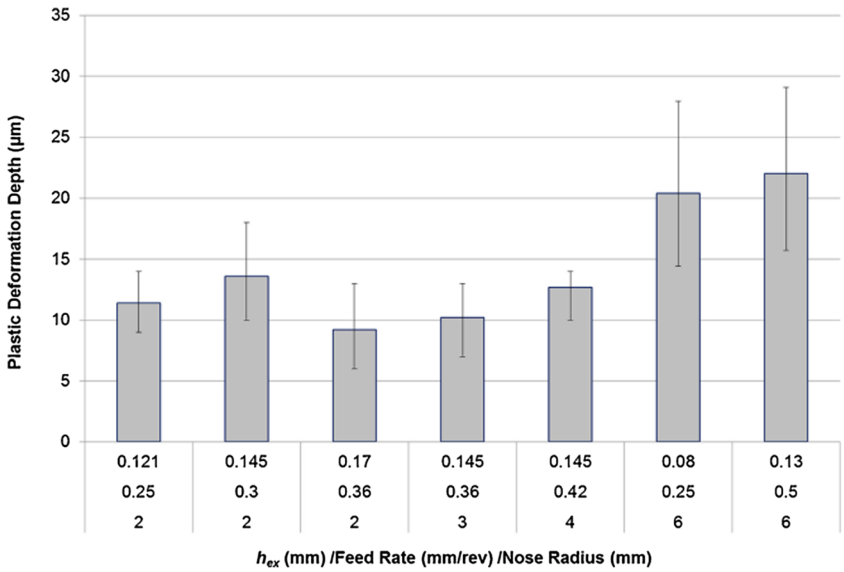

Fig. 15 Plastic deformation depth for Inconel 718 formed using cutting tools with different tool nose radius [117]

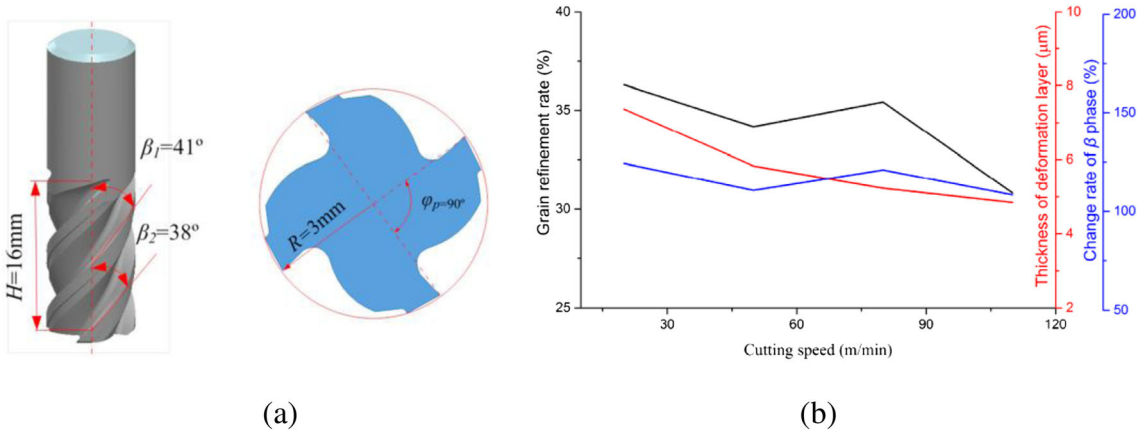

Fig. 16 Variation of microstructural features for Ti6Al4V machined with 4-flute and variable helix angles end milling tools (**a**) schematic diagram for end milling tools; (**b**) variation of microstructural features for Ti6Al4V [118]

with round shape, chamfered cutting edge and negative rake angle could generate primarily compressive residual stresses. Generally, round inserts produced compressive residual stresses on the machined surface while square inserts produced tensile residual stresses. When the workpiece material near machined surface is heated and elongated more than the bulk material, the machined surface area expands and experiences a compressive residual stress from the less deformed bulk material. A sharp cutting edge leads to higher values of tensile residual stress than the honed cutting edge, while chamfered cutting edge generates more compressive residual stress. The compression imposed on the machined surface by large edge honed tools is much severer than that caused by small edge honed tools. Thus more compressive residual stress is prone to be induced with large honed edge tools compared with the small ones [123].

The effects of chamfered and honed cutting edges on residual stress formation have been investigated as illustrated in Fig. 17 [79]. The chamfered plus honed edge results in larger contact area between the cutting edge and the deformed material ahead of the cutting edge, which causes greater plowing effect and thereby greater plastic deformation of the workpiece material. Consequently, the additional plowing due to the honed radius compared to chamfered tools can induce more compressive residual stresses.

As shown in Fig. 18, the effects of chamfered cutting edge on residual stresses of machined surface for Inconel 718 using ceramic cutting tools were assessed [97]. It was reported that compressive residual stresses were generated with 20° chamfered insert (i.e. the commercial chamfer in Fig. 18), while the magnitude of residual stresses increased when the tool with 15° chamfered (i.e. the modified chamfer in Fig. 18) and honed edge was used. Matsumoto et al. [124] have confirmed that the honed edge combined the double chamfered geometries can offer greater subsurface penetration and then produce larger values of maximum compressive stress.

The effect of negative tool rake angle on the residual stress formation is similar with that of the chamfered cutting edge, while the positive tool rake angle tends to induce the tensile residual stress. However, Arunachalam et al. [96] revealed that the smallest tool nose radius (0.8 mm) resulted in compressive residual stresses while the larger radius resulted in tensile residual stresses, which is different from the common sense. They attributed the abnormal phenomenon to the poor thermal conductivity of Inconel 718, which results in the

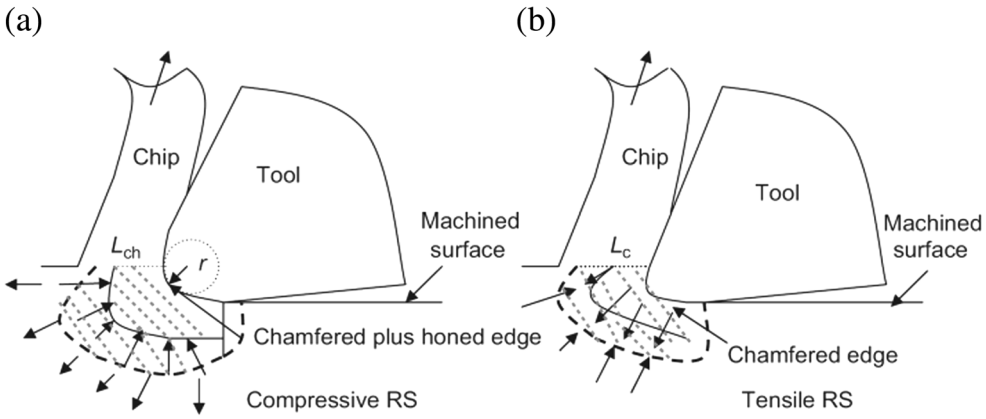

Fig. 17 Illustration for the effect of tool edge shape on residual stresses in machining of Inconel 718 [79]

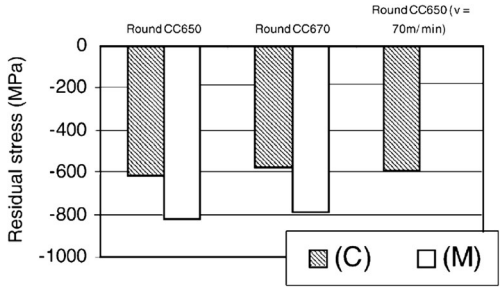

Fig. 18 Residual stresses after turning of Inconel 718 at $V_c = 70$ and 500 m/min, $f = 0.1$ mm/rev, and $a_p = 0.35$ mm with different chamfered edge cutting tools (C: commercial chamfer, M: modified chamfer) [97]

dominant role of plastic deformation associated with thermal effects than the plowing effect for the larger tool radius.

Sharman et al. [117] investigated the effects of tool nose radius on the residual stress distribution using coated tungsten carbide tools at such fixed cutting parameters as the cutting speed of 40 m/min and depth of cut of 0.25 mm. The tool nose radius was varied from 2 mm to 6 mm and the feed rate was varied from 0.25 mm/rev to 0.5 mm/rev. The variation of residual stress profiles in cutting direction under different tool nose radii can be seen in Fig. 19 [117]. The results showed that an increase in tool nose radius resulted in deeper tensile and compressive residual stress distribution when the cutting parameters were fixed, and they proposed that the shift to a deeper tensile and compressive stress layer with larger tool nose radius could be attributed to the depth increase of the deformed subsurface microstructure. The investigation in finish turning regime for two aerospace grade titanium alloys including Ti6Al4V and Ti-6246 considered the effects of tool nose radius on machined surface integrity [125], in which the appropriate range of tool nose radius suitable to generate the compressive residual stress which can promote fatigue-inhibiting consequently was proposed.

Micro hardness is another important parameter to characterize the mechanical properties of machined surface. The

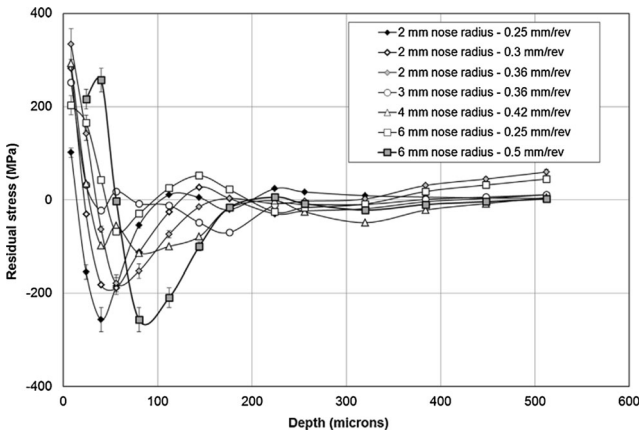

Fig. 19 Variation of residual stress profiles in cutting direction under different tool nose radii (error bars show the uncertainty of measurement) [117]

turning experiments of Inconel 718 using PCBN rhomboidal shaped insets with different cutting edge geometries, which include 30° chamfer with 100 μm land (labeled as CWI), 20° chamfer with 100 μm land (labeled as CWII), and 30° chamfer with 100 μm land plus honed edge (labeled as CH) were performed [79]. It can be seen from Fig. 20 that under different cutting parameters, the effects of cutting edge geometry on the micro hardness of machined subsurface are different. At low cutting speed of 125 m/min combined with feed rate of 0.05 mm/rev and depth of cut of 1 mm, the micro hardness of machined surface obtained using the tool with chamfer plus honed edge is the largest. It can be attributed to the severe compression on the machined surface caused by the chamfer plus honed cutting edge. However, with the cutting speed increasing to 475 m/s, the effect of chamfer plus honed cutting edge on the machined surface micro hardness decreases, while the value of micro hardness obtained with the tool of 20° chamfered edge is the largest.

Through establishment of a quantitative relationship between material yield strength and average micro hardness for the machined surface, the variation of material yield strength with depth below the machined surface for Inconel 718 obtained with different cutting edge geometries were obtained [79]. Because the material yield strength has positive relationship with the micro hardness, the yield strength profiles of machined subsurface for 718 obtained with different cutting edge geometries are the same with those of the micro hardness profiles.

Through turning experiments of Inconel 100 alloy, the effects of cutting edge radius on the variation of machined surface micro hardness were investigated with two cutting speeds ($V_c = 12$ and 24 m/min), a constant feed rate ($f = 0.05$ mm/rev) and a constant depth of cut ($a_p = 1$ mm), under dry cutting conditions [76]. Uncoated tungsten carbide (WC/Co) cutting inserts with three different edge radii (r_β) with $r_\beta = 5 \pm 0.5$ μm (sharp edge), $r_\beta = 10 \pm 0.7$ μm and $r_\beta = 25 \pm 1.0$ μm, as well as TiAlN coated inserts with $r_\beta = 10 \pm 0.7$ μm were researched. It can be seen from Fig. 21 that larger cutting tool edge radius caused a higher hardness profile into the depth from the machined surface at both cutting speeds. Among the uncoated cutting tools with three different edge radii, the cutting tool with sharp edge of $r_\beta = 5 \pm 0.5$ μm provided the lowest hardness profile into the depth of Inconel 100 alloy, while the cutting tool with cutting edge radius of $r_\beta = 25 \pm 1.0$ μm produced severe deformation field and the hardest subsurface. It has been demonstrated that the cutting tool with large edge radius is not suggested to be used in finished process during industrial applications where hardened machined surface layer is not demanded.

Another research of Arisoy and Özel [93] focused on the effects of cutting tool micro-geometry on the micro hardness profile of the machined surface for Ti6Al4V (Fig. 22). The green dashed line in Fig. 22 indicates the mean hardness of

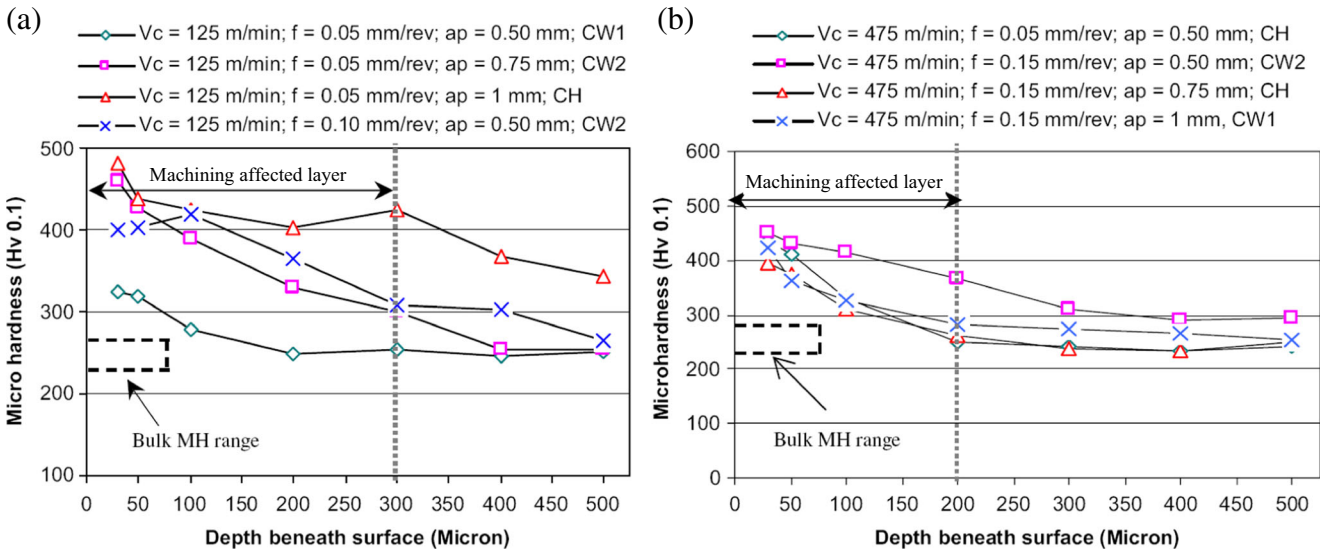

Fig. 20 Micro hardness profiles of machined subsurface for Inconel 718 obtained with different cutting edge geometries [79]

bulk material for Ti6Al4V. Unlike the results for machining of Inconel 100 with the same cutting tools, the machined surfaces were found to be softer than the bulk material due to the microstructural changes. The effects of tool edge radius on hardness profiles indicate that the largest tool edge radius for WC/Co tool with $r_\beta = 25 \pm 1.0$ μm generated the highest surface micro hardness. However, the machined surface hardness produced with the tool with $r_\beta = 10 \pm 0.7$ μm is the lowest, which was also different form the result of that for Inconel 100 as shown in Fig. 21. Increasing the feed rate results in increased machined hardness which can be attributed to the larger cutting forces loaded on the machined surface.

The effects of tool rake face texture on the micro hardness variation with depth below the machined surface for Ti6Al4V were revealed [111]. The different textures fabricated on the tool rake face have been introduced as shown in Fig. 11. It was found that the micro hardness of machining affected layer generated with non-textured tools was larger than those

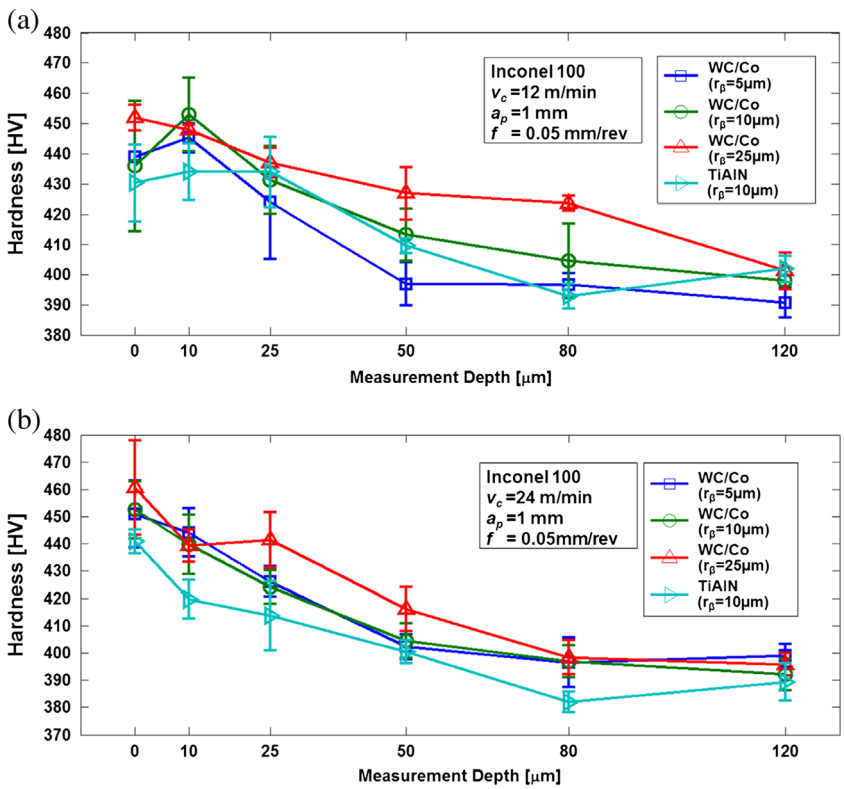

Fig. 21 Micro hardness profiles of machined subsurface for Inconel 100 generated using different cutting tools with varied cutting edge radii (**a**) $V_c = 12$ m/min; (**b**) $V_c = 24$ m/min (f = 0.05 mm/rev, $a_p = 1$ mm) [76]

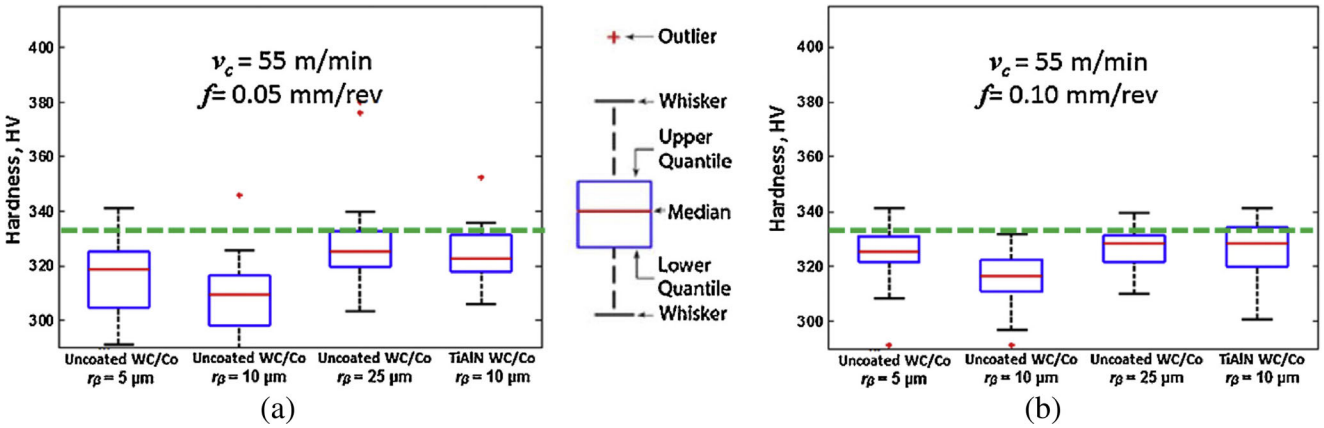

Fig. 22 Effects of cutting tool edge radius on micro hardness profile of the machined subsurface for Ti6Al4V (**a**) V_c = 55 m/min, f = 0.05 mm/rev; (**b**) V_c = 55 m/min, f = 0.10 mm/rev [93]

obtained with textured tools. The distribution and variation patterns for micro hardness of machined surface did not depend on the cutting speed and coating type. Comparatively, the micro hardness of machining affected layer obtained with PE.T tool is the most approached to the micro hardness of bulk material. Combined the geometrical characteristics and mechanical properties of machined surface, the PE.T tool presented the best cutting performance for Ti6Al4V, which generated the best surface quality evolving the lowest surface roughness and the slightest hardened surface layer.

Table 1 provides a check list and summary of the important studies dealt with the effects of tool structures on machined surface integrity during machining of titanium and nickel alloys reviewed in this paper.

6 Influence of tool material on machined surface integrity

6.1 Influence of tool material on geometrical characteristics of machined surface

As the same with cutting tool structure, varied cutting tool materials also generate different machined surface integrity due to different interaction between the tool and workpiece. Under different cutting parameters, the influence of cutting tool material on machined surface integrity also changes.

The research of Ezugwu and Tang [99] found that machining of Inconel 718 with the mixed-oxide ceramic tools generally produced better surface finish than with the pure oxide ceramics because of their improved hot hardness, fracture toughness and wear resistance. Tanaka et al. [126] attempted to optimize the material structures of PCBN to improve the cutting performance and prolong the cutting tool life during machining of nickel alloys. They suggested that a low CBN content with TiN-based ceramic binder exhibited excellent wear resistance in high speed machining of Inconel 718. Akhtar et al. [127] investigated the effects of cutting tool material on machined surface integrity of Inconel 718 during face milling process, in which two kinds of cutting tools of TiAlN coated cemented carbide inserts and SiC whisker-reinforced coated ceramic inserts were used. The surface roughness generated with the two different tools was researched. Considering the high hardness and high strength for ceramic material, the ceramic inserts can be used under much higher cutting speeds that those used for cemented carbide inserts. However, the high brittleness for ceramic inserts generated worse surface roughness than the cemented carbide ones. So the ceramic inserts are recommended to be used in rough and semi finish machining of Inconel 718 with high machining efficiency, while the TiAlN coated cemented carbide inserts are recommended to be used in finishing process with high machining quality. The comparison of machined surface morphology obtained with cemented carbide and ceramic inserts have demonstrated this conclusion further [127]. The ceramic insert generated a poor surface finish due to adherence of material debris while the coated cemented carbide insert generated a better surface finish.

Generally, coating tools are used to improve the cutting performance and modify the machined surface roughness during machining of titanium and nickel alloys, because the coating are always used to improve either edge preparation prior to coating or alternation of edge radius with deposition process [7]. The roles of coating materials, coating layer number (i.e. single, bilayer or multilayer configuration) or coating technique (PVD or CVD) could be researched by maintaining the identical geometry of cutting edge. In order to improve the cutting performance and prolong the tool life during machining of titanium and nickel alloys, Biksa et al. [128] attempted the application of nano-multilayered AlTiN/Me_xN PVD coatings (where Me_x is a transition metal of V-VI groups of periodic table) on cemented carbide tools. Such coated cemented carbide tools have the advantage of noticeably lower friction coefficient at elevated temperatures during machining process.

Table 1 Summary of cutting tool structure on machined surface integrity of titanium and nickel alloys

Reference	Workpiece material	Tool structure	Cutting parameters	Remarks
Ezugwu and Tang [99]	Inconel 718	Turning, round and rhomboid-shaped ceramic tools	$V_c = 152$ m/min $f = 0.125$ mm/rev $a_p = 2$ mm	Round inserts produced a better surface finish.
Arunachalam et al. [20, 96]	Inconel 718	Turning, varied insert shape, cutting edge preparation and nose radius	$V_c = 60$ m/min $f = 0.1$ mm/rev $a_p = 0.5$ mm	Insert with round shape, honed cutting edge, negative type and large nose radius decreased surface roughness.
Zhang and Liu [81]	Applicable for different materials	Turning, wiper and conventional inserts	Applicable for varied parameters	Wiper insert can decrease the surface roughness.
Ulutan and Özel [103]	Ti6Al4V	Turning, varied cutting edge geometry	$V_c = 50$, 100 m/min $f = 0.1$, 0.2 mm/rev $a_p = 2$ mm	Cutting force was lowed and generated better surface quality.
Yang and Liu [108]	Ti6Al4V	Milling, end milling tool with varied helix angles (38° and 41°)	$V_c = 20$–110 m/min $f = 0.02$ mm/rev $a_e = 0.5$–2.0 mm	Varied helix angles decreased the surface defects.
Arulkirubakaran and Senthilkumar [111]	Ti6Al4V	Turning, cutting inserts with textured patterns on rake face	$V_c = 60$, 90, 120 m/min $f = 0.1$ mm/rev $a_p = 0.5$ mm	Textures on tool rake face decreased machined surface roughness, produced lower micro hardness of machining affected layer.
Jafarian et al. [116]	Inconel 718	Orthogonal cutting, tools with honed edge and chamfer angle	$V_c = 60$ m/min $f = 0.05$, 0.075, 0.1 mm/rev	Both chamfer angle and honed edge increased surface hardness while decreased surface grain size. Machining affected layer depth was more sensitive to the tool edge type.
Arisoy et al. [76]	Inconel 100	Turning, varied cutting edge radii of 5 μm, 10 μm and 25 μm	$V_c = 12$, 24 m/min $f = 0.05$ mm/rev $a_p = 1$ mm	Size of grains and precipitates depended on the cutting edge radius. Larger cutting tool edge radius caused a higher hardness profile into the depth from surface.
Arisoy and Özel [93]	Ti6Al4V	Turning, varied cutting edge radii of 5 μm, 10 μm and 25 μm	$V_c = 55$, 90 m/min $f = 0.05$, 0.1 mm/rev $a_p = 2$ mm	Effects of cutting edge micro geometries on surface grain size varied with cutting parameters. Largest tool edge radius generated the highest surface micro hardness.
Sharman et al. [117]	Inconel 718	Turning, varied tool nose radii of 2–6 mm	$V_c = 40$ m/min $f = 0.25$–0.5 mm/rev $a_p = 0.25$ mm	Larger tool nose radius produced larger plastic deformation depth and deeper residual stress.
Yang and Liu [118]	Ti6Al4V	Milling, end milling tools with varied helix angles of 38° and 41°	$V_c = 20$–110 m/min $f = 0.02$–0.05 mm/rev $a_e = 0.5$–2.0 mm	End milling tools with varied helix angles generated better surface quality and slighter microstructure alteration.
Coelho et al. [97]	Inconel 718	Turning, tool cutting edge with commercial and modified chamfer	$V_c = 70$, 500 m/min $f = 0.1$ mm/rev $a_p = 0.35$ mm	Compressive residual stresses were increased using the cutting tool with modified chamfer.
Pawade et al. [79]	Inconel 718	Turning, insets with different cutting edge geometries including chamfer and honed edges	$V_c = 125$, 300, 475 m/min $f = 0.05$, 0.10, 0.15 mm/rev $a_p = 0.50$, 0.75, 1.0 mm	Insert with chamfer plus honed edge produced the largest micro hardness and yield strength profiles of machined subsurface.
Abboud et al. [125]	Ti6Al4V and Ti-6246	Turning, varied tool nose radii of 0.2–1.6 mm	$V_c = 20$–90 m/min $f = 0.05$–0.25 mm/rev $a_p = 0.1$–0.3 mm	Tool nose radius range suitable to generate compressive residual stress was proposed.

They recommended nano-multilayered AlTiN/MoN coated cemented carbide tools for machining of Inconel 718 and AlTiN/VN coated cemented carbide tools for machining of Ti6Al4V. Nalbant et al. [98] investigated the effects of coating material and coating layer number on the machined surface roughness of Inconel 718 using CVD quadruple (top layer is TiN), triple (top layer is Al_2O_3) and single (TiN) coated cemented carbide inserts. Their results showed that the average surface roughness generated with single layer (TiN) coated cemented carbide inserts was much smaller than those generated with multicoated Al_2O_3 and TiN inserts. The coating layer number and coating material have significantly effects on the average surface roughness of Inconel 718. Liu et al. [129] performed the turning experiments of Inconel 718 under the same cutting parameters with uncoated and TiCN coated Sialon ceramic inserts prepared by PVD technique. It was revealed that the cutting performance of Sialon ceramic cutting inserts was improved remarkably through treatment of TiCN coating on the inserts for machining of nickel alloys, which could improve machined surface quality consequently. Although the dominant failure mechanisms of the coated and uncoated inserts are all abrasive and adhesive wear, the wear rate of coated insert is much lower than that of the uncoated insert.

The comparison of cutting performance for CVD and PVD coated cutting tools and corresponding finished surface quality have also been researched. Thakur et al. [130] compared the cutting performance of multicoated TiN/TiAlN (PVD) coated and TiN/Al_2O_3/TiCN (CVD) coated tungsten carbide tools during high speed turning of Inconel 718. The effect of coating materials on cutting force, cutting temperature, vibration, and acoustic emission was recorded, analyzed, and reported. Their results illustrated that TiN/Al_2O_3/TiCN (CVD) coated tool outperformed the TiN/TiAlN (PVD) coated tool in terms of machinability parameters such as cutting force and cutting temperature. In result, better finished surface for Inconel 718 is expected to be produced with the former one than the latter one.

Besides the cutting inserts, the effect of cutting tool materials on machined surface integrity for solid milling tools has also attracted wide attention. Ucun et al. [131] investigated the effect of coating material on tool wear and machined surface quality during micro milling of Inconel 718 with coated and uncoated WC-Co micro milling tools under dry and lubricated conditions. It was found that the cutting tools coated with AlTiN, TiAlN+AlCrN, and AlCrN exhibited better cutting performances compared to those coated with TiAlN+WC/C and DLC.

However, different observation and different conclusion has also been reported for the effect of tool coatings on surface roughness of titanium or nickel alloys [132]. The variation of machined surface roughness for Inconel 718 generated with TiN coated and uncoated PCBN tools were investigated [133, 134]. The results as shown in Fig. 23(a) illustrated that TiN coated PCBN tool resulted in poor surface finish than its uncoated one. The comparison of machined surface morphology generated with coated and uncoated inserts indicated that the built-up edge formation on machined surface for coated CBN tool was much severer than that for uncoated one. It was explained by rougher surface morphology of the coating tool associated with larger cutting edge radius compared to the uncoated tool.

Similar observation was also noted by other research [135] which studied machined surface roughness of Inconel 825 using uncoated cemented carbide and CVD multilayer coated (TiN/TiCN/Al_2O_3/ZrCN) inserts as illustrated in Fig. 23(b). It can be seen from Fig. 23(b) that the CVD multilayer coated tool resulted in deterioration in surface finish compared to the uncoated insert under entire investigated cutting speed range.

In addition to the surface roughness, the surface defects generated on the machined surface of Inconel 825 which is another important geometrical index to characterize the surface integrity were investigated [136]. Such surface defects of smeared materials, feed marks, debris and re-deposited material were observed on the machined surface (Fig. 24). It was further noted that the coated (TiN/TiCN/Al_2O_3/ZrCN) tool could not improve machined surface morphology with the presence of debris and re-deposited material, which might be attributed to the lower thermal conductivity of Al_2O_3 coating. It results in higher temperature rise on the machined surface compared to that produced using uncoated cemented carbide insert. Consequently, the high temperature is apt to induce plastic flow of workpiece material and easy adhesion of chip fragments on machined surface [137, 138].

As one of the most widely used nickel alloys, the surface defects of Inconel 718 induced during machining process have been researched extensively. Fig. 25 presents different surface defects induced during machining of Inconel 718 with different tool materials. With the cemented carbide tools, the machined surface defects mainly include surface tearing and cracked carbide, which are usually caused by large cutting force [12, 139, 140]. Comparatively, the surface defects induced by CBN tools mainly include material smearing, feed marks and metal debris, which are usually caused by high cutting temperature leading to severe plastic deformation and material adhesion [137, 139].

The burr formation during micro machining is one of the main geometrical characteristics for the machined quality. Through micro milling operation on nickel alloy of Nimonic 75 using uncoated and TiAlN coated tungsten carbide micro end mills, the effects of cutting tool material on burr formation were researched [141]. Figure 26 shows the slot morphologies obtained at a cutting length of 30 mm and 300 mm using uncoated and TiAlN coated micro tools. It can be seen that much larger top burr occurred after machining with uncoated micro end milling tools compared to those obtained with TiAlN coated tools. It is explained that the increase in tool wear resistance for TiAlN coated micro-tool leads to the

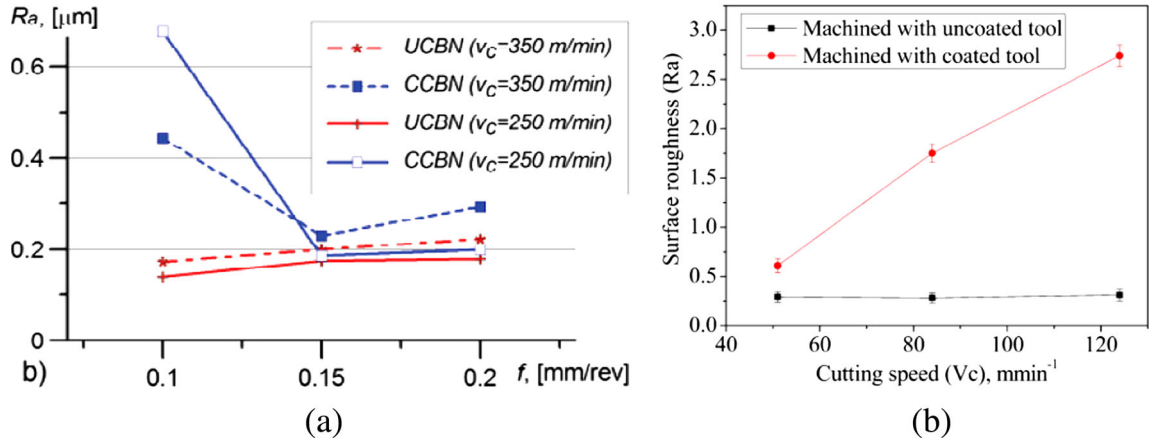

Fig. 23 Comparison of machined surface roughness generated with different cutting tool materials (**a**) workpiece material: Inconel 718, coated and uncoated PCBN inserts, $V_c = 250$, 350 m/min, $a_p = 0.3$ mm [133]; (**b**) workpiece material: Inconel 825, coated and uncoated cemented carbide inserts, $f = 0.198$ mm/rev, $a_p = 1$ mm [135]

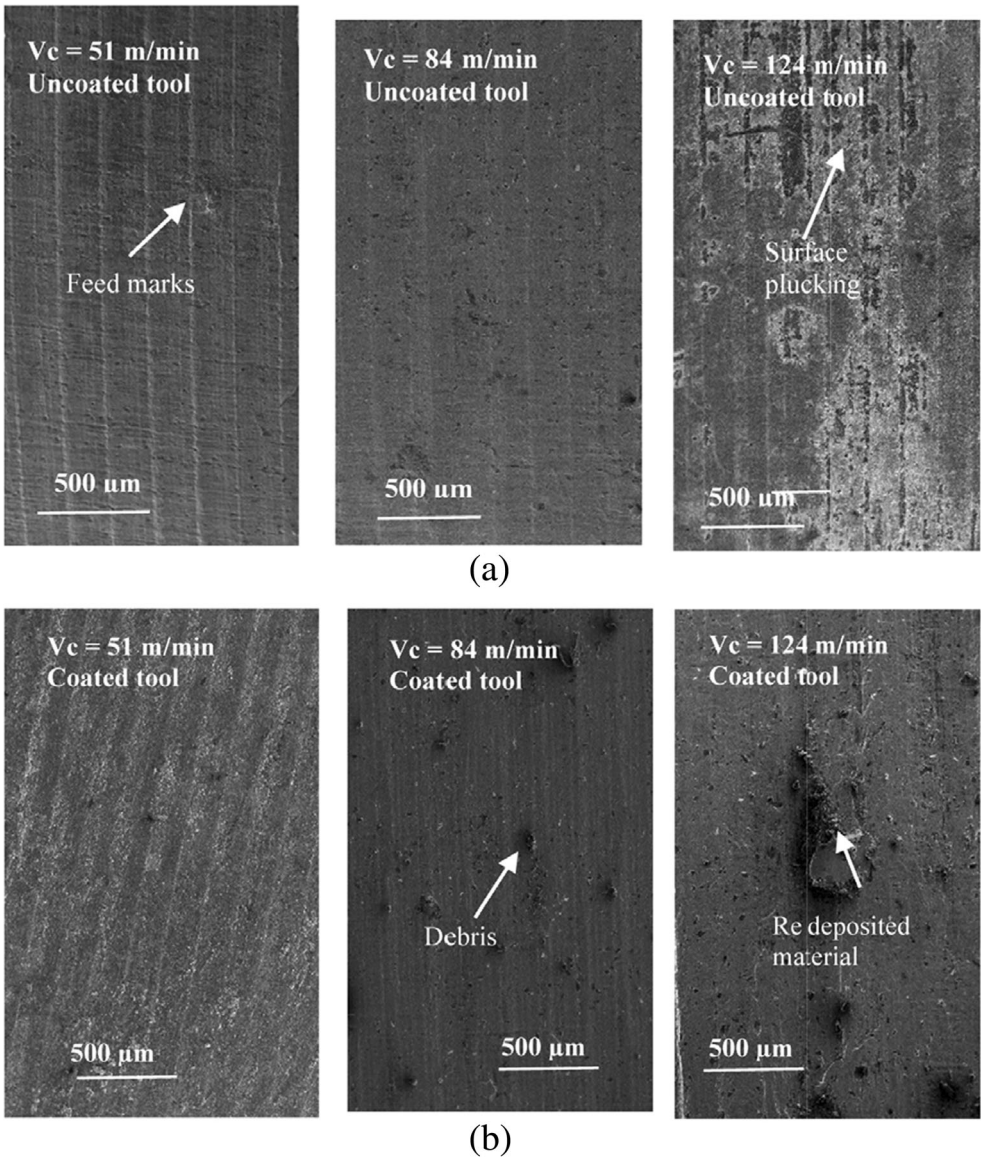

Fig. 24 SEM images of surface defects on machined surface of Inconel 825 generated with uncoated and multilayer coated ($TiN/TiCN/Al_2O_3/ZrCN$) inserts [136]

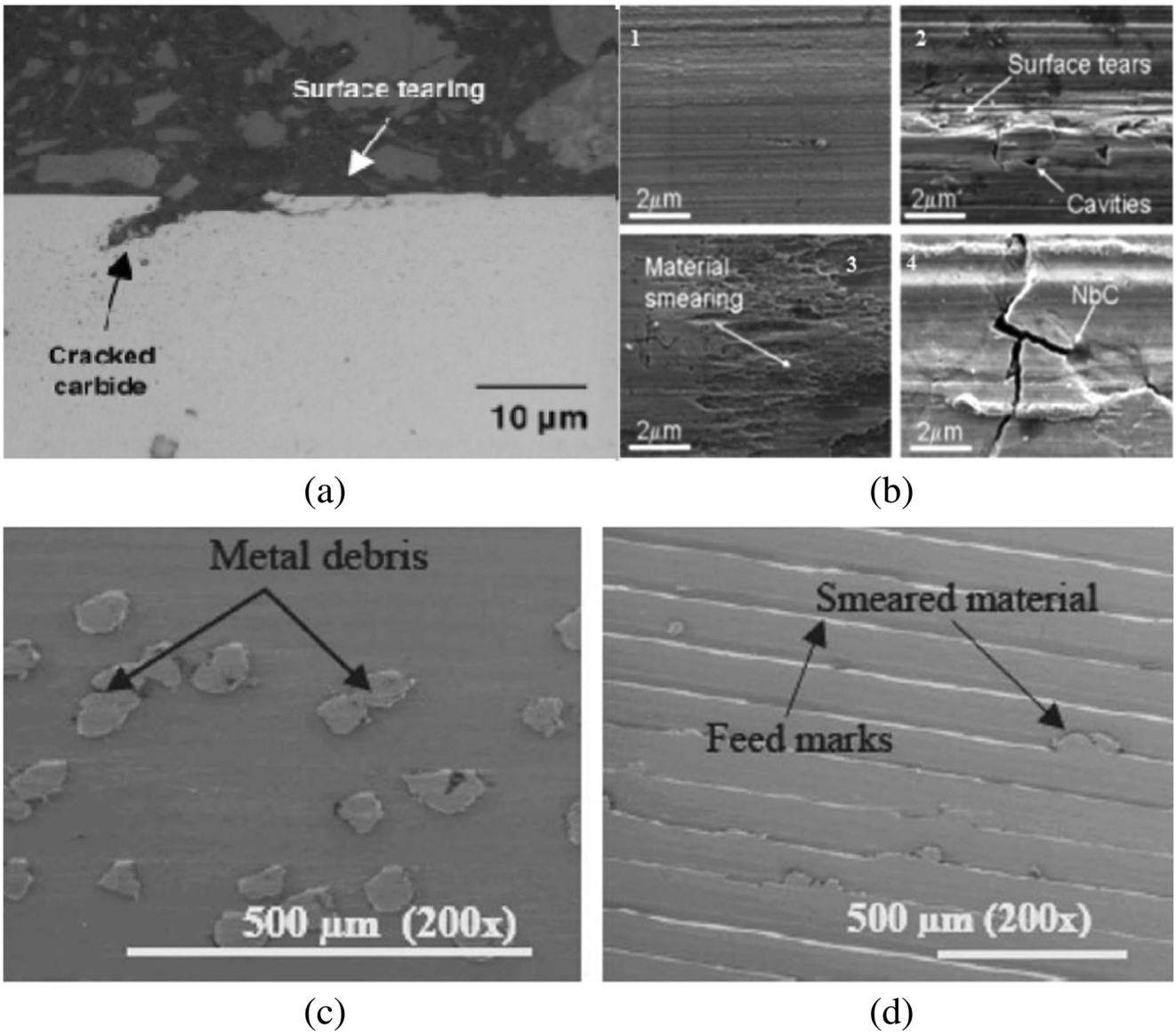

Fig. 25 Surface defects induced during machining of Inconel 718 (**a**) cracked carbide and surface tearing, WC tool [12]; (**b**) $f = 0.15$ mm/rev and $a_p = 0.25$ mm (1) $V_c = 90$ m/min, WC tool, (2) $V_c = 90$ m/min, WC tool, (3) $V_c = 300$ m/min, CBN tool, (4) $V_c = 300$ m/min, CBN tool [139]; (**c**) metal debris formed at $V_c = 125$ m/min, $f = 0.05$ mm/rev, and $a_p = 0.5$ mm, PCBN tool [137]; (**d**) smeared material and feed marks formed at $V_c = 125$ m/min, $f = 0.1$ mm/rev, and $a_p = 0.75$ mm, PCBN tool [137]

alleviation of burr formation especially under longer cutting length. Through comparison of machined surface roughness generated with both uncoated and coated tools, Swain et al. [141] found that the surface roughness generated with TiAlN coated micro end milling tools was also lower than that obtained with uncoated ones, which was in agreement with the variation of burr formation formed using different tools.

6.2 Influence of tool material on microstructure alterations of machined surface

Machining affected layer always exhibits different microstructure from the interior of the bulk workpiece material, which is caused by thermomechanical processing on the machined surface during machining process. The cutting tool material is also an essential factor affecting the plastic deformation within the machined subsurface, so different cutting tool materials output varied microstructure alterations after machining.

The microstructural difference of the subsurface layers for Inconel 718 generated with PCBN and whisker-reinforced ceramic (Al_2O_3-SiC_w) cutting tools were presented at cutting speeds of 200 m/min and 350 m/min, and a constant feed rate of 0.1 mm/rev and depth of cut of 0.3 mm [142]. The microstructure alterations of grain bending, deformation twin bands and slip bands were observed for all machined surfaces obtained with both tools (Fig. 27), and the microstructure alterations

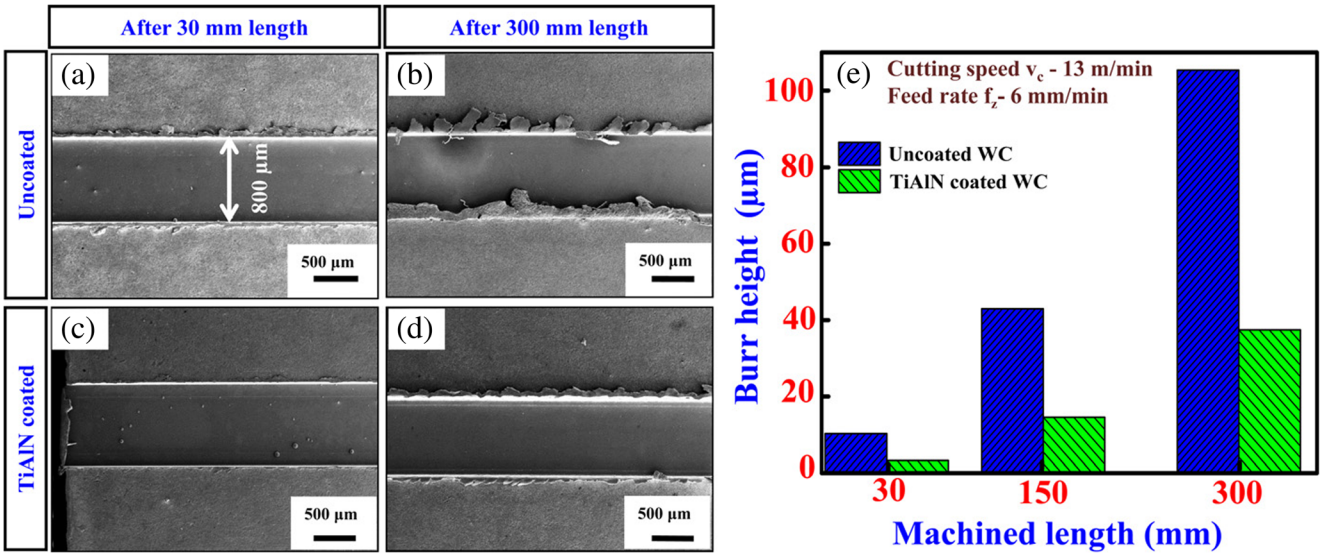

Fig. 26 Morphologies of burr formation generated with (**a**), (**b**) uncoated and (**c**), (**d**) TiAlN coated micro end milling tools after machining lengths of 30 mm and 300 mm; (**e**) variation of burr height with machining length [141]

were more distinguishable under higher cutting speed. It can be seen from Fig. 27 that severer and deeper plastic deformation within machining affected layer was generated with ceramic tools (Fig. 27a, b) than that generated with PCBN tools (Fig. 27c, d), which is associated with higher cutting temperature for ceramic tools due to their poor thermal conductivity. Nevertheless, the nano-crystalline microstructure within the near surface layer has no significant difference between the ceramic and PCBN tools, which suggests that the cutting tool material has little effect on the formation of nano-structured layer for Inconel 718.

The surface deformation and microstructure alteration during longitudinal turning of Inconel 718 with uncoated and coated PCBN inserts exhibit the influences of tool material

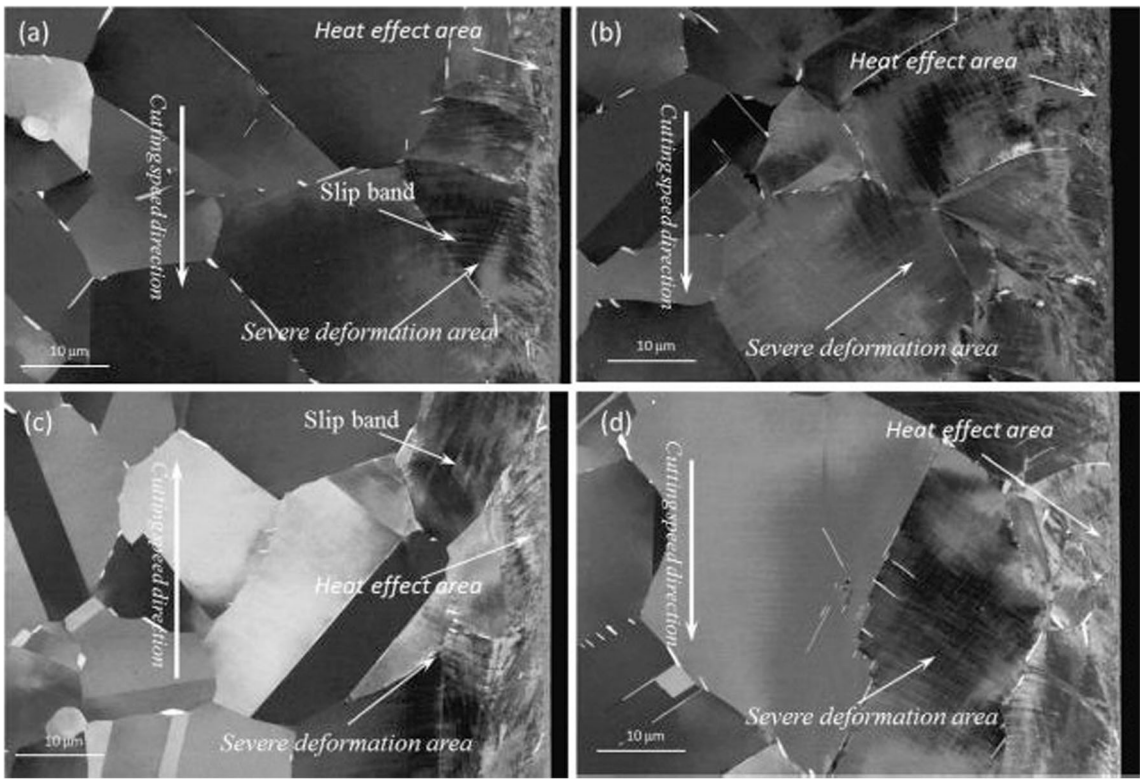

Fig. 27 Morphology of microstructure alterations in the machined subsurface for Inconel 718 generated with (**a**, **b**) an Al_2O_3-SiCw cutting tool and (**c**, **d**) a PCBN cutting tool [142]

on nickel alloy machining [133]. Significant bending and elongation of grain boundaries and slip lines in the direction of cutting were found within the machining affected layer. The authors also indicated that the application of coated PCBN tools resulted in more severe grain elongation, which was explained by the increase of the cutting temperature within the deformation zone due to the insulation effect of the coating. In addition, the effect of larger cutting edge radius of the coated tools also contributed to enhanced plowing effect and severer material plastic deformation on machined surface.

After the workpiece is machined, the subsurface usually exhibits different behavior from the bulk material. Sometimes the microstructure alteration of machining affected layer causes it to be harder than the bulk workpiece material and appear as white under optical or scanning electron microscope (SEM). Then this layer is usually called as the "white layer" [143, 144]. The effects of uncoated and TiN/TiCN/Al_2O_3/ZrCN coated cemented carbide inserts on the white layer formation of machined surface for Inconel 825 have been focused on [136]. Figure 28 shows the SEM images of machined subsurface produced with uncoated and TiN/TiCN/Al_2O_3/ZrCN coated cemented carbide inserts under different cutting speeds. It can be seen that the white layer occurred under all investigated cutting parameters for both two kinds of inserts. The results clearly demonstrated that the white layer thickness formed by uncoated insert was larger than the coated insert particularly at the cutting speeds of 54 m/min and 84 m/min. This phenomenon was attributed to the reason that Al_2O_3 having low thermal conductivity and other coating materials like TiN, TiCN and ZrCN possessing excellent anti friction properties, which could reduce the formation of thermally affected layer and decrease the white layer thickness.

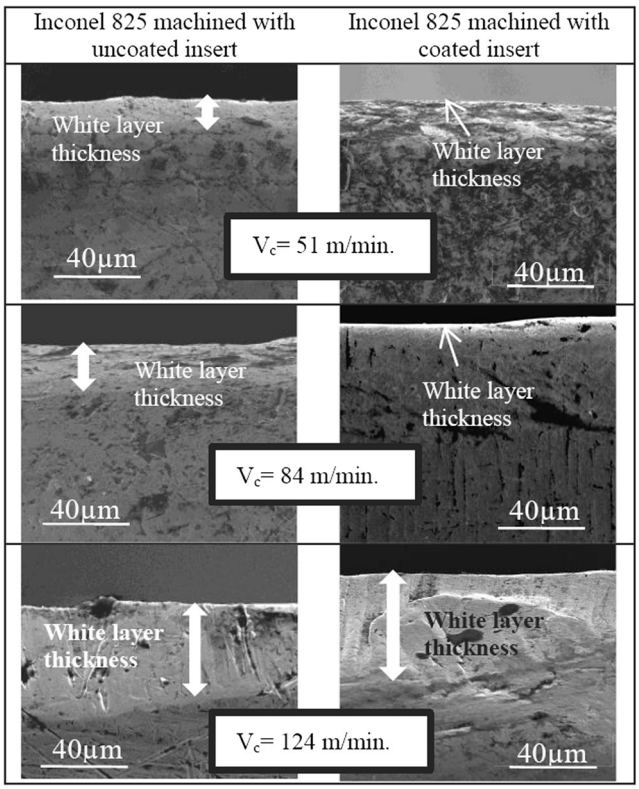

Fig. 28 SEM images for machined subsurface of Inconel 825 formed with coated and uncoated cemented carbide inserts under different cutting speeds [136]

The effect of multilayer coating (TiN/TiCN/Al_2O_3/ZrCN) on micro-morphology of the machined surface for Inconel 825 was also researched [136]. Dynamic recrystallization was seen on the machined surface at V_c = 124 m/min, f = 0.198 mm/rev and a_p = 1 mm after machining of Inconel 825 as shown in Fig. 29. It can be seen that the machined surface generated with uncoated insert exhibited formation of new undeformed recrystallized grains due to high cutting temperature, while the machined surface generated with coated insert just exhibited the pre stage of grain growth due to absence of high cutting temperature which was required for grain growth (Fig. 29b).

The research on the effects of TiAlN coating on microstructure evolution of machined surface for Inconel 100 indicated that the machined surface formed using TiAlN coated tool possessed smaller primary γ' grains and larger secondary γ' grains, which contributed to the lower hardness alteration for the machined surface [76]. Meanwhile, Arisoy and Özel [93] investigated the effect of TiAlN coating on microstructure evolution of machined surface for Ti6Al4V as shown in Fig. 30. It was indicated that the average grain size on the machined surface induced by TiAlN coated WC/Co tool was larger than that induced by uncoated tool, which was attributed to the thermal restriction of the coated tool resulting in less grain growth.

6.3 Influence of tool material on mechanical properties of machined surface

Variation of tool material also plays an important role on mechanical properties of machined surface for titanium and nickel alloys. The physical and mechanical properties of cutting tool materials, especially the thermal conductivity of cutting tool, are important factors to determine the residual stress distribution within the machining affected layer. Generally, the cutting tool materials with lower thermal conductivity tend to cause more tensile residual stress due to the dominance of thermal influence [96, 97, 142]. In addition, the different thermal and mechanical stresses caused by different tool materials also affect the micro hardness distribution and the plastic deformation depth. Due to this fact, mixed alumina ceramic insert is prone to cause higher tensile stress than PCBN tools during machining of Inconel 718 [96, 97, 142], because more compressive residual stress on machined surface tend to be produced with PCBN tool due to its higher thermal conductivity responsible for effective dissipation of heat from the cutting zone [142]. Similar conclusions for generation of higher surface tensile stress have also been reported with tools

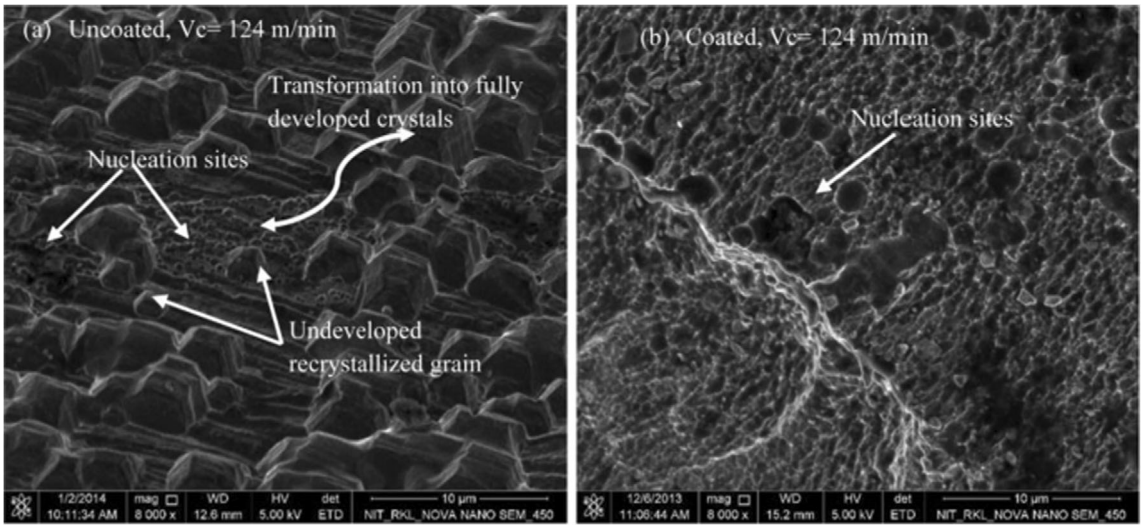

Fig. 29 SEM images of micro-morphology of machined surface for Inconel 825 formed with (**a**) uncoated insert and (**b**) coated insert at $V_c = 124$ m/min, $f = 0.198$ mm/rev, $a_p = 1$ mm [136]

having lower thermal conductivity coating materials [82, 133]. Surface tensile residual stress and micro hardness can also be decreased through lowering friction between the tool-chip and the tool-workpiece interfaces.

The research of Akhtar et al. [127] indicated that the ceramic inserts produced very high tensile residual stresses on the machined surface of Inconel 718, while the carbide inserts generated mostly compressive surface residual stresses and comparable surface micro hardness. It can thus be concluded that carbide inserts generated much better surface physical properties compared to the ceramic inserts in finish machining of Inconel 718.

Figure 31 presents the influences of PCBN and whisker-reinforced ceramic (Al_2O_3-SiC_w) cutting tools on the in-depth residual stresses within machined subsurface of Inconel 718 [142]. The results indicated that much higher tensile residual stresses were generated by whisker reinforced ceramic tools than PCBN tools, which was attributed to the dominant thermal effect during machining and the poor thermal conductivity of whisker-reinforced ceramic inserts [142]. The surface residual stresses generated by PCBN tools are more compressive, which are demanded to be achieved to improve the mechanical property of machined surface and the working performance of components.

Different tool materials of uncoated and TiN coated PCBN tools were used in another literature to investigate the difference of in-depth residual stress of Inconel 718 generated (Fig. 32) [133]. The results suggested that the surface residual stresses caused by TiN coated PCBN tools were more tensile than those caused by uncoated PCBN tools, which was attributed to the lower thermal conductivity of coated PCBN tools and high thermally-related contribution to the residual stress formation. Furthermore, the depth of residual stress profile for coated PCBN tools (about 120 μm) was larger than that for uncoated PCBN tools (about 100 μm). Similar results were obtained in the research of Sharman et al. [145] on surface residual stress generation of Inconel 718 as shown in Fig. 33. It was indicated in Fig. 10 that the residual stress profiles for machined surface of Inconel 718 were more tensile for TiCN/Al_2O_3/TiN coated WC Tool than uncoated WC tool. Compared with Figs. 32 and 33, it can be seen that the surface residual stresses of Inconel 718 generated with PCBN tools are much more compressive than those generated with WC tools, regardless of the tools are coated or not.

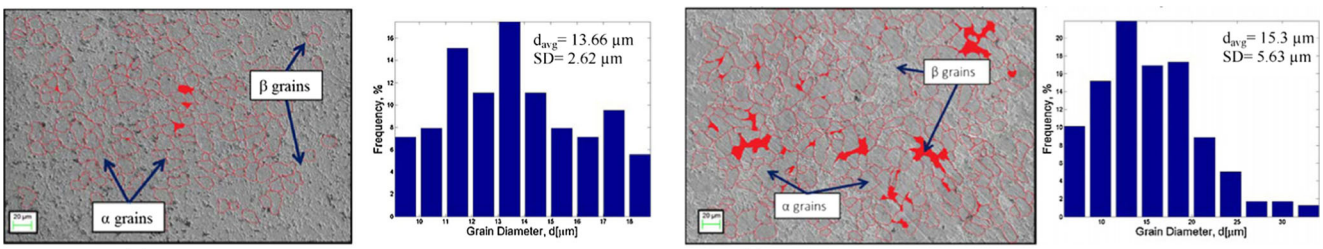

(a) WC/Co tool (r_β=10 μm), v_c=90 m/min, f=0.10mm/rev (b) TiAlN coated WC/Co tool (r_β=10 μm), v_c=90 m/min, f=0.10mm/rev

Fig. 30 SEM images and grain size distributions of machined surface for Ti6Al4V generated under $V_c = 90$ m/min and $f = 0.05$ mm/rev with (**a**) uncoated WC/Co tool; (**b**) TiAlN coated WC/Co tool [93]

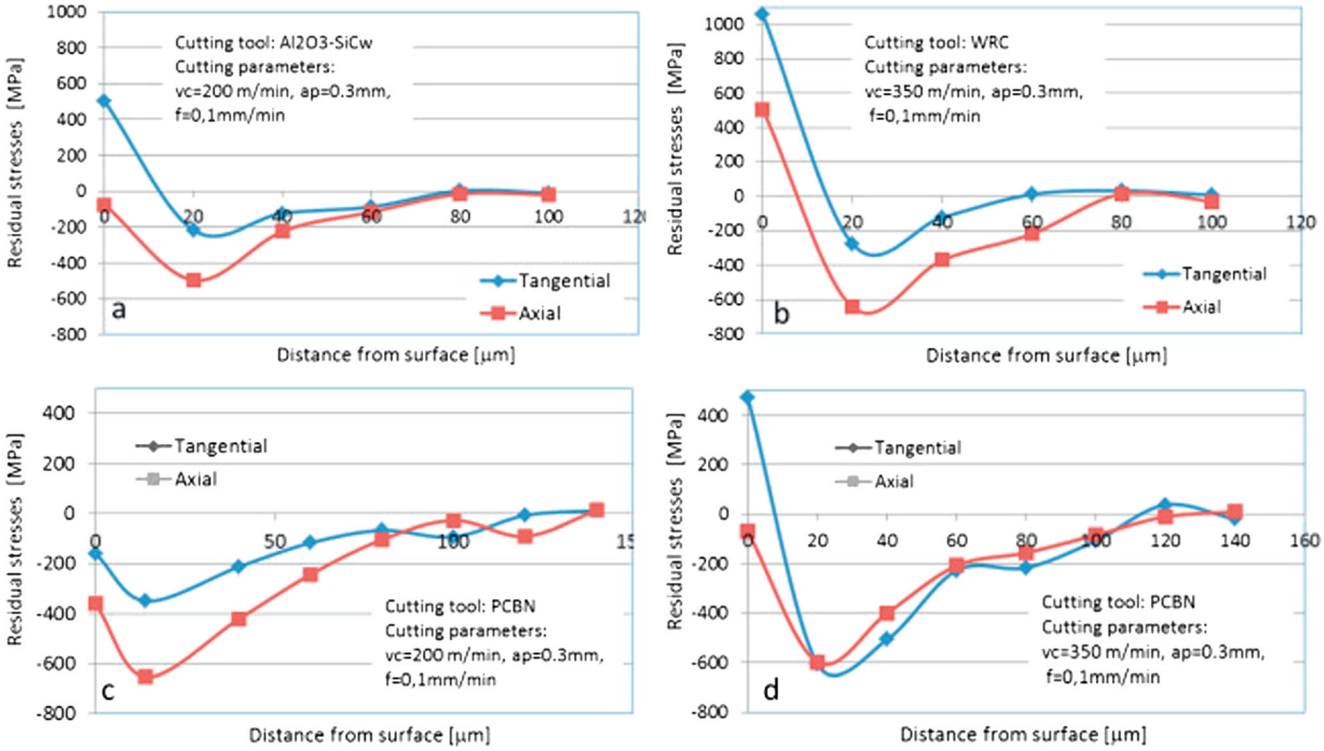

Fig. 31 In-depth residual stress profiles in machined subsurface of Inconel 718 generated with (**a**), (**b**) Al_2O_3-SiC_w cutting tools and (**c**), (**d**) PCBN cutting tools, respectively [142]

However, the effect of tool coating on the residual stress distribution within machined subsurface for nickel alloys has some contradiction. Different observations were noted for the residual stresses generated with uncoated tools exhibiting higher tensile stresses than those generated with coated tools during machining of Inconel 718 [146] and Inconel 100 [147].

Moreover, another research investigated the influence of tool coating on machined surface integrity during dry turning of Inconel 718 with PVD coated (TiAlN coating with 2 μm in thickness) and uncoated carbide tools [146]. Profiles of in-depth residual stresses along the cutting direction ($\sigma_{//}$) and the feed direction ($\sigma_{\perp}$) induced by machining with coated and uncoated cutting tools are presented in Fig. 34. It can be seen that the residual stresses caused by coated tools have several different characteristics compared with those caused by uncoated tools including: (i) lower surface ($\sigma_{//}$ and $\sigma_{\perp}$) residual stresses; (ii) deeper tensile stress layer; and (iii) higher maximum residual stresses within subsurface and the maximum value being shifted closer to the surface. Similar results were obtained in the research of Ulutan and Özel [147] on surface residual stress generation of Inconel 100 as shown in Fig. 35. Although the coating materials used in different researches were different, the contradiction of residual stress generation could be attributed to either the difference in properties of tool coating and workpiece materials, or difference in the machining conditions.

In-depth variation of micro hardness with distance from the machined surface for Inconel 825 under different cutting speeds (51, 84 and 124 m/min) were investigated using

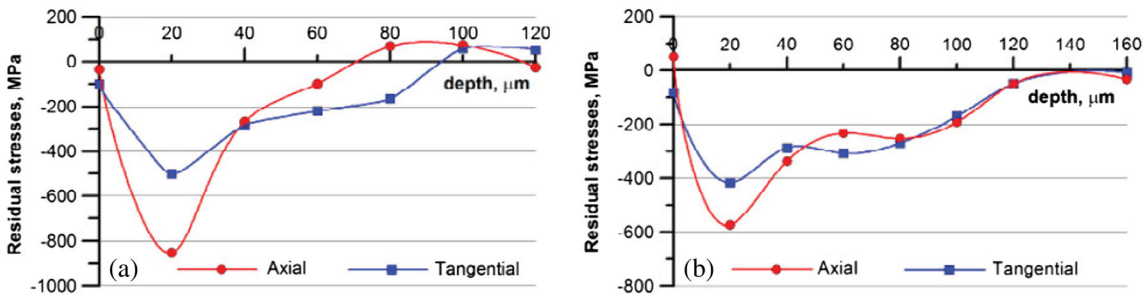

Fig. 32 In-depth residual stress profiles for machined subsurface of Inconel 718 generated with (**a**) uncoated and (**b**) TiN coated PCBN tools (V_c = 300 m/min, f = 0.1 mm/rev, new tool) [133]

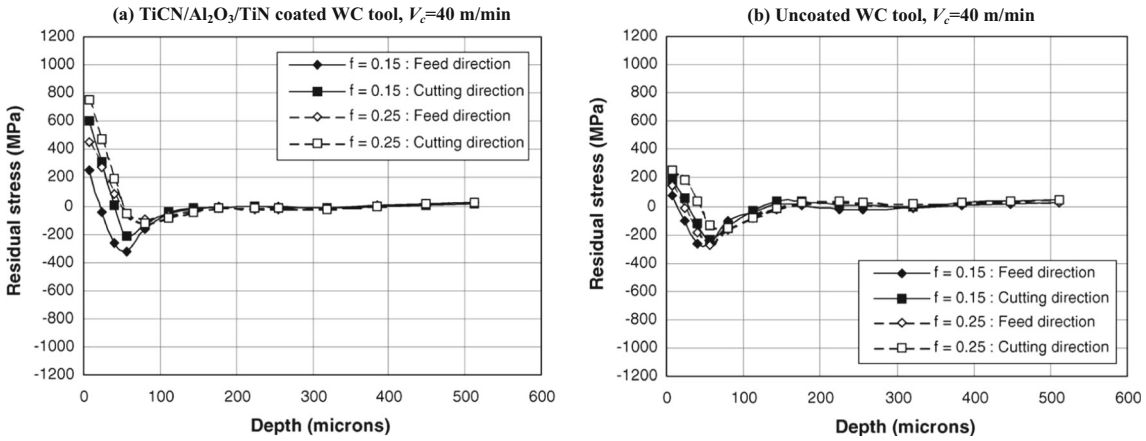

Fig. 33 In-depth residual stress profiles for machined subsurface of Inconel 718 generated with (**a**) TiCN/Al_2O_3/TiN coated WC and (**b**) uncoated WC tools [145]

uncoated and coated carbide inserts (Fig. 36) [136]. It was indicated that an overall decrease for the micro hardness from machined surface to the bulk material occurred, which was attributed to the variation in the grain or crystallite size within machining affected layer. SEM images of the microstructure as shown in Fig. 36 obtained at two different depths demonstrate the increase in grain size with the depth from the machined surface increasing. The variation of micro hardness in machining affected layer generated with uncoated and CVD multilayer coated tools could be attributed to the difference in the friction co-efficient between the tool and workpiece. Low friction co-efficient of coated tool results in lower tool wear rate, which then leads to the alleviation of both thermally and mechanically induced plastic deformation and lower micro hardness of the machined surface compared to the uncoated tool.

Table 2 provides a check list and summary of the important studies dealt with the effects of tool materials on machined surface integrity during machining of titanium and nickel alloys reviewed in this paper.

7 Influence of tool wear on machined surface integrity

Tool wear has significant influence on the machined surface integrity during machining process, especially for the machining of difficult-to-machine materials including titanium and nickel alloys, which is accompanied with sever tool wear [148–150]. Tool wear induces alteration of machined surface integrity through changing cutting edge geometry or tool coating detachment (for coated tools). Tool flank wear (denoted by *VB*) has more prominent influence on machined surface due to their direct contact, and it is always regarded as the tool wear criterion [151, 152]. Although excessive tool wear rate is not demanded in machining process, the effects of tool wear on machined surface quality are not always detrimental. Research on the influence of tool wear on machined surface integrity can help to instruct selection of appropriate cutting tools and replacement of worn tools in time to guarantee the requirements of machined surface quality.

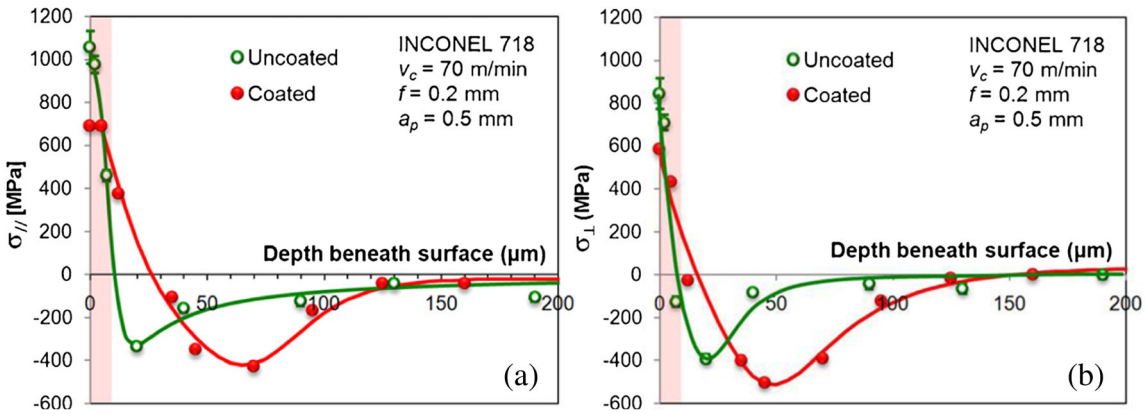

Fig. 34 In-depth residual stress distribution after machining of Inconel 718 with uncoated and coated tools (**a**) $\sigma_{//}$ in cutting direction; (**b**) $\sigma_{\perp}$ in feed direction [146]

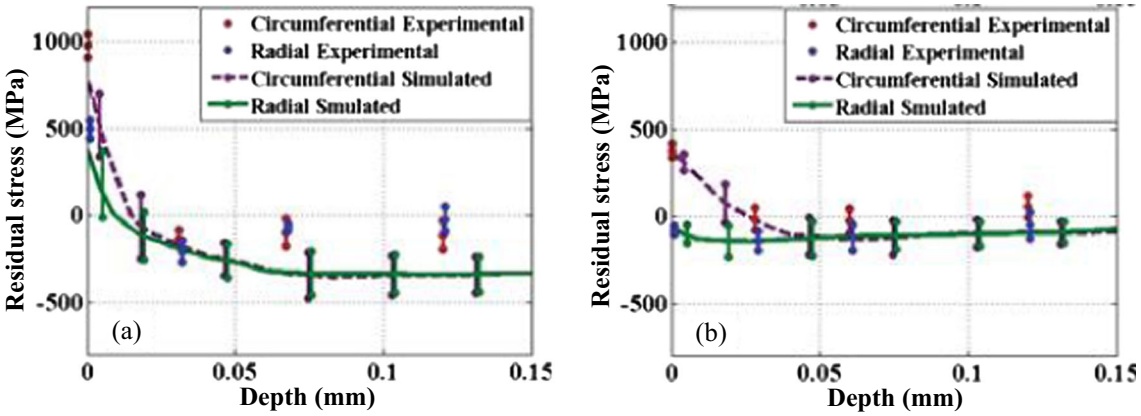

Fig. 35 Comparison of residual stresses after face turning of Inconel 100 at $V_c = 12$ m/min, $f = 0.05$ mm/rev and $a_p = 1$ mm with (**a**) WC/Co tool and (**b**) TiAlN coated WC/Co tool [147]

7.1 Influence of tool wear on geometrical characteristics of machined surface

Tool wear, especially the tool flank wear changes the cutting edge geometry, which influences the tool-workpiece contact behavior and the geometrical characteristics of machined surface.

During turning of Inconel 718 with TiCN/Al_2O_3/TiN coated WC insert, the machined surface roughness was found to be improved (as shown in Fig. 37) due to the location of wear scar on the tool flank face away from the trailing edge [153]. The relatively flat worn flank face played a similar role of "wiper" and removed the peaks of the feed marks. The difference of 3D surface roughness maps of Inconel 718 generated with the new and worn TiCN/Al_2O_3/TiN coated WC inserts has also been researched. The results indicated that the increasing of tool wear for TiCN/Al_2O_3/TiN coated WC insert resulted in decreasing of R_a values under investigated cutting parameters as shown in Fig. 37. However, the wear of uncoated WC insert resulted in increased surface roughness due to small notch occurring at the trailing edge, and other workers have also obtained similar results [99, 154]. It means that the influence of tool wear on machined surface roughness depends on the tool material and tool wear patterns [153].

Aspinwall et al. [155] performed the ball end milling experiments with TiAlCrN multi-layer coated carbide tools to investigate the influence of tool wear on machined surface roughness of Inconel 718 under different tool orientation/workpiece angles. It can be seen from Fig. 38 that lower surface roughness was generated with worn tools except in the case of horizontal upwards operation, of which the results were reversed. The formation of a "wiper flat" along the tool cutting edge in tool-workpiece interface is beneficial to improve the surface roughness. The abnormity for horizontal upwards machining was explained by the vibration/chatter occurring during tool engagement for the worn tools.

The influences of tool wear on machined surface roughness of titanium alloy have also been researched. The effect of tool flank wear on surface integrity during orthogonal dry cutting of Ti6Al4V using CVD Al_2O_3 coated carbide inserts with cutting edge radius of 10 μm was studied [152]. Figure 39 presents the 3D surface topographies of the machined surface

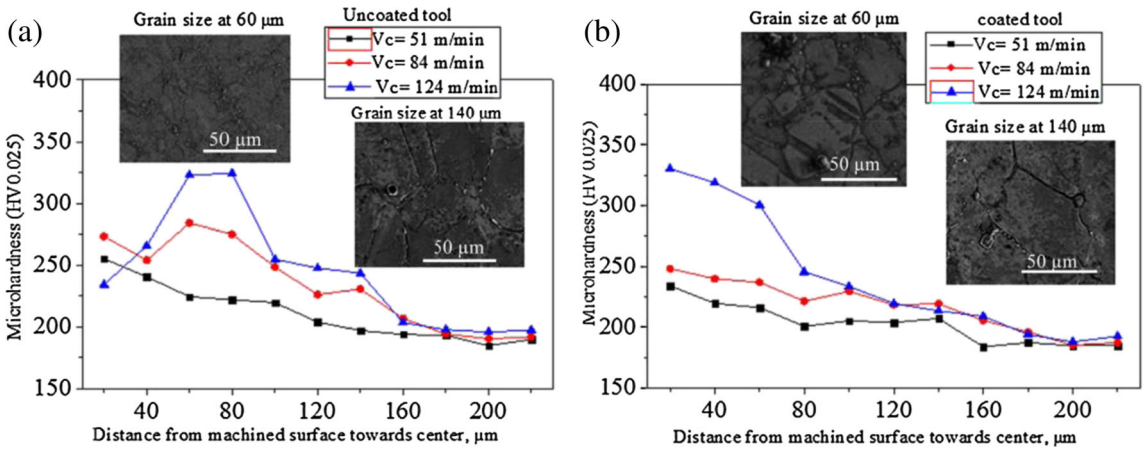

Fig. 36 Variation of micro hardness with distance from machined surface towards bulk material for Inconel 825 generated with (**a**) uncoated and (**b**) CVD multilayer coated carbide inserts [136]

Table 2 Summary of cutting tool material on machined surface integrity of titanium and nickel alloys

Reference	Workpiece material	Tool material	Cutting parameters	Remarks
Ezugwu and Tang [99]	Inconel 718	Turning, pure oxide and mixed-oxide ceramic tools	$V_c = 152$ m/min $f = 0.125$ mm/rev $a_p = 2$ mm	Mixed-oxide ceramic tools generally produced better surface finish.
Biksa et al. [128]	Inconel 718 and Ti6Al4V	Turning, varied insert shape, cutting edge preparation and nose radius	$V_c = 40$–60 m/min for Inconel 718 and 150 m/min for Ti6Al4V $f = 0.125$ mm/rev $a_p = 0.25$ mm	AlTiN/MoN coated cemented tool was recommended for machining of Inconel 718 and AlTiN/VN coated tool was recommended for machining of Ti6Al4V.
Nalbant et al. [98]	Inconel 718	Turning, CVD quadruple (top layer is TiN), triple (top layer is Al_2O_3) and single (TiN) coated carbide inserts	$V_c = 15$–75 m/min $f = 0.2$ mm/rev $a_p = 2$ mm	Coating layer number and coating material had significantly effects on the surface roughness.
Liu et al. [129]	Inconel 718	Turning, uncoated and PVD TiCN coated Sialon ceramic insert	$V_c = 150$ m/min $f = 0.1$ mm/rev $a_p = 0.5$ mm	TiCN coating improved the cutting performance of Sialon ceramic cutting inserts remarkably.
Thakur et al. [130]	Inconel 718	Turning, TiN/TiAlN (PVD) coated and TiN/Al_2O_3/TiCN (CVD) coated tools	$V_c = 50$–90 m/min $f = 0.05$–0.2 mm/rev $a_p = 0.5$ mm	TiN/Al_2O_3/TiCN (CVD) coated tool outperformed TiN/TiAlN (PVD) coated tool.
Tanaka et al. [126]	Inconel 718	Orthogonal cutting, different PCBN cutting tools	$V_c = 20$, 100, 300 m/min $f = 0.1$ mm/rev	A low CBN content with TiN-based ceramic binder exhibited excellent wear resistance.
Ucun et al. [127]	Inconel 718	Milling, coated and uncoated WC-Co micro milling tools	$V_c = 48$ m/min $f = 1.25$–5 μm/z $a_e = 0.1$, 0.15, 0.2 mm	Milling tools coated with AlTiN, TiAlN+AlCrN, and AlCrN exhibited better cutting performances.
Akhtar et al. [127]	Inconel 718	Milling, TiAlN coated and SiC whisker-reinforced coated ceramic inserts	$V_c = 30$–900 m/min $f = 0.02$–0.12 mm/z $a_e = 0.2$–1.0 mm	Ceramic inserts were recommended to be used in rough and semi finish machining, while TiAlN coated inserts were recommended to be used in finishing process.
Bushlya et al. [133] and Zhou et al.[134]	Inconel 718	Turning, TiN coated and uncoated PCBN inserts	$V_c = 250$, 350 m/min $f = 0.15$ mm/rev $a_p = 0.3$ mm	TiN coated PCBN tool resulted in poorer surface finish and more tensile residual stress than its uncoated one.
Thakur et al. [135, 136]	Inconel 825	Turning, uncoated and CVD coated TiN/TiCN/Al_2O_3/ZrCN inserts	$V_c = 51$, 84, 124 m/min $f = 0.198$ mm/rev $a_p = 1$ mm	CVD multilayer coated tool resulted in deterioration in surface finish and lower micro hardness compared to the uncoated insert. The white layer thickness formed by uncoated insert was larger than the coated insert.
Swain et al. [141]	Nimonic 75	Milling, uncoated and TiAlN coated tungsten carbide micro-end mills	$V_c = 11$–18 m/min $f = 6$–15 mm/min $a_e = 120$ μm	TiAlN coated micro tools decreased the burr formation compared with uncoated micro tools.
Zhou et al. [142]	Inconel 718	Turning, PCBN and whisker-reinforced ceramic (Al_2O_3-SiC_w) inserts	$V_c = 200$, 350 m/min $f = 0.1$ mm/rev $a_p = 0.3$ mm	Ceramic tools produced severer and deeper plastic deformation as well as much higher tensile residual stresses than PCBN tools.
Sharman et al. [145]	Inconel 718	Turning, TiCN/Al_2O_3/TiN coated and uncoated WC inserts	$V_c = 40$, 80, 120 m/min $f = 0.15$, 0.25 mm/rev $a_p = 0.25$ mm	TiCN/Al_2O_3/TiN coated insert produced more tensile residual stress than uncoated insert.
Outeiro et al. [146]	Inconel 718	Turning, PVD coated (TiAlN-2 μm) and uncoated carbide tools	$V_c = 70$ m/min $f = 0.2$ mm/rev $a_p = 0.5$ mm	Coated tools produced lower surface residual stresses, larger thickness of tensile layer and higher residual stresses in machined subsurface.
Ulutan and Özel [147]	Inconel 100	Turning, TiAlN coated and uncoated WC/Co cutting inserts	$V_c = 12$, 24 m/min $f = 0.05$ mm/rev $a_p = 1$ mm	Coated tools produced lower surface residual stresses, and higher residual stresses in machined subsurface.

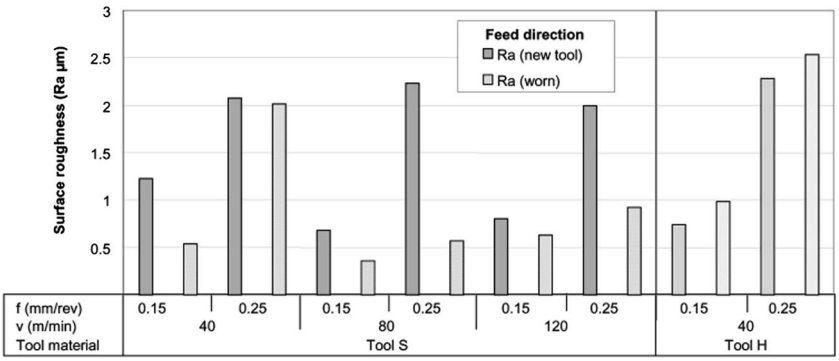

Fig. 37 Machined surface roughness after turning of Inconel 718 using TiCN/Al_2O_3/TiN coated and uncoated WC inserts with constant depth of cut of 0.25 mm [153]

under different tool flank wear states under the cutting speed of 60 m/min, the feed rate of 0.1 mm/r, and cutting width of 2 mm, based on which 3D surface roughness S_a under different tool flank wear states were measured. Their results indicated that the surface roughness first increased and then decreased with the tool flank wear increasing from zero to 0.3 mm, which was caused by different wear morphologies of tool flank face under different wear states. Nevertheless, the research of Yang et al. [151] reported contradictory results, in which the machined surface roughness of Ti-1023 presented a monotone increasing trend with the increase of tool flank wear. The experiments conducted by Yang et al. [151] was wet milling experiments on near-β titanium alloy Ti-1023 with single layer PVD TiAlN coated carbide tools. The reason for the contradiction of surface roughness variation may lie in the differences in workpiece material, cutting tool or cutting environments, etc.

The machined surface defects of Inconel 718 generated with new and worn tools during high speed turning process have been compared detailedly in literature [134], in which the whisker-reinforced Al_2O_3 inserts having an edge radius of 20 μm and a chamfer angle of 20° were used. Figure 40 presents the surface damage generated with new and worn inserts under dry cutting and cutting parameters of $V_c = 200$ m/min, $f = 0.1$ mm/rev and $a_p = 0.1$ mm/rev. It can be seen from Fig. 40(a–d) that the new insert induced such surface defects as built-up edge formation, side flow and tearing. Although the tool flank face wear is beneficial to decrease the surface roughness with a certain degree, the surface defects caused by the worn tool with the flank wear of 0.3 mm are still obvious

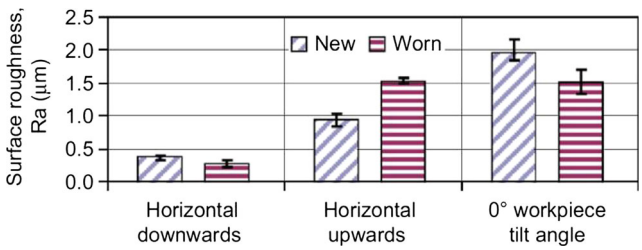

Fig. 38 Influence of tool wear on machined surface roughness generated with new and worn tools under different tool orientation/workpiece angles during ball end milling of Inconel 718 [155]

as shown in Fig. 40(d–f) due to the plastic flow of workpiece material in the cutting zone. In addition, the features of material side flow, ridges or grooves were observed more frequently with tool wear increasing, which can be attributed to the greater material plastic flow on the machined caused by the higher cutting temperatures and higher cutting forces with worn tools.

Other research has pointed out that long and straight grooves are prone to be formed by the plowing effect of individual small built-up edges occurring on the cutting edge, while small fragments of the built-up edges detachment tend to result in short and straight grooves on the machined surface [156]. The feature of ridges was found both in the feed mark region and between the feed marks. With regard to the formation of severe side flow under the tool flank wear of 0.3 mm as shown in Fig. 40(e) and Fig. 40(g), the reason was associated with the increase of cutting edge radius with the tool flank wear aggravating. The increase of cutting edge radius leads to the increase of the minimum chip thickness. Then it causes much severer material side flow in the area of feed marks, where the workpiece material is deformed through plowing effect when the chip thickness is less than the minimum chip thickness [157]. Furthermore, the higher temperature and higher level stress intensify induced by worn tools also intensify the material side flow [158].

The ridges and grooves formation on machined surface of Inconel 718 within feed marks associated with the cutting edge damage are depicted in Fig. 41 [134]. Firstly, the carbides in workpiece material of Inconel 718 produce the grooves on the tool flank surface as shown in Fig. 41(c). Then the groove formed on the trailing edge grows with the cutting time and acts as a forming tool leading to formation of high ridges on the machined surface as shown in Fig. 41(b). The ridges generated on the machined surface can be regarded as the mapping of the grooves located on the trailing edge of the cutting tool, and the grooves formed on the machined surface can be regarded as the mapping of the hard particles on the tool flank face.

The research on the effects of tool flank wear on machined surface defects of Ti6Al4V with CVD Al_2O_3 coated carbide inserts found that the machined surface topography was

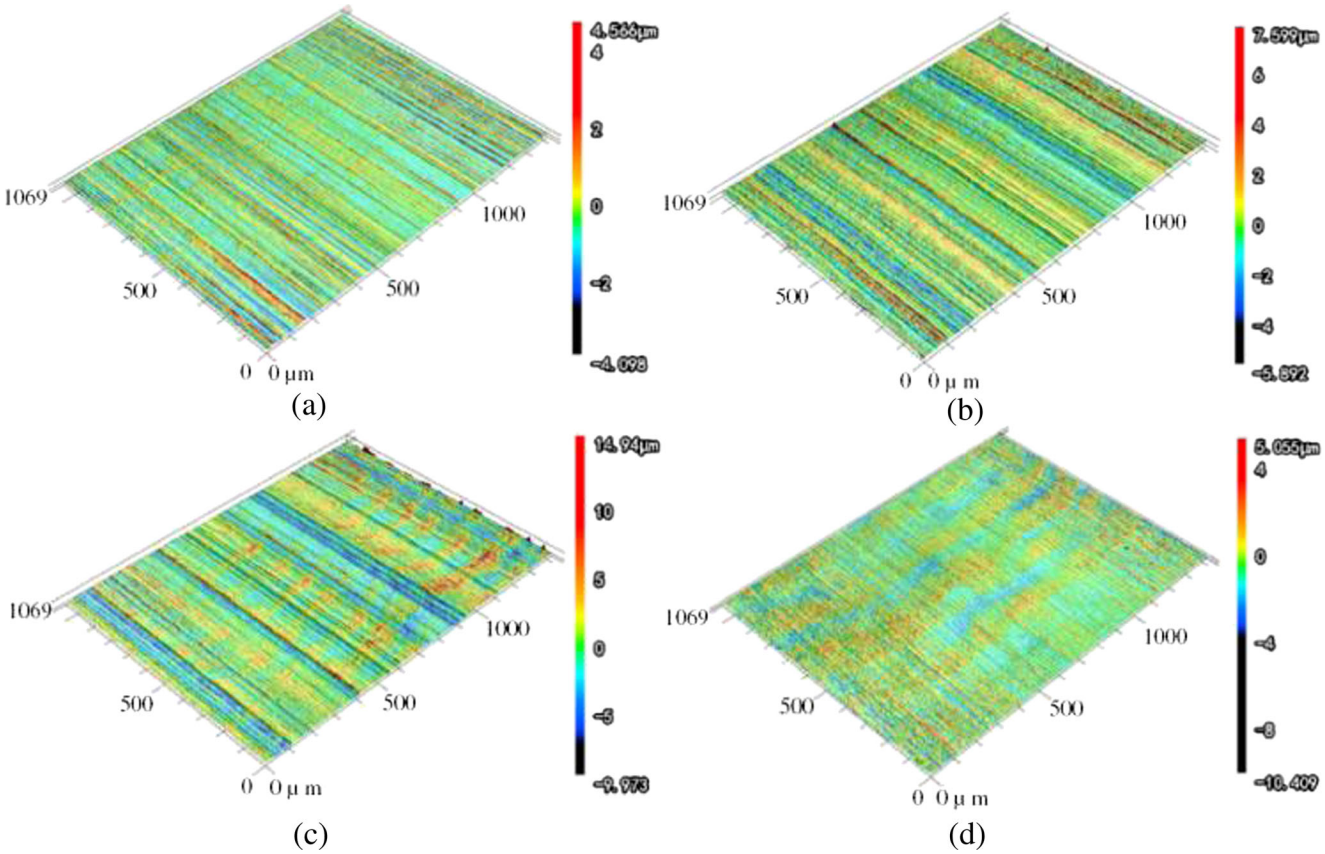

Fig. 39 3D surface topographies of Ti6Al4V generated with different tool flank wear states (**a**) new tool; (**b**) $VB = 0.1$ mm; (**c**) $VB = 0.2$ mm; (**d**) $VB = 0.3$ mm [152]

relatively smooth accompanied with few common defects of grooves and folds when machining with new tool [152]. With the tool flank wear increasing, adhered material particles and material tearing surface occurred due to the effect of extrusion for worn tools. When the tool flank wear reached 0.3 mm, surface material burning and plastic flows were observed due to the high cutting temperature and large cutting force between the tool-workpiece interface. It was suggested that the tool flank face wear with less than 0.2 mm is the most suitable to guarantee the surface integrity during orthogonal dry cutting of Ti6Al4V. Based on the research results of Yang et al. [151], the machined surface defects of near-β titanium alloy Ti-1023 evolves from micro-voids and smeared material to groove and pitting corrosion with the tool wear increasing.

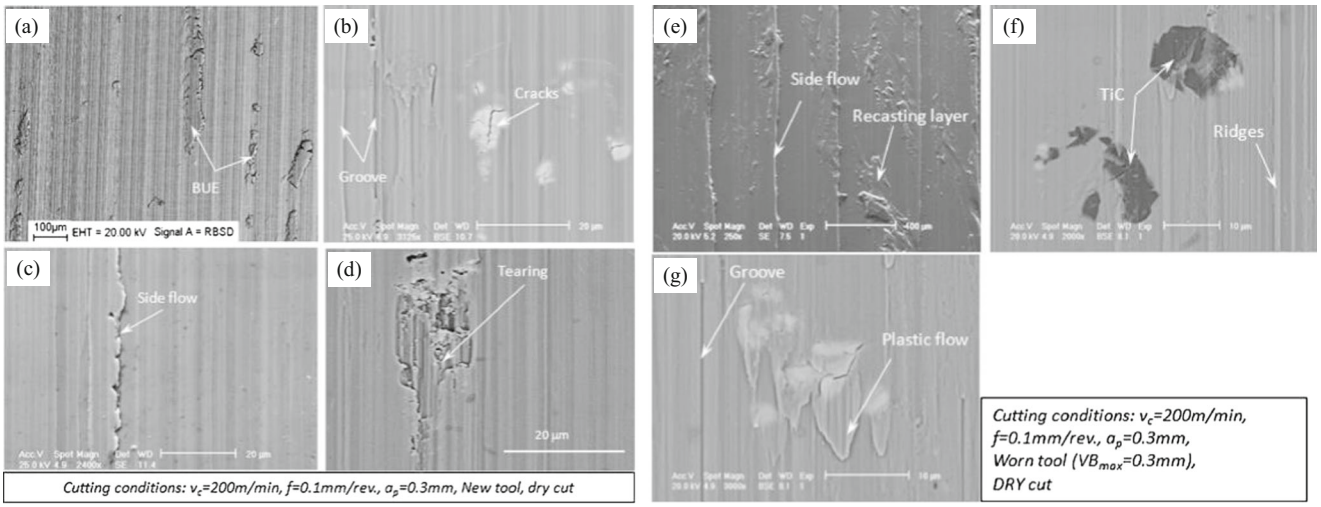

Fig. 40 Machined surface defects of Inconel 718 generated with (**a**–**d**) new tools and (**e**–**g**) worn tools [134]

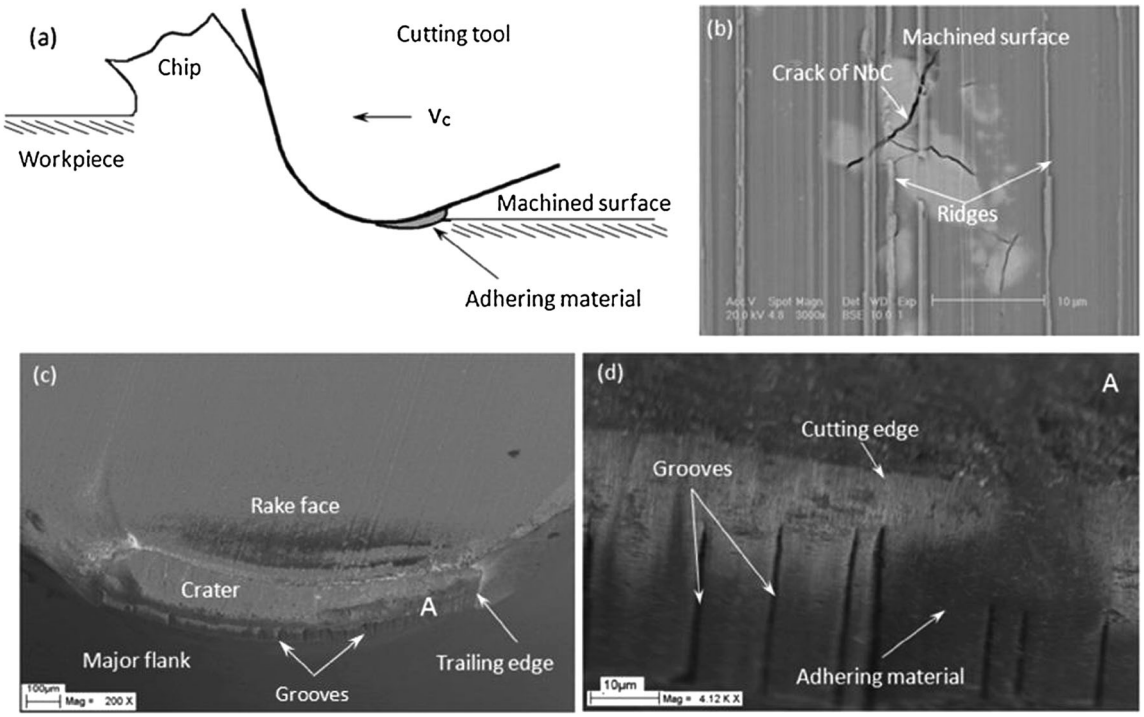

Fig. 41 (**a**) A schematic diagram showing the mechanism of ridge formation; (**b**) ridges located on the machined surface; (**c**), (**d**) grooves located on the tool flank face [134]

The formation of micro-voids was associated with the carbide particles within the workpiece material, while the pitting corrosion was attributed to the high local cutting temperature generated on the machined surface when machining with worn tools. Yang et al. [151] predicted that the cutting temperature generated with the worn tools under the investigated cutting parameters exceeded 1000 °C, which was prone to induce the material burning, phase transformation and material debris attachment on the machined surface.

7.2 Influence of tool wear on microstructure alterations of machined surface

The influence of tool wear on machined surface integrity has been researched through in-depth analysis of microstructure alteration of machined surface and subsurface for titanium and nickel alloys. Different micro-examination techniques including OM, SEM, EBSD and EDS, etc., have been adopted to analyze the microstructure alteration of machined subsurface [5].

The increase of tool flank wear causes severer plastic deformation of machined surface due to the intensified mechanical and thermal loadings applied on the tool-workpiece interface. Both of plastic deformation degree (indicated by inclined red lines in Fig. 42) and plastic deformation depth increased with the tool flank face wear increasing were observed. The results showed that nearly no distinct microstructure deformation or deformed grain observed near the machined surface layer machining using the new tool. The plastic deformation depth of machining affected area increased to 48 μm at the tool flank wear of 0.3 mm and fine grain zone occurred near the machined surface, which is always observed under severe plastic deformation process [159, 160]. Similar results were also found by the research of Yang et al. [151] and Hughes et al. [161].

The microstructure alterations of machined surface for Ti-6242S generated with the new tool and worn tool (VB = 0.3 mm) under milling parameters of V_c = 100 m/min, f = 0.15 mm/z, a_p = 2.5 mm and a_e = 8.8 mm are shown in Fig. 43 [60]. It was indicated that the increase in tool wear induced the microstructural alterations within the machining affected layer. The researches on the microstructure alteration beneath the machined surface of Inconel 718 generated with new and worn tools under different cutting parameters have also demonstrated the increase of more significant plastic deformation and relatively deeper microstructure alteration with the tool wear increasing [153, 154].

Through comparison of the plastic deformation depth quantitatively during turning of Inconel 718 with new and worn tools at V_c = 40–120 m/min, f = 0.15–0.25 mm/rev, and a_p = 0.25 mm (Fig. 44) [153], it was demonstrated that increasing of tool wear exaggerated the plastic deformation depth, especially under lower cutting speeds of 40 m/min, which could be explained by the severe rubbing of tool-workpiece interface caused by the increase of tool-workpiece contact area due to reduction of tool flank angle [162].

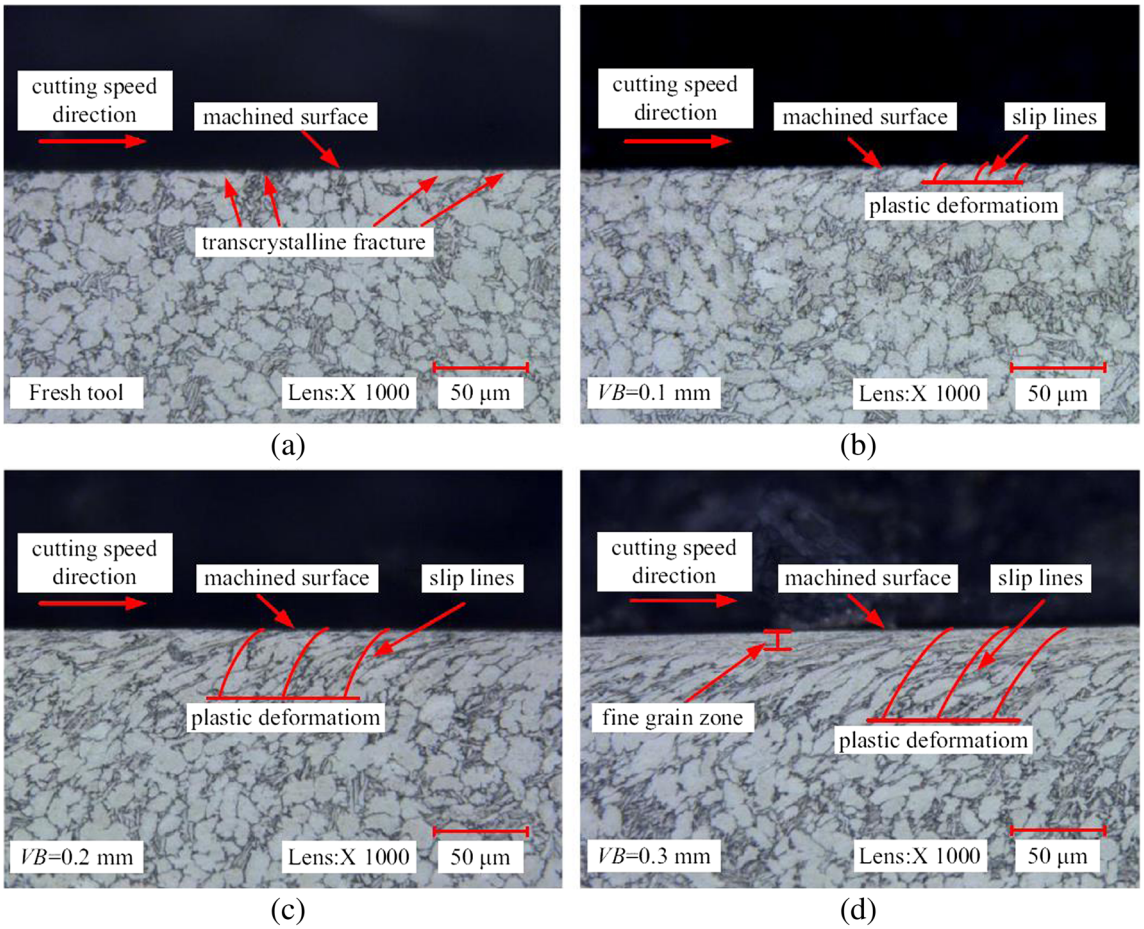

Fig. 42 Microstructure of machined subsurface for Ti6Al4V generated with different tool flank wear states (**a**) new tool; (**b**) $VB = 0.1$ mm; (**c**) $VB = 0.2$ mm; (**d**) $VB = 0.2$ mm [152]

It has been found that the microstructure alteration beneath the machined surface can lead to while layer formation near the outside layer when the effect of strain aging is dominant [143, 144]. The white layer often presents higher micro hardness than the bulk material, which tends to induce the crack formation and its formation is unexpected during machining process. Axinte et al. [163] investigated the variation of white layer formation for powder metallurgy nickel alloy RR_X under different tool wear conditions (Fig. 45). It was found that the uniformly worn tool generated discontinuous and thin

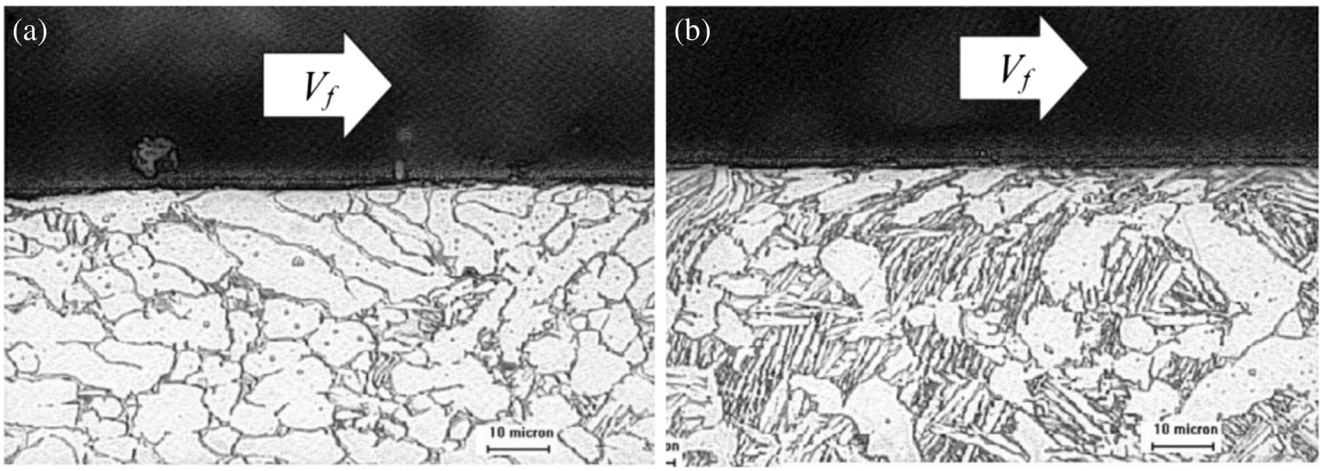

Fig. 43 Microstructure alteration beneath the machined surface of Ti-6242S produced by uncoated carbide tool ($V_c = 125$ m/min, $f = 0.20$ mm/tooth, $a_a = 2.5$ mm, $a_r = 8.8$ mm) (**a**) new tool; (**b**)$VB = 0.3$ mm [60]

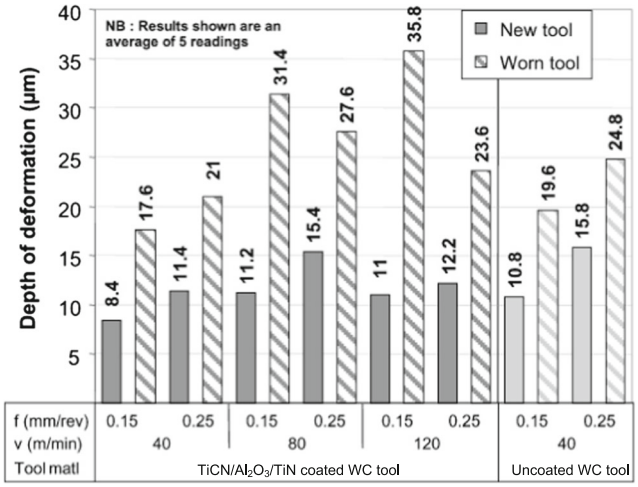

Fig. 44 Influence of tool wear on plastic deformation depth after turning of Inconel 718 at $V_c = 40–120$ m/min, $f = 0.15–0.25$ mm/rev, and $a_p = 0.25$ mm [153]

while layer as shown in Fig. 45(a) and (c), and nearly no signs of strain or microstructure deformation were seen beneath the white layer. Nevertheless, the tool with chipped cutting edge generated relatively continuous and thicker white layer accompanied with obvious material drag beneath the white layer as shown in Fig. 45(b) and (d). The difference can be attributed to more intense friction occurred for the chipped tool leading to severer machining related heat concentration for powder nickel alloys with low thermal conductivity. Du and Liu [143] and Ibrahim et al. [164] have also researched the influences of cutting parameters and tool conditions on the while layer formation of powder metallurgy nickel alloy FGH 95 and Ti6Al4V, respectively.

The effects of tool wear on the extent of subsurface deformation and microstructure modification for Inconel 718 can be shown more clearly with BSE images of machined surface [165]. Figure 46 presents the BSE images of machining affected layer generated with new, semi-worn ($VB_{max} = 0.15$ mm) and worn ($VB_{max} = 0.3$ mm) tools, respectively. It indicates that all machined subsurface generated with different tool wear states contain three zones, of which zone 1 is the near surface region, zone 2 is the deformation zone, and zone 3 is the bulk material. Zhou et al. [165] explained that zone 1 is formed by both strong mechanical (friction force) and local thermal load during machining process and the topography in this area clearly demonstrates the feature of re-solidification rather than simple shearing. Zone 2 is the deformation layer which exhibits clear bending and elongation of grain boundaries and slip bands. With the tool wear increasing, both the thicknesses of zone 1 and zone 2 increase due to the severer mechanical and thermal loading on the tool-workpiece interface. For the near surface microstructure generated with the worn tool as shown in Fig. 46(d), a nano-crystalline structure layer with about 1~2 μm thickness was formed which was explained that the temperature experienced in this region was close to the material melting temperature (1260~1336 °C [166]) during machining process.

EBSD is an advanced microstructure characterization technique which is beneficial to analyze the machining induced deformation through providing quantitative information about the grain orientation and intragranular mis-orientations [160, 167,

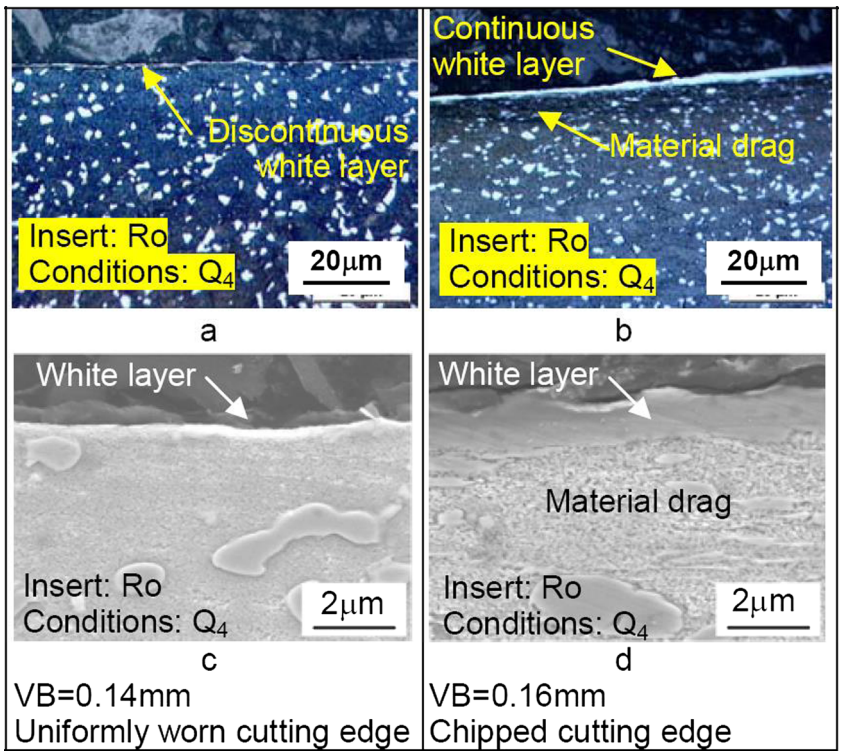

Fig. 45 Optical and SEM micrographs of white layers generated after turning of nickel alloy RR_x with (**a**) uniformly worn and (**b**) chipped ceramic tool at $V_c = 175–200$ m/min, $f = 0.15–0.25$ mm/rev, $a_p = 1–2$ mm [163]

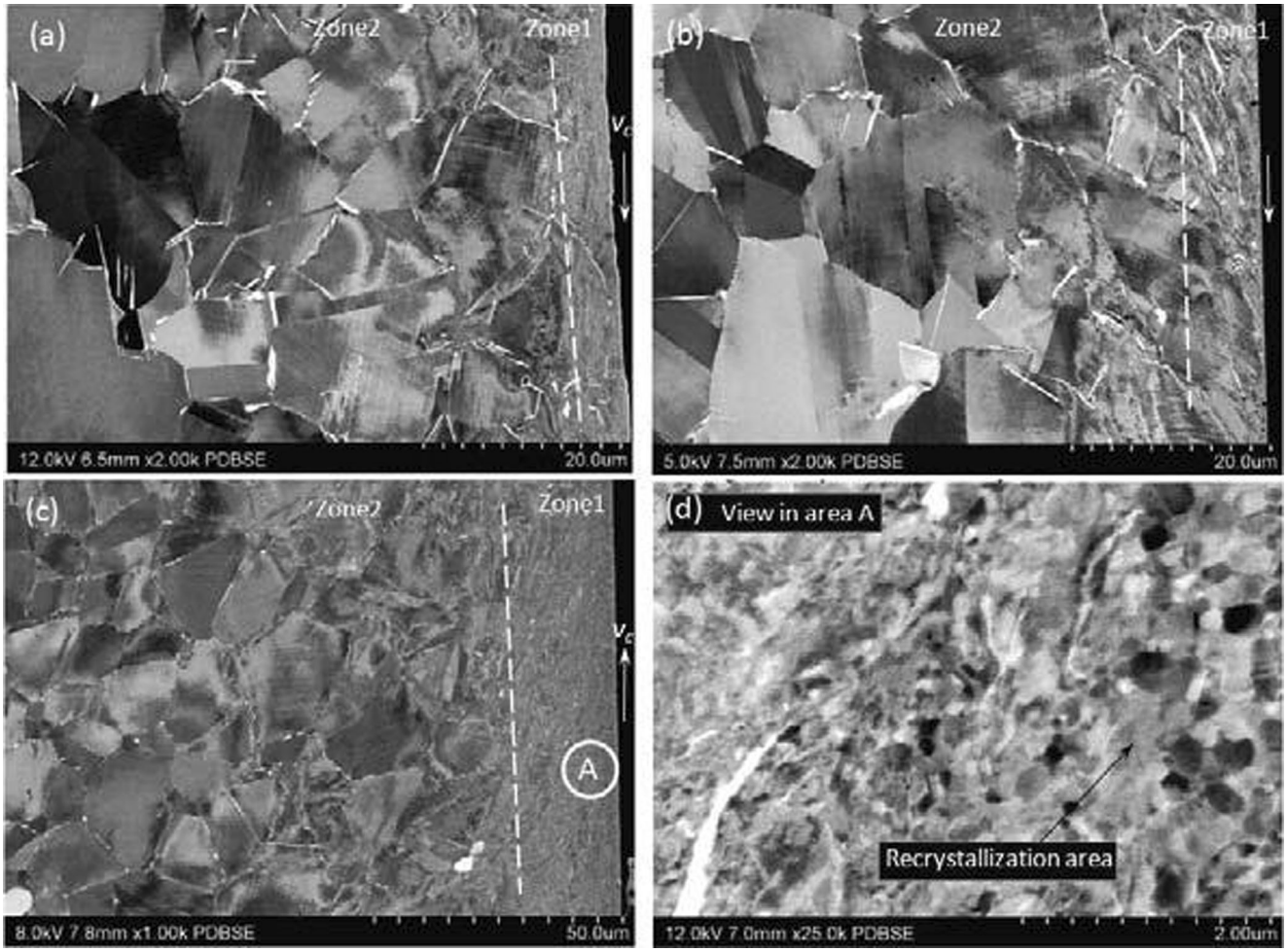

Fig. 46 BSE images indicating the effects of (**a**) new tool; (**b**) semi-worn tool; (**c**) worn tool, on extent of subsurface deformation and microstructure modification and (**d**) refinement of microstructure during turning of Inconel 718 at $V_c = 300$ m/min, $f = 0.2$ mm/rev and $a_p = 0.3$ mm [165]

168]. The EBSD images of machined subsurface layer for Inconel 718 generated with different tool wear conditions were also analyzed (Fig. 47). It can be seen that the lattice rotation increases towards the machined surface caused by the plastic deformation. The sub-grain boundaries and the associated gradients provide evidence of increasing intragranular mis-orientation and plastic activity form the bulk material to the machined surface for all three different tool wear conditions. With the tool flank wear increasing from 0 to 0.3 mm, the thickness of concentrated deformation layer increases from about 10 μm to about 50 μm. The percentage of deformed area in the machined affected zone increases dramatically from less than 20% for new tool to over than 80% for worn tool as shown in Fig. 47(d). The deformation depth for machined surface reached to 250 μm for the worn tool, while that was just about 50 μm for the machined surface produced with the new tool. It was also demonstrated that the increases in mechanical effects (including the stress and the strain) were associated with the increase of the subsurface deformation.

Meanwhile, Agmell et al. [169] investigated the subsurface deformation of Inconel 718 machined with new tool and worn tool with the aid of BSE and EBSD analyses. It can be figured out from the results that the material within the machining affected layer experienced excessive deformation near the machined surface, where a layer containing smaller grain structure was produced. With the distance from the machined surface increasing, the material plastic deformation decreased and a larger grain structure was present towards the bulk material. Their research presented the relative strain as a function of the distance from the machined surface measured by EBSD technique (Fig. 48), which demonstrated that the relative strain generated by the worn tool was much larger than that generated by the new tool.

Machined surface generated with different tool wear conditions also differs due to different phase transformations. Based on the research of Liang and Liu [152], the percentage of β phase near the machined surface of Ti6Al4V generated with difference tool wear condition varied obviously. They found that the percentage of β phase near machined surface generated with new tool was much larger than that of the bulk material, while the percentage of β phase generated with the worn had no obvious variation compared with the bulk material. Combined with EDS analysis for the machined surface,

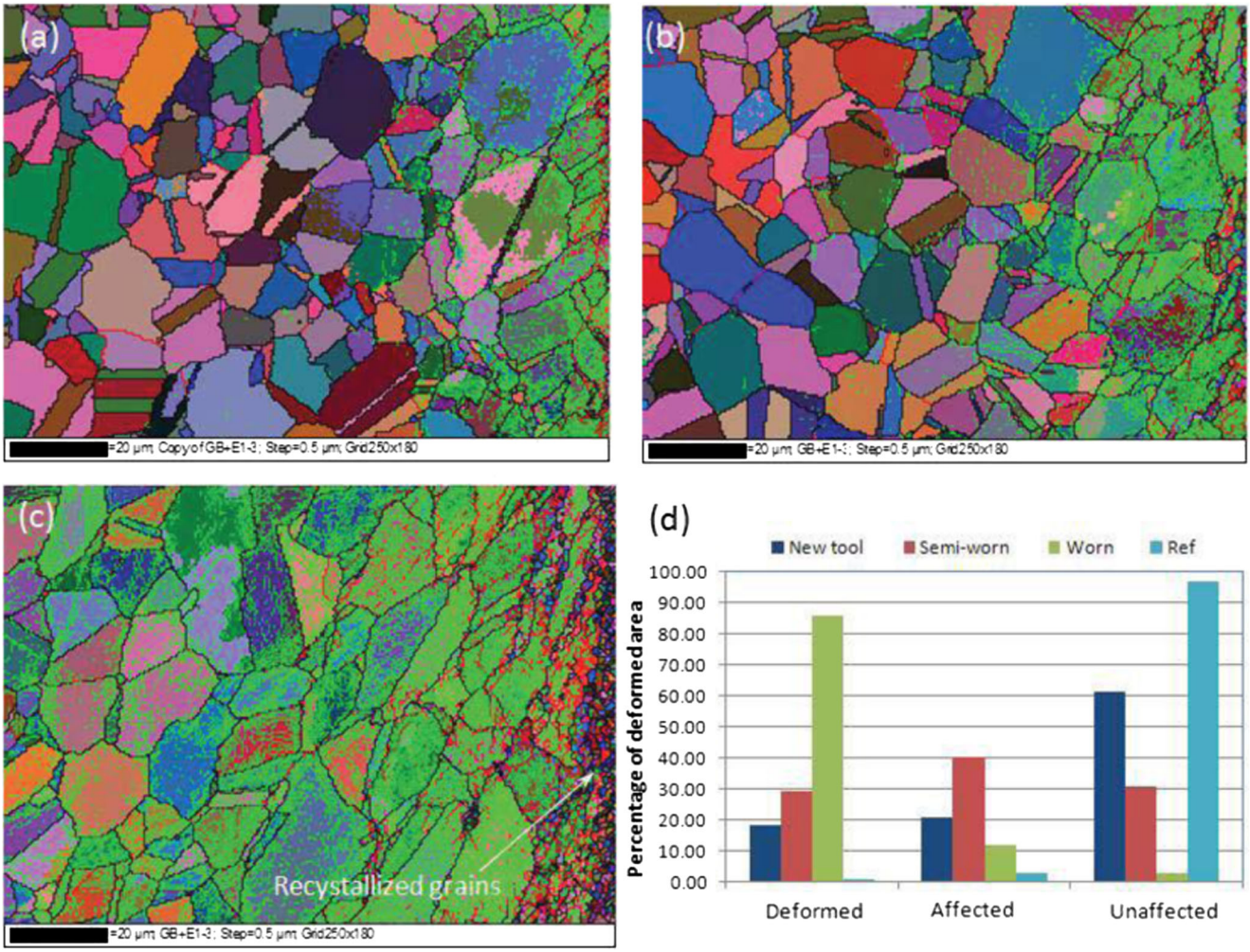

Fig. 47 EBSD images of machined subsurface layer for Inconel 718 generated with (**a**) new tool, (**b**) semi-worn tool, (**c**) worn tool and (**d**) percentage of deformation area [165]

the authors proposed that the contents of element C and element O increased to 1.08 and 2.45%, respectively, when machining with the worn tool of $VB = 0.3$ mm. It was explained that the low percentage of β phase generated with the worn tool was caused by the emergence of elements C and O which belong to the stable elements of α phase, and the increases of elements C and O could stabilize more α phase of Ti6Al4V [170–172].

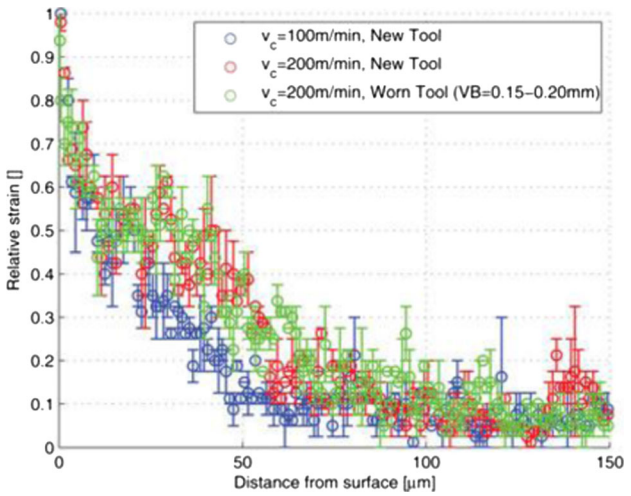

Fig. 48 Relative strain in machining affected layer of Inconel 718 generated with different tool wear states [169]

7.3 Influence of tool wear on mechanical properties of machined surface

As found for the other characteristics of surface integrity, tool wear also has significant influence on the mechanical properties of machined surface including the residual stress profile and micro hardness distribution. The influences of tool wear on the in-depth residual stress profiles of Inconel 718 generated with two kinds of tools as TiCN/Al_2O_3/TiN coated WC tool and uncoated WC tool were researched (Fig. 49) [145]. All the worn tools had average flank wear of 0.25 mm. The results indicated that the residual stresses beneath the machined surface became much more compressive and penetrated to a

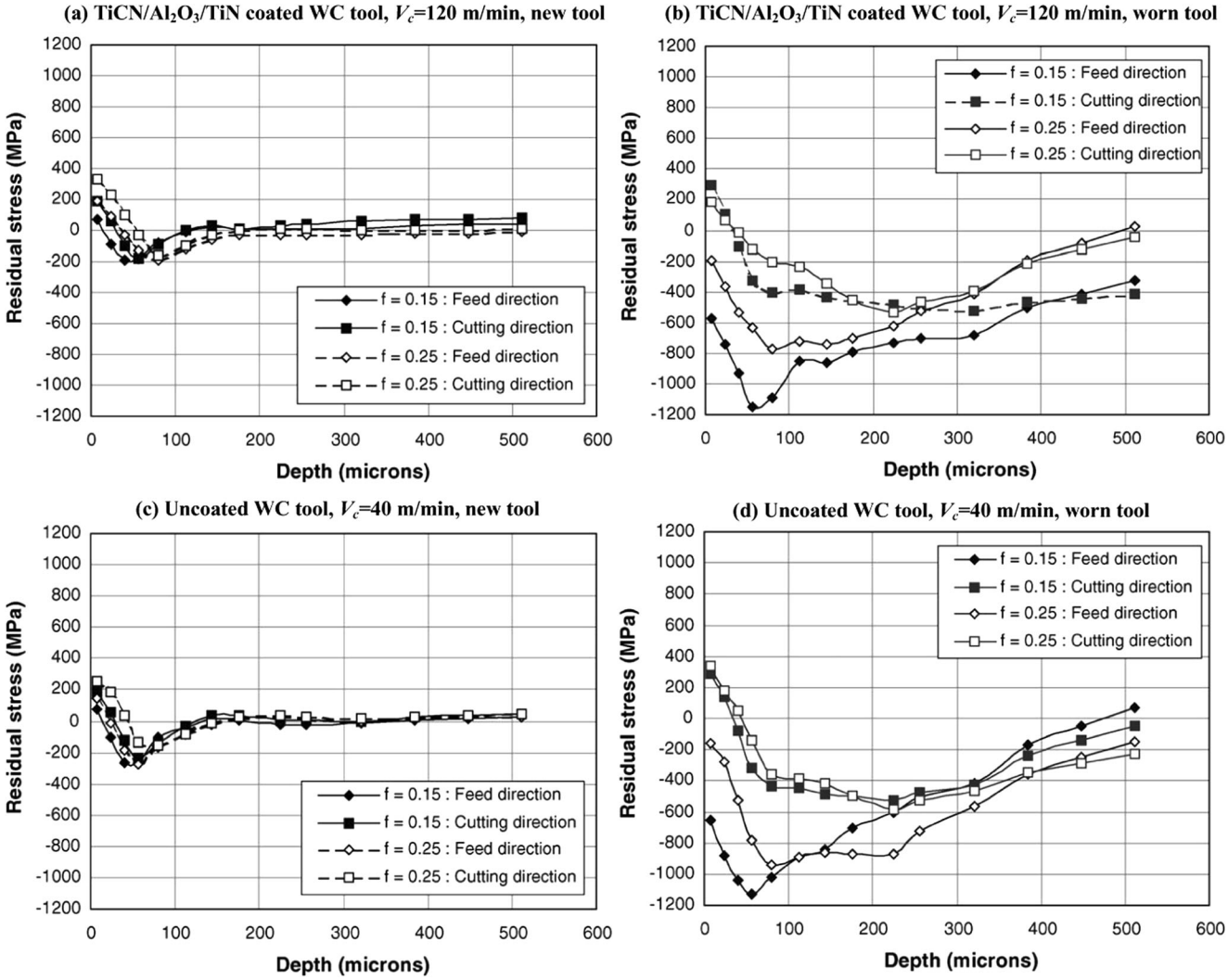

Fig. 49 In-depth residual stress profiles of Inconel 718 generated with (**a**), (**c**) new tools and (**b**), (**d**) worn tools [145]

deeper depth for the worn tools regardless of the tool type. The depth of a significant level of compressive stress reached up to 500 μm beneath the workpiece surface for the worn tools, while the depth of compressive stress was just about 150 μm for the new tools. It was explained that an increase in rubbing or plowing leaded to greater plastic deformation of the workpiece surface, which then produced increased depth of deformation and residual stress variation [117, 145].

Through comparison of in-depth residual stress profiles of Inconel 718 generated with the new and worn PCBD tools numbered DCC500 as shown in Fig. 50 [173], it was found that the worn insert in Test B induced the highest subsurface residual stress levels (− 1268 MPa and − 930 MPa in the feed and cutting directions, respectively) with the distance from machined surface extending to about 450 μm, as opposed to about 100–150 μm when machining with new inserts.

However, some other researchers obtained the contrary results for the residual stress profiles generated with the new and worn tools. Figure 51 shows one study for orthogonal cutting of Ti6Al4V at $V_c = 320$ m/min, $f = 0.1$ mm/rev and $a_w = 1$ mm, which suggested that with the tool flank wear increasing, the surface residual stresses became more tensile due to increased temperature [174]. In addition, the peak compressive residual stresses became less compressive, and the residual stresses deep into the bulk material became tensile rather than compressive as the new tool. The work in literature [152] also draw the similar conclusions through research on the residual stress profiles after orthogonal cutting of Ti6Al4V at $V_c =$ 60 m/min, $f = 0.1$ mm/rev and $a_w = 2$ mm. They concluded that with the tool flank wear increasing, the residual stresses near the machined surface became less compressive.

Aspinwall et al. [155] investigated the influence of tool wear on in-depth residual stress profiles of Inconel 718 after end milling process as shown in Fig. 52, and they suggested that the effect of tool wear on the surface residual stresses varied depending on the cutter orientation and workpiece angle. The peak compressive residual stresses occurred in the machined subsurface also changed inconsistently. However,

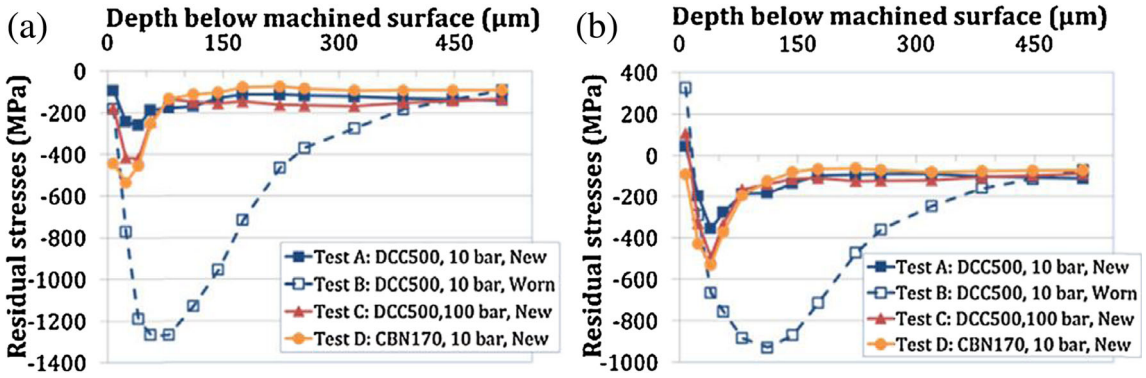

Fig. 50 In-depth residual stress profiles of Inconel 718 generated with new and worn tools in (**a**) feed and (**b**) cutting directions [173]

the machining affected layer became much deeper with the tool wear increasing. Figure 52 presents the combined effects of cutter orientation, workpiece tilt angle as well as tool wear on the residual stresses of machined surface for Inconel 718 after end milling process, and it indicates that it is possible to change the residual stresses from tensile to compressive, or alter the residual stress magnitude by adjusting the cutter orientation or the workpiece tilt angle under different tool wear conditions [155].

The research of Peng et al. [175] found that worn tool tended to result in higher tensile residual stress near the machined surface, higher compressive residual stress beneath the heat affected layer as well as deeper peak of compressive stress, simultaneously. They suggested that the increase in tensile residual stress on the machined surface could be attributed to higher cutting temperature caused due to rubbing and plowing between the machined surface and the worn tool flank face. It also induced higher degree of plastic deformation leading to increased compressive stress within the machined subsurface. Meanwhile, it was pointed out that the effects of tool wear on residual stresses along cutting and feed directions were different, which was explained by the reason that the radial and feed force components increased more prominently compared to the cutting force component [175].

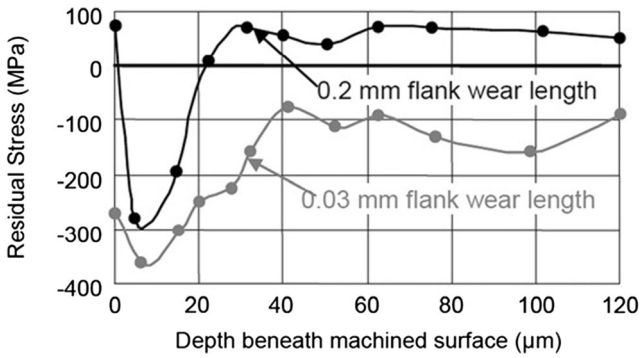

Fig. 51 Effect of tool flank wear on residual stress profiles after turning of Ti6Al4V at $V_c = 320$ m/min, $f = 0.1$ mm/rev and $a_p = 1$ mm [174]

The effects of tool wear on the micro hardness profiles of machined subsurface after machining can also be tracked in some literatures. The research of [173] indicated that nearly no variation in material micro hardness (average value for the bulk material was about 30 HK0.025) was observed perpendicular to the feed direction when turning with new inserts except for the CrAlN 2 coated insert (Fig. 53). The CrAlN 2 coated insert produced a hardened layer of up to 544 HK0.025, and it was explained that the greater coating thickness (5.5 μm) of this insert compared to the others (1–3 μm) resulted in a larger cutting edge radius and increased rubbing as well as material deformation. For all investigated cutting tools, Soo et al. [173] found that the machined surface turned with worn inserts typically exhibited elevated hardness levels of up to about 80 $HK_{0.025}$ and the machining affected layer depth reached to about 100 μm below the machined surface.

Similar results have also been obtained by Sadat and Reddy [176] and Sharman et al. [153] in machining of Inconel 718. Sharman et al. [153] researched the effects of tool wear on micro hardness depth profiles after turning of Inconel 718 with TiCN/Al_2O_3/TiN coated WC tool and uncoated WC tool (Fig. 54). They found that the depth of micro hardness increase was limited to around 50 mm when machining with new tools, and the maximum micro hardness of the machined surface was about 450 $HK_{0.05}$. Nevertheless, the machined surfaces produced with worn tools were harder (the maximum value is 500$HK_{0.05}$) and the affected layer depth was larger (about 200 μm) than those produced with new tools under the same cutting parameters. The reason lies in that machining with worn tools leads to larger tool/workpiece contact area and enhances the hardening effect on the machined surface [153, 176].

The research of Ginting and Nouari [60] on Ti-6242S and the research of Liang and Liu [152] on Ti6Al4V also demonstrated the severer hardening effects of tool wear on machined surface. It can be seen from Fig. 55 that both the micro hardness and the hardened layer thickness increased when machining with the worn tools for uncoated and TiN/TiC/TiCN coated carbide tools [60]. It was found that with the tool flank wear increasing from 0 to 0.2 mm, both of the micro hardness and

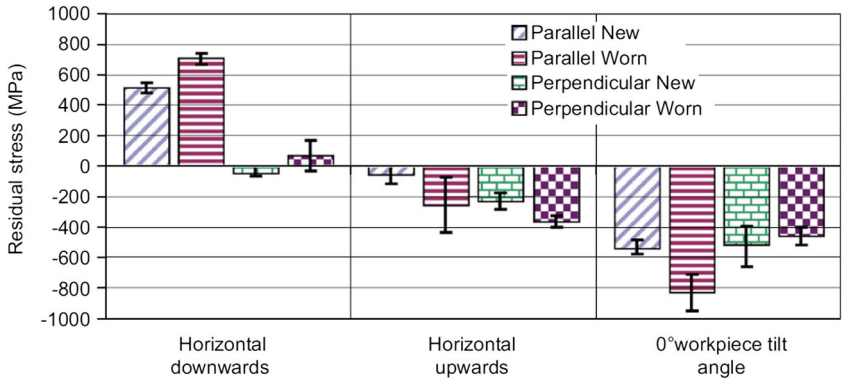

Fig. 52 Residual stress on machined surface of Inconel 718 generated with new and worn tools under different cutter orientations and workpiece tilt angles [155]

the depth of machining hardened layer increased [152]. However, a softened zone near the machined surface was found when the tool flank wear increased to 0.3 mm, which could be explained by the predominant thermal softening effect caused by severe friction between tool-workpiece interface. The poor thermal conductivity of Ti6Al4V may also enhance the thermal softening of machined surface under severe tool flank wear.

Table 3 provides a check list and summary of the important studies dealt with the effects of tool wear on machined surface integrity during machining of titanium and nickel alloys reviewed in this paper.

8 Research limitations and latest ideas

According to the review of considerable amount of literatures, it has been found that some issues about the effects of tool parameters on machined surface integrity are still open during machining titanium and nickel alloys. These open issues and limitations for the current research are listed as following.

- The current research on the effects of tool parameters (including tool structure, tool material and tool wear) on machined surface integrity mainly depends on practical experiments or empirical data. For example, theoretical models of surface roughness considering the effects of tool structures are still lacking. The variation of machined surface roughness generated with different tool structures need to be determined based on experiments. The effects of tool material or tool wear on the residual stress profiles of machined surface are also rarely theoretical analyzed. If one parameter for the cutting tool is changed, all the geometrical characteristics, microstructure alteration, or mechanical properties of machined surface are unknown and need to be measured with experiments. The research cost is high and sometimes it is impossible to carry out all experiments because there are too many different cutting tools. There is great significance to predict the variation of machined surface integrity with one given tool before practical machining. After then, the most appropriate cutting tools can be selected efficiently to improve the machined surface quality.
- For one certain cutting tool used in machining one kind of workpiece material, the current research on the characteristics of machined surface integrity is limited to just one or several incomplete evaluation parameters. The geometrical characteristics, microstructure alteration, or mechanical properties of machined surface are partially focused on in one individual literature. Particularly, there is little research about the effects of tool parameters on phase transformation of machined surface. According to the current research, it is hard to evaluate if the machined surface integrity generated with one given cutting tool can be qualified. Systematic research on the effects of tool parameters (including tool structure, tool material and tool wear of one cutting tool) on all characterized parameters of machined surface integrity should be conducted to provide synthetic evaluation for the tool cutting performance.
- The weights of geometrical characteristics, microstructure alteration, as well as mechanical properties in overall evaluation of machined surface integrity are not straightforward for one machined components. According to the current research, the above three aspects of machined surface are hard to be qualified simultaneously with one fixed cutting tool. Improvement in geometrical characteristics of machined surface may weaken the microstructural

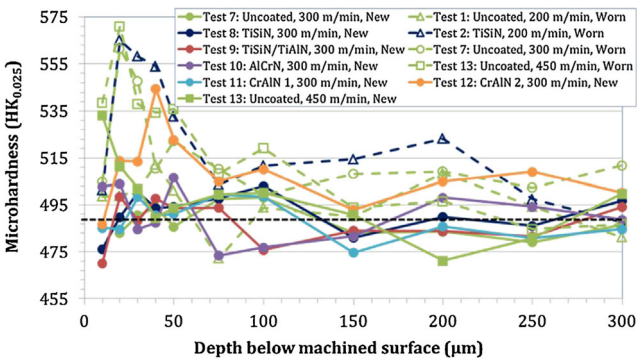

Fig. 53 Micro hardness profiles perpendicular to feed direction after turning of Inconel 718 [173]

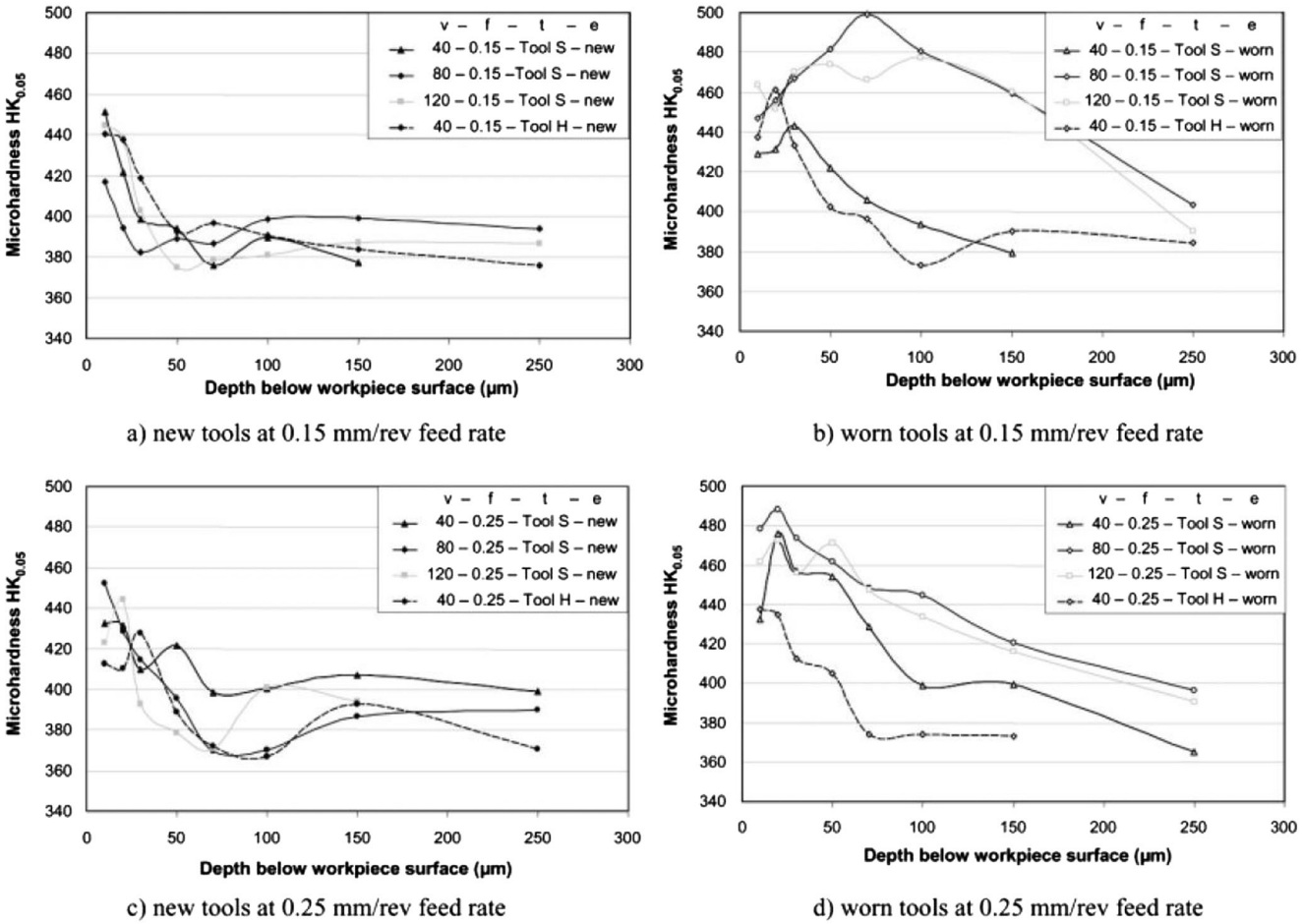

Fig. 54 Effect of tool wear on micro hardness profiles after turning of Inconel 718 with different tools (Tool S: TiCN/Al_2O_3/TiN coated WC tool, Tool H: uncoated WC tool) [153]

alteration or physical properties of machined surface. It is urgent to obtain the influence of cutting tool parameters on different aspects of machined surface integrity, in addition to the weights of different evaluation parameters on the machined surface quality. Then the largest beneficial influence of the cutting tool on machined surface quality can be developed while the detrimental influence of the cutting tool is controlled to be the least.

- The relationships of different evaluation parameters of machined surface integrity have not been known clearly. When the cutting tool structure, tool material or tool wear condition is changed, the geometrical characteristics,

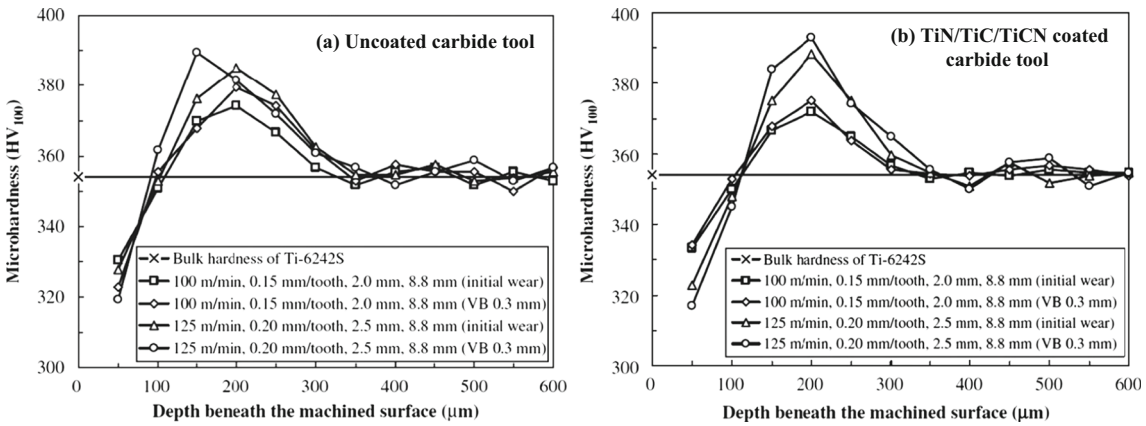

Fig. 55 Effect of tool wear on micro hardness profiles after milling of Ti-6242S under V_c = 100–125 m/min, f = 0.15–0.2 mm/z, a_p = 2–2.5 mm with (**a**) uncoated and (**b**) TiN/TiC/TiCN coated carbide tools [60]

Table 3 Summary of cutting tool wear on machined surface integrity of titanium and nickel alloys

Reference	Workpiece material	Tool condition	Cutting parameters	Remarks
Sharman et al. [145, 153]	Inconel 718	Turning, TiCN/Al_2O_3/TiN coated and uncoated WC inserts, $VB = 0.25$ mm	$V_c = 40, 80, 120$ m/min $f = 0.15, 0.25$ mm/rev $a_p = 0.25$ mm	Tool flank wear decreased machined surface roughness, exaggerated plastic deformation depth, and produced higher level of compressive stress and increased the depth of residual stress.
Liang and Liu [152]	Ti6Al4V	Orthogonal cutting, CVD Al_2O_3 coated carbide inserts, $VB = 0.1, 0.2, 0.3$ mm	$V_c = 60$ m/min $f = 0.1$ mm/rev $a_w = 2$ mm	Surface roughness first increased and then decreased with the tool flank wear i ncreasing from zero to 0.3 mm. Tool flank wear increased both of plastic deformation degree and deformation depth.
Yang et al. [151]	Ti-1023	Milling, PVD TiAlN coated carbide inserts, $VB = 0.1, 0.2, 0.35$ mm	$V_c = 20$–300 m/min $f = 0.08$ mm/z $a_e = 1$ mm	Machined surface roughness presented a monotone increasing trend with tool flank wear. Worn tools produced defects of groove and pitting corrosion.
Aspinwall et al. [155]	Inconel 718	Milling, coated ball end milling tools, $VB = 0.3$ mm	$V_c = 90$ m/min $f = 0.2$ mm/z $a_p = 0.2$ mm $a_e = 0.5$ mm	Lower surface roughness was generated with worn tools except for horizontal upwards operation. Effect of tool wear on surface residual stresses depended on cutter orientation and workpiece angle.
Zhou et al. [138]	Inconel 718	Turning, whisker-reinforced Al_2O_3 insert, $VB = 0.3$ mm	$V_c = 100$–400 m/min $f = 0.1, 0.15, 0.2$ mm/rev $a_p = 0.3$ mm	Tool flank wear decreased the surface roughness, but surface defects were still obvious.
Ginting and Nouari [60]	Ti-6242S	Milling, cutting inserts with textured patterns on rake face	$V_c = 100$ m/min $f = 0.15$ mm/rev $a_p = 2.5$ mm $a_e = 8.8$ mm	Tool flank wear increased significant plastic deformation and relatively deeper microstructure alteration.
Axinte et al. [163]	Nickel alloy RR_X	Turning, uniformly worn and chipped ceramic tool	$V_c = 175$–200 m/min $f = 0.15$–0.25 mm/rev $a_p = 1$–2 mm	Tool with chipped cutting edge generated relatively continuous and thicker white layer compared with uniformly worn tool.
Zhou et al. [165]	Inconel 718	Turning, whisker reinforced alumina ceramic insert, $VB = 0.15, 0.3$ mm	$V_c = 300$ m/min $f = 0.2$ mm/rev $a_p = 0.3$ mm	Increase of tool wear enlarged the microstructure alteration thicknesses of machined surface.
Agmell et al. [169]	Inconel 718	Orthogonal cutting, Whisker reinforced alumina ceramic insert, $VB_{max} = 0.2$ mm	$V = 100, 200$ m/min $f = 0.2$ mm/rev	Relative strain of the machined subsurface generated by worn tool was much larger than that generated by new tool.
Soo et al. [173]	Inconel 718	Turning, new and worn PCBD tools, $VB_{max} = 0.2$ mm	$V_c = 200$–450 m/min $f = 0.15$ mm/rev $a_p = 0.2$ mm	Worn insert induced higher subsurface residual stress levels, higher micro hardness and larger distance extending from machined surface.
Chen et al. [174]	Ti6Al4V	Orthogonal cutting, uncoated carbide tools, $VB = 0.03, 0.2$ mm	$V_c = 320$ m/min $f = 0.1$ mm/rev $a_w = 1$ mm	Surface residual stresses became more tensile with the tool flank wear increasing.
Peng et al. [175]	Inconel 718	Turning, whisker reinforced alumina ceramic insert, $VB = 0.15, 0.3$ mm	$V_c = 200$ m/min $f = 0.2$ mm/rev $a_p = 0.3$ mm	Worn tool produced higher tensile residual stress near machined surface, higher compressive residual stress beneath heat affected layer and deeper peak of compressive stress.

microstructure alteration, as well as mechanical properties of the machined surface will be changed. However, it remains unknown about the relationships for the variation of surface geometrical characteristics and the variation of surface microstructure or physical properties. Because the measurement of physical properties of machined surface is complexed especially in practical production, the explicit correspondence between geometrical characteristics and physical properties of machined surface will be beneficial to monitor the machined surface online. For example, if the residual stress profile could be ascertained from other more simple measurements of surface integrity (e.g. surface roughness), the residual stress can be monitored through measurement of surface roughness instead. Further, the effects of tool parameters on the machined surface integrity can be understood more comprehensively. In general, an increase in surface defects results in a general increase in the level of tensile residual stress, but the measurements of

surface defects could still not be used to predict the actual residual stress state with any degree of certainty [145].

- The research of tool parameters on machined surface integrity mainly focuses on turning process, while little work on the milling process and solid milling tools can be tracked. Although there are some similarities for the influence of turning tools and milling tools on the machined surface integrity, there are still some particularities for different cutting process that should be pay more attention to. Similarly, the current researches on titanium and nickel alloys are mainly limited to Ti6Al4V and Inconel 718 as summarized in Tables 1, 2 and 3. Further research on machined surface integrity of titanium and nickel alloys should be carried out based on different components or mechanical properties of the workpiece materials.

Through the review of current relevant literatures, the latest idea about the research for the influence of tool parameters on machined surface integrity should consider the requirements of service performance (e.g. fatigue life) for machined components. The characteristics of machined surface integrity (including geometrical characteristics, microstructure alteration and mechanical properties) play important roles on working performance and service life of components. Components working under different loading conditions have different demands for the machined surface integrity. The primary task is to realize which parameter of machined surface is the most one that determine or influence the component service performance. Then the cutting tool parameters can be adjusted to produce the demanded machined surface quality. It is vital important to establish the mapping relationships among the cutting tool parameters, machined surface integrity, and the service performance of machined components.

9 Conclusions

The quality and service performance of a product is directly determined by the surface integrity achieved by final manufacturing process. Surface integrity covers the geometrical characteristics (geometrical morphology, surface roughness and surface defects, etc.), the microstructure alteration (plastic deformation layer, grain size and texture, phase transformation, etc.) and the mechanical properties (the state of residual stress and micro hardness) of the machined surface. The tool parameters including tool structure, tool material and tool wear have significant influences on the machined surface integrity.

This review paper provides an overview of the effects of tool parameters on the machined surface integrity during turning and milling of titanium and nickel alloys. Improvements of surface integrity of titanium and nickel alloys are challengeable subjects in the area of manufacture due to their low machinability. Some specific conclusions drawn in this review are summarized as following.

- Geometrical characteristics of machined surface are closely related to the tool structures such as tool shape, tool angles, and cutting edge geometries, etc. Round insert with large nose radius, negative rake angle and cutting tools with chamfer, hone or wiper edge can generally lower the machined surface roughness. Variable microgeometry of cutting edge for inserts and variable helix angles for solid end milling tools can lower the machined surface roughness and alleviate the surface defects by suppressing the cutting vibration. Cutting tools with micro textures fabricated on the rake face or flank face have also been developed to lower the surface roughness though improving the friction behavior between tool-chip or tool-workpiece interfaces.
- Cutting edge geometry has significant influence on the microstructure alteration of machined surface. Increases of both chamfer angle and hone radius result in the decrease of surface grain size and increase of machined surface micro hardness, and this variation is more insensitive for chamfered tool than honed tool. Larger tool nose radius generally induces larger plastic deformation depth due to higher cutting forces.
- Cutting tools with round shape, chamfered cutting edge and negative rake angle generate primarily compressive residual stresses. Increase in tool nose radius always results in deeper tensile and compressive residual stress. Larger cutting tool edge radius induces a higher hardness profile into the depth from the machined surface.
- The tool cutting performance is generally improved through coating treatment, but the machined surface roughness produced with the coated tools may not be better than the uncoated ones due to rougher coating surface morphology associated with larger cutting edge radius compared to the uncoated tool. The cutting tools with poor thermal conductivity generate deeper plastic deformation and severer microstructural alteration due to the higher cutting temperature.
- The physical and mechanical properties of cutting tool materials, especially the thermal conductivity of cutting tool, play an important role on the residual stress distribution within the machining affected layer. Cutting tool materials with lower thermal conductivity tend to cause more tensile residual stress due to the dominance of thermal influence. Cutting tool materials with low friction coefficient results in lower tool wear rate, and leads to the alleviation of both thermally and mechanically induced plastic deformation, as well as the lower micro hardness of the machined surface.
- The worn flank face of cutting tools plays a similar role of "wiper" and can lower the machined surface roughness.

Nevertheless, the tool flank wear cannot alleviate the surface defects due to the greater material plastic deformation on the machined surface caused by higher cutting temperatures and higher cutting forces with worn tools. Through providing effective resistance to tool wear plowing, plastic deformation and surface defects such as grooves, ridges and tearing can be significantly controlled.

- With the tool flank wear increasing, both of plastic deformation degree and plastic deformation depth of machining affected layer increase, accompanied with more serious microstructure alteration and phase transformation. In addition, the residual stresses beneath the machined surface generated by the worn tools generally become more compressive and penetrate to a deeper depth. The machined surface produced with the worn inserts typically exhibits elevated micro hardness levels extending to a deeper affected layer.

Acknowledgements The authors would like to acknowledge the financial support from the National Natural Science Foundation of China (51705293, 51425503), and the Major Science and Technology Program of High-end CNC Machine Tools and Basic Manufacturing Equipment (2014ZX04012014 and 2015ZX04005008). This work was also supported by project funded by China Postdoctoral Science Foundation (2017M610422), International Postdoctoral Exchange Fellowship Program and grants from Taishan Scholar Foundation (TS20130922).

References

1. Yang XP, Liu CR (1999) Machining titanium and its alloys. Mach Sci Technol 3(1):107–139
2. Arrazola PJ, Garay A, Iriarte LM, Armendia M, Marya S, Maître FL (2009) machinability of titanium alloys (Ti6Al4V and Ti555.3). J Mater Process Technol 209(5):2223–2230
3. Choudhury IA, El-Baradie MA (1998) Machinability of nickel-base super alloys: a general review. J Mater Process Technol 77(1–3):278–284
4. Dudzinski D, Devillez A, Moufki A, Larrouquère D, Zerrouki V, Vigneau J (2004) A review of developments towards dry and high speed machining of Inconel 718 alloy. Int J Mach Tools Manuf 44(4):439–456
5. Ulutan D, Özel T (2011) Machining induced surface integrity in titanium and nickel alloys: A review. Int J Mach Tools Manuf 51(3):250–280
6. Wang B, Liu ZQ (2014) Investigations on the chip formation mechanism and shear localization sensitivity of high-speed machining Ti6Al4V. Int J Adv Manuf Technol 75(5-8):1065–1076
7. Thakur A, Gangopadhyay S (2016) State-of-the-art in surface integrity in machining of nickel-based super alloys. Int J Mach Tools Manuf 100:25–54
8. Wang B, Liu ZQ (2017) Acoustic emission signal analysis during chip formation process in high speed machining of 7050-T7451 aluminum alloy and Inconel 718 superalloy. J Manuf Process 27:114–125
9. Reed RC (2006) The Superalloys: Fundamentals and Applications. Cambridge University Press, New York
10. Ezugwu EO, Bonney J, Yamane Y (2003) An overview of the machinability of aero-engine alloys. J Mater Process Technol 134(2):233–253
11. M'Saoubi R, Axinte D, Soo SL, Nobel C, Attia H, Kappmeyer G, Engin S, Sim WM (2015) High performance cutting of advanced aerospace alloys and composite materials. CIRP Ann Manuf Technol 64(2):557–580
12. Pervaiz S, Rashid A, Deiab I, Nicolescu M (2014) Influence of tool materials on machinability of titanium- and nickel-based alloys: a review. Mater Manuf Process 29(3):219–252
13. Grzesik W (2008) Advanced machining processes of metallic materials: theory, modeling and applications, 1st edn. Elsevier, Amsterdam
14. Zhu DH, Zhang XM, Ding H (2013) Tool wear characteristics in machining of nickel-based superalloys. Int J Mach Tools Manuf 64(1):60–77
15. Imran M, Mativenga PT, Gholinia A, Withers PJ (2014) Comparison of tool wear mechanisms and surface integrity for dry and wet micro-drilling of nickel-base superalloys. Int J Mach Tools Manuf 76(1):49–60
16. Da Silva RB, Sales WF, Costa ES, Ezugwu EO, Bonney J, Da Silva MB, Machado ÁR (2017) Surface integrity and tool life when turning of Ti-6Al-4V with coolant applied by different methods. Int J Adv Manuf Technol 93(5-8):1893–1902
17. Ezugwu EO, Wang ZM (1997) Titanium alloys and their machinability a review. J Mater Process Technol 68:262–274
18. Guo YB, Li W, Jawahir IS (2009) Surface integrity characterization and prediction in machining of hardened and difficult-to-machine alloys: a state-of-the-art research review and analysis. Mach Sci Technol 13(4):437–470
19. Obikawa T, Kamio A, Takaoka H, Osada A (2011) Micro-texture at the coated tool face for high performance cutting. Int J Mach Tools Manuf 51(12):966–972
20. Arunachalam RM, Mannan MA, Spowage AC (2004) Surface integrity when machining age hardened Inconel 718 with coated carbide cutting tools. Int J Mach Tools Manuf 44(14):1481–1491
21. Cantero JL, Díaz-Álvarez J, Miguélez MH, Marín NC (2013) Analysis of tool wear patterns in finishing turning of Inconel 718. Wear 297(1-2):885–894
22. Groover MP (2010) Fundamentals of modern manufacturing: materials, processes, and systems, 4th edn. Wiley, New York
23. Leyens C, Peters M (2006) Titanium and titanium alloys. Wiley, New York
24. Wang T, Wan Y, Kou ZJ, Cai YK, Wang B, Liu ZQ (2016) Construction of a bioactive surface with micro/nano-topography on titanium alloy by micro-milling and alkali-hydrothermal treatment. Proc Inst Mech Eng H J Eng Med 230(12):1086–1095
25. Liu SY, Wang B, Zhang PR (2016) Effect of glucose concentration on electrochemical corrosion behavior of pure titanium TA2 in Hanks' simulated body fluid. Materials 9(11):874 (11 pages)
26. Saravanan I, Perumal AE, Balasubramanian V (2016) A study of frictional wear behavior of Ti6Al4V and UHMWPE hybrid composite on TiN surface for bio-medical applications. Trib Int 98:179–189
27. Wang B, Liu ZQ (2015) Shear localization sensitivity analysis for Johnson-Cook constitutive parameters on serrated chips in high speed machining of Ti6Al4V. Simul Model Pract Theory 55:63–76
28. Sun S, Brandt M, Dargusch MS (2009) Characteristics of cutting forces and chip formation in machining of titanium alloys. Int J Mach Tools Manuf 49(7):561–568
29. Thomas M, Turner S, Jackson M (2010) Microstructural damage during high-speed milling of titanium alloys. Scripta Mater 62(5):250–253
30. Cui WF, Jin Z, Guo AH, Zhou L (2009) High temperature deformation behavior of a+b-type biomedical titanium alloy Ti-6Al-7Nb. Mater Sci Eng A 499(1):252–256

31. Jemielniak K (2009) Finish turning of Inconel 718. Adv Manuf Sci Technol 33(1):59–69
32. Kadam GS, Pawade RS (2017) Surface integrity and sustainability assessment in high-speed machining of Inconel 718—an eco-friendly green approach. J Clean Prod 147:273–283
33. Navas VG, Arriola I, Gonzalo O, Leunda J (2013) Mechanisms involved in the improvement of Inconel 718 machinability by laser assisted machining (LAM). Int J Mach Tools Manuf 74(4):19–28
34. Iturbe A, Giraud E, Hormaetxe E, Garay A, Germain G, Ostolaza K, Arrazola PJ (2017) Mechanical characterization and modelling of Inconel 718 material behavior for machining process assessment. Mater Sci Eng A 682:441–453
35. Sims CT, Stoloff NS, Hagel WC (eds) (1987) Superalloys II: high temperature materials for aerospace and industrial power. Wiley, New York
36. Durand-Charre M (1997) The microstructure of superalloys. Gordon & Breach Science Publishers, Amsterdam
37. Astakhov VP, Xiao XR (2008) A methodology for practical cutting force evaluation based on the energy spent in the cutting system. Mach Sci Technol 12(3):325–347
38. Wang B, Liu ZQ (2016) Cutting performance of solid ceramic end milling tools in machining hardened AISI H13 steel. Int J Refrac Met Hard Mater 55:24–32
39. Smith GT (2008) Cutting tool technology-industrial handbook. Springer-Verlag, London
40. Astakhov VP, Davim JP (2008) Machining: fundamentals and recent advances. Springer, London
41. Bayer AM, Becherer BA, Vasco T (1989) High speed steel. ASM handbook, vol 16: machining, pp 51–59
42. Kupczyk MJ, Komolka J (2015) High durability of cutting insert edges made of nanocrystalline cemented carbides. Int J Refrac Met Hard Mater 49(1):225–231
43. Lorentzon J, Järvstråt N (2008) Modelling tool wear in cemented-carbide machining alloy 718. Int J Mach Tools Manuf 48(10): 1072–1080
44. Noordin MY, Venkatesh VC, Chan CL, Abdullah A (2001) Performance evaluation of cemented carbide tools in turning AISI 1010 steel. J Mater Process Technol 116(1):16–21
45. Davim JP (2008) Machining; fundamentals and recent advances. Springer-Verlag, London
46. Koseki S, Inoue K, Sekiya K, Morito S, Ohba T, Usuki H (2017) Wear mechanisms of PVD-coated cutting tools during continuous turning of Ti-6Al-4V alloy. Precis Eng 47:434–444
47. Da Silva RB, Machado ÁR, Ezugwu EO, Bonney J, Sales WF (2013) Tool life and wear mechanisms in high speed machining of Ti-6Al-4V alloy with PCD tools under various coolant pressures. J Mater Process Technol 213(8):1459–1464
48. Yigit R, Celik E, Findik F, Koksal S (2008) Tool life performance of multilayer hard coatings produced by HTCVD for machining of nodular cast iron. Int J Refrac Met Hard Mater 26(6):514–524
49. Settineri L, Bucciotti F, Cesano F, Faga MG (2007) Surface properties of diamond coatings for cutting tools. CIRP Ann Manuf Technol 56(1):573–576
50. Ferreira R, Carou D, Lauro CH, Davim JP (2016) Surface roughness investigation in the hard turning of steel using ceramic tools. Mater Manuf Process 31(5):648–652
51. North B (1987) Ceramic cutting tools, a review. Int J High Technol Ceram 3:113–127
52. Aruna M, Dhanalakshmi V, Mohan S (2010) Wear analysis of ceramic cutting tools in finish turning of Inconel 718. Int J Eng Sci Technol 2(9):4253–4262
53. Uhlmann E, Hübert C (2011) Tool grinding of end mill cutting tools made from high performance ceramics and cemented carbides. CIRP Ann Manuf Technol 60(1):359–362
54. Çelik A, Lazoglu I, Kara A, Kara F (2015) Investigation on the performance of SiAlON ceramic drills on aerospace grade CFRP composites. J Mater Process Technol 223:39–47
55. Ceramic based solutions. http://www.pesmag.co.uk/features/93/20136/2376/
56. Gerchman MC (1986) Specifications and manufacturing considerations of diamond machined optical components, Proc. SPIE 0607, Optical Component Specifications for Laser-based Systems and Other Modern Optical Systems, 36
57. Dearnley PA, Grearson AN (1986) Evaluation of principal wear mechanisms of cemented carbides and ceramics used for machining titanium alloy IMI 318. Mater Sci Technol 2(1):47–58
58. Rashid RAR, Palanisamy S, Sun S, Dargusch MS (2016) Tool wear mechanisms involved in crater formation on uncoated carbide tool when machining Ti6Al4V alloy. Int J Adv Manuf Technol 83(9-12):1457–1465
59. Davoodi B, Eskandari B (2015) Tool wear mechanisms and multi-response optimization of tool life and volume of material removed in turning of N-155 iron-nickel-base superalloy using RSM. Measurement 68:286–294
60. Ginting A, Nouari M (2009) Surface integrity of dry machined titanium alloys. Int J Mach Tools Manuf 49(3):325–332
61. Ren XP, Liu ZQ (2016) Influence of cutting parameters on work hardening behavior of surface layer during turning superalloy Inconel 718. Int J Adv Manuf Technol 86(5-8):2319–2327
62. Mather I (1934) Determination of initial stress by measuring the deformation around drilled holes. Trans ASME 56(4):249–254
63. Zuccarello B, Menda F, Scafidi M (2016) Error and uncertainty analysis of non-uniform residual stress evaluation by using the ring-core method. Exp Mech 56(9):1531–1546
64. Smith M, Levesque J-B, Bichler L, Sediako D, Gholipour J, Wanjara P (2017) Residual stress analysis in linear friction welded in-service Inconel 718 superalloy via neutron diffraction and contour method approaches. Mater Sci Eng A 691:168–179
65. Moussaoui K, Segonds S, Rubio W, Mousseigne M (2016) Studying the measurement by X-ray diffraction of residual stresses in Ti6Al4V titanium alloy. Mater Sci Eng A 667:340–348
66. Withers PJ (2013) Synchrotron X-ray diffraction, practical residual stress measurement methods. Wiley, New York
67. Teti R, Jemielniak K, O'Donnell G, Dornfeld D (2010) Advanced monitoring of machining operations. CIRP Ann Manuf Technol 59(2):717–739
68. Jawahir IS, Brinksmeier E, M'Saoubi R, Aspinwall DK, Outeiro JC, Meyer D, Umbrello D, Jayal AD (2011) Surface integrity in material removal processes: recent advances. CIRP Ann Manuf Technol 60(2):603–626
69. Subhas BK, Bhat R, Ramachandra KS, Balakrishna HK (2000) Simultaneous optimization of machining parameters for dimensional instability control in aero gas turbine components made of Inconel 718 alloy. ASME J Manuf Sci Eng 122(3):20–31
70. Axinte DA, Dewes RC (2002) Surface integrity of hot work tool steel after high speed milling-experimental data and empirical models. J Mater Process Technol 127(3):325–335
71. Joshi SV, Vizhian SP, Sridhar BR, Jayaram K (2008) Parametric study of machining effect on residual stress and surface roughness of nickel base super alloy UDIMET 720. Adv Mater Res 47-50: 13–16
72. Shi J, Wang JY, Liu CR (2006) Modeling white layer thickness based on the cutting parameters of hard machining. J Eng Manuf 220(2):119–128
73. Sridhar BR, Devananda G, Ramachandra K, Bhat R (2003) Effect of machining parameters and heat treatment on the residual stress distribution in titanium alloy IMI-834. J Mater Process Technol 139(1):628–634
74. Yang D, Liu ZQ, Ren XP, Zhuang P (2016) Hybrid modeling with finite element and statistical methods for residual stress prediction

in peripheral milling of titanium alloy Ti-6Al-4V. Int J Mech Sci 108-109:29–38
75. El-Axir MH (2002) A method of modeling residual stress distribution in turning for different materials. Int J Mach Tools Manuf 42(9):1055–1063
76. Arisoy YM, Guo CS, Kaftanoğlu B, Özel T (2016) Investigations on microstructural changes in machining of Inconel 100 alloy using face turning experiments and 3D finite element simulations. Int J Mech Sci 107:80–92
77. Capello E (2005) Residual stresses in turning part I: influence of process parameters. J Mater Process Technol 160(2):221–228
78. Ulutan D, Arisoy YM, Özel T, Mears L (2014) Empirical modeling of residual stress profile in machining nickel-based superalloys using the sinusoidal decay function. Procedia CIRP 13:365–370
79. Pawade RS, Joshi SS, Brahmankar PK (2008) Effect of machining parameters and cutting edge geometry on surface integrity of high-speed turned Inconel 718. Int J Mach Tools Manuf 48(1):15–28
80. Yang D, Liu ZQ (2015) Surface plastic deformation and surface topography prediction in peripheral milling with variable pitch end mill. Int J Mach Tools Manuf 91:43–53
81. Zhang PR, Liu ZQ (2016) Modeling and prediction for 3D surface topography in finish turning with conventional and wiper inserts. Measurement 94:37–45
82. Ulutan D, Alaca BE, Lazoglu I (2007) Analytical modelling of residual stresses in machining. J Mater Process Technol 183(1):77–87
83. Wu DW, Matsumoto Y (1990) The effect of hardness on residual stresses in orthogonal machining of AISI 4340 steel. ASME J Eng Ind 112(3):245–252
84. Liu CR, Barash MM (1976) The mechanical state of the sublayer of a surface generated by chip-removal process—part 2: cutting with a tool with flank wear. ASME J Eng Ind 98(4):1202–1208
85. Liang SY, Su JC (2007) Residual stress modeling in orthogonal machining. CIRP Ann Manuf Technol 56(1):65–68
86. Soo SL, Aspinwall DK, Dewes RC (2004) Three-dimensional finite element modelling of high-speed milling of Inconel 718. Proc Inst Mech Eng B: J Eng Manuf 218(11):1555–1561
87. Guo YB, Liu CR (2002) 3D FEA modeling of hard turning. ASME. J Manuf Sci Eng 124(2):189–199
88. Marusich TD, Ortiz M (2010) Modeling and simulation of high-speed machining. Int J Numer Meth Eng 38(21):3675–3694
89. Ding HT, Shin YC (2014) Dislocation density-based grain refinement modeling of orthogonal cutting of titanium. ASME. J Manuf Sci Eng 136(4):152–161
90. Wang QQ, Liu ZQ, Wang B, Song QH, Wan Y (2016) Evolutions of grain size and micro-hardness during chip formation and machined surface generation for Ti-6Al-4V in high-speed machining. Int J Adv Manuf Technol 82(9-12):1725–1736
91. Calamaz M, Coupard D, Girot F (2008) A new material model for 2D numerical simulation of serrated chip formation when machining titanium alloy Ti-6Al-4V. Int J Mach Tools Manuf 48(3):275–288
92. Ranganath S, Guo C, Hegde P (2009) A finite element modeling approach to predicting white layer formation in nickel superalloys. CIRP Ann Manuf Technol 58(1):77–80
93. Arisoy YM, Özel T (2015) Prediction of machining induced microstructure in Ti-6Al-4V alloy using 3-D FE-based simulations: Effects of tool micro-geometry, coating and cutting conditions. J Mater Process Technol 220:1–26
94. Seddiki O, Harnagea C, Levesque L, Mantovani D, Rosei F (2014) Evidence of antibacterial activity on titanium surfaces through nanotextures. Appl Surf Sci 308(3):275–284
95. Kwong J, Axinte DA, Withers PJ, Hardy MC (2009) Minor cutting edge-workpiece interactions in drilling of an advanced nickel-based superalloy. Int J Mach Tools Manuf 49(7):645–658
96. Arunachalam RM, Mannan MA, Spowage AC (2004) Residual stress and surface roughness when facing age hardened Inconel 718 with CBN and ceramic cutting tools. Int J Mach Tools Manuf 44(9):879–887
97. Coelho RT, Silva LR, Braghini A Jr, Bezerra AA (2004) Some effects of cutting edge preparation and geometric modifications when turning Inconel 718™ at high cutting speeds. J Mater Process Technol 148(1):147–153
98. Nalbant M, Altın A, Gökkaya H (2007) The effect of coating material and geometry of cutting tool and cutting speed on machinability properties of Inconel 718 super alloys. Mater Des 28(5):1719–1724
99. Ezugwu EO, Tang SH (1995) Surface abuse when machining cast iron (G-17) and nickel-base superalloy (Inconel 718) with ceramic tools. J Mater Process Technol 55(2):63–69
100. Dogra M, Sharma VS, Dureja J (2011) Effect of tool geometry variation on finish turning—a review. J Eng Sci. Technol Rev 4(1):1–13
101. Özel T, Karpat Y, Srivastava A (2008) Hard turning with variable micro-geometry PcBN tools. CIRP Ann Manuf Technol 57(1):73–76
102. Özel T (2009) Computational modelling of 3D turning: influence of edge micro-geometry on forces, stresses, friction and tool wear in PcBN tooling. J Mater Process Technol 209(11):5167–5177
103. Ulutan D, Özel T (2011) Effects of tool micro-geometry and coatings in turning of Ti-6Al-4V titanium alloy. Conference: NAMRC, At Corvallis, OR, 39:395–402
104. Davim JP, Figueira L (2007) Comparative evaluation of conventional and wiper ceramic tools on cutting forces, surface roughness, and tool wear in hard turning AISI D2 steel. Proc Inst Mech Eng B J Eng Manuf 221(4):625–633
105. Grzesik W, Wanat T (2006) Surface finish generated in hard turning of quenched alloy steel parts using conventional and wiper ceramic inserts. Int J Mach Tools Manuf 46(15):1988–1995
106. Dombovari Z, Stepan G (2012) The effect of helix angle variation on milling stability. ASME J Manuf Sci Eng 134(5):051015 (6 pages)
107. Sims ND, Mann B, Huyanan S (2008) Analytical prediction of chatter stability for variable pitch and variable helix milling tools. J Sound Vib 317(3-5):664–686
108. Yang D, Liu ZQ (2015) Surface topography analysis and cutting parameters optimization for peripheral milling titanium alloy Ti-6Al-4V. Int J Refrac Met Hard Mater 51:192–200
109. Wang B, Liu ZQ, Su GS, Ai X (2015) Brittle removal mechanism of ductile materials with ultrahigh-speed machining. ASME J Manuf Sci Eng 137(6):061002 (9 pages)
110. Sutter G, List G (2013) Very high speed cutting of Ti-6Al-4V titanium alloy - change in morphology and mechanism of chip formation. Int J Mach Tools Manuf 66:37–43
111. Arulkirubakaran D, Senthilkumar V (2017) Performance of TiN and TiAlN coated micro-grooved tools during machining of Ti-6Al-4V alloy. Int J Refrac Met Hard Mater 62:47–57
112. Kawasegi N, Ozaki K, Morita N, Nishimura K, Yamaguchi M (2017) Development and machining performance of a textured diamond cutting tool fabricated with a focused ion beam and heat treatment. Precis Eng 47:311–320
113. Sugihara T, Nishimoto Y, Enomoto T (2017) Development of a novel cubic boron nitride cutting tool with a textured flank face for high-speed machining of Inconel 718. Precis Eng 48:75–82
114. Field M, Kahles JF (1971) Review of surface integrity of machined components. Ann CIRP 20(2):153–162
115. Arrazola PJ, Özel T, Umbrello D, Davies M, Jawahir IS (2013) Recent advances in modelling of metal machining processes. CIRP Ann Manuf Technol 62(2):695–718
116. Jafarian F, Umbrello D, Jabbaripour B (2016) Identification of new material model for machining simulation of Inconel 718 alloy and the effect of tool edge geometry on microstructure changes. Simul Model Pract Th 66:273–284

117. Sharman ARC, Hughes JI, Ridgway K (2015) The effect of tool nose radius on surface integrity and residual stresses when turning Inconel 718™. J Mater Process Technol 216:123–132
118. Yang D, Liu ZQ (2016) Quantification of microstructural features and prediction of mechanical properties of a dual-phase Ti-6Al-4V alloy. Materials 9(8):628 (14 pages)
119. Cullity BD (1978) Elements of X-ray diffraction. Addison-Wesley Publishing Company, California
120. Jang DY, Liou JH, Watkins TR, Kozaczek KJ, Hubbard CR (1995) Characterization of surface integrity in machined austenitic stainless steel. Manuf Sci Eng 3(1):399–413
121. El-Khabeery MM, Fattouh M (1989) Residual stress distribution caused by milling. Int J Mach Tools Manuf 29(3):391–401
122. Bellows G (1972) Applying surface integrity principles in jet engine production. Met Eng Quart 55–58
123. Thiele JD, Melkote SN (2000) The effect of tool edge geometry on workpiece subsurface deformation and through-thickness residual stress for hard turning of AISI 52100 steel. J Manuf Process 2(4): 270–276
124. Matsumoto Y, Hashimoto F, Lahoti G (1999) Surface integrity generated by precision hard turning. Ann CIRP 48(1):59–62
125. Abboud E, Attia H, Shi B, Damir A, Thomson V, Mebrahtu Y (2016) Residual stresses and surface integrity of Ti-alloys during finish turning-guidelines for compressive residual stresses. Procedia CIRP 45:55–58
126. Tanaka H, Sugihara T, Enomoto T (2016) High speed machining of Inconel 718 focusing on wear behaviors of PCBN cutting tool. Procedia CIRP 46:545–548
127. Akhtar W, Sun JF, Chen WY (2016) Effect of machining parameters on surface integrity in high speed milling of super alloy GH4169/Inconel 718. Mater Manuf Process 3(5):620–627
128. Biksa A, Yamamoto K, Dosbaeva G, Veldhuis SC, Fox-Rabinovich GS, Elfizy A, Wagg T, Shuster LS (2010) Wear behavior of adaptive nano-multilayered AlTiN/MexN PVD coatings during machining of aerospace alloys. Trib Int 43(8):1491–1499
129. Liu J, Ma CY, Tu GZ, Long Y (2016) Cutting performance and wear mechanism of Sialon ceramic cutting inserts with TiCN coating. Surf Coat Technol 307:146–150
130. Thakur DG, Ramamoorthy B, Vijayaraghavan L (2012) Some investigations on high speed dry machining of aerospace material Inconel 718 using multicoated carbide inserts. Mater Manuf Process 27(10):1066–1072
131. Ucun I, Aslantas K, Bedir F (2013) An experimental investigation of the effect of coating material on tool wear in micro milling of Inconel 718 super alloy. Wear 300(1-2):8–19
132. Motorcu AR, Kus A, Durgun I (2014) The evaluation of the effects of control factors on surface roughness in the drilling of Waspaloy superalloy. Measurement 58:394–408
133. Bushlya V, Zhou J, Ståhl JE (2012) Effect of cutting conditions on machinability of superalloy Inconel 718 during high speed turning with coated and uncoated PCBN Tools. Procedia CIRP 3:370–375
134. Zhou JM, Bushlya V, Ståhl JE (2012) An investigation of surface damage in the high speed turning of Inconel 718 with use of whisker reinforced ceramic tools. J Mater Process Technol 212(2):372–384
135. Thakur A, Gangopadhyay S, Maity KP (2014) Effect of cutting speed and CVD multilayer coating on machinability of Inconel 825. Surf Eng 30(7):516–523
136. Thakur A, Mohanty A, Gangopadhyay S (2014) Comparative study of surface integrity aspects of Incoloy 825 during machining with uncoated and CVD multilayer coated inserts. Appl Surf Sci 320:829–837
137. Pawade RS, Joshi SS, Brahmankar PK, Rahman M (2007) An investigation of cutting forces and surface damage in high-speed turning of Inconel 718. J Mater Process Technol 192-193:139–146
138. Zhou JM, Bushlya V, Avdovic P, Ståhl JE (2012) Study of surface quality in high speed turning of Inconel 718 with uncoated and coated CBN tools. Int J Adv Manuf Technol 58(1-4):141–151
139. M'Saoubi R, Larsson T, Outeiro J, Guo Y, Suslov S, Saldana C, Chandrasekar S (2012) Surface integrity analysis of machined Inconel 718 over multiple length scales. CIRP Ann Manuf Technol 61(1):99–102
140. Ranganath S, Guo CS, Holt S (2009) Experimental investigations into the carbide cracking phenomenon on Inconel 718 superalloy material. ASME Int Manuf Sci Eng Conf 2:33–39
141. Swain N, Venkatesh V, Kumar P, Srinivas G, Ravishankar S, Barshilia HC (2017) An experimental investigation on the machining characteristics of Nimonic 75 using uncoated and TiAlN coated tungsten carbide micro-end mills. CIRP J Manuf Sci Technol 16:34–42
142. Zhou JM, Bushlya V, Peng RL, Chen Z, Johansson S (2014) Analysis of subsurface microstructure and residual stresses in machined Inconel 718 with PCBN and Al2O3-SiCw tools. Procedia CIRP 13:150–155
143. Du J, Liu ZQ (2012) Effect of cutting speed on surface integrity and chip morphology in high-speed machining of PM nickel-based superalloy FGH95. Int J Adv Manuf Technol 60(9-12): 893–899
144. Aramcharoen A, Mativenga PT (2008) White layer formation and hardening effects in hard turning of H13 tool steel with CrTiAlN and CrTiAlN/MoST-coated carbide tools. Int J Adv Manuf Technol 36(7):650–657
145. Sharman ARC, Hughes JI, Ridgway K (2006) An analysis of the residual stresses generated in Inconel 718™ when turning. J Mater Process Technol 173(3):359–367
146. Outeiro JC, Pina JC, M'Saoubi R, Pusavec F, Jawahir IS (2008) Analysis of residual stresses induced by dry turning of difficult-to-machine materials. CIRP Ann Manuf Technol 57(1):77–80
147. Ulutan D, Özel T (2013) Multiobjective optimization of experimental and simulated residual stresses in turning of nickel-alloy IN100. Mater Manuf Process 28(7):835–841
148. Musfirah AH, Ghani JA, Che Haron CH (2017) Tool wear and surface integrity of inconel 718 in dry and cryogenic coolant at high cutting speed. Wear 376-377:125–133
149. Costes JP, Guillet Y, Poulachon G, Dessoly M (2007) Tool-life and wear mechanisms of CBN tools in machining of Inconel 718. Int J Mach Tools Manuf 47(7-8):1081–1087
150. Bermingham MJ, Palanisamy S, Dargusch MS (2012) Understanding the tool wear mechanism during thermally assisted machining Ti-6Al-4V. Int J Mach Tools Manuf 62:76–87
151. Yang HC, Chen ZT, Zhou ZT (2015) Influence of cutting speed and tool wear on the surface integrity of the titanium alloy Ti-1023 during milling. Int J Adv Manuf Technol 78(5-8):1113–1126
152. Liang XL, Liu ZQ (2017) Experimental investigations on effects of tool flank wear on surface integrity during orthogonal dry cutting of Ti-6Al-4V. Int J Adv Manuf Technol 93(5-8):1617–1626
153. Sharman ARC, Hughes JI, Ridgway K (2004) Workpiece surface integrity and tool life issues when turning Inconel 718™ nickel based superalloy. Mach Sci Technol 8(3):399–414
154. Ezugwu EO, Wang ZM, Okeke CI (1999) Tool life and surface integrity when machining Inconel 718 with PVD and CVD coated tools. Trib Trans 42(2):353–360
155. Aspinwall DK, Dewes RC, Ng E-G, Sage C, Soo SL (2007) The influence of cutter orientation and workpiece angle on machinability when high-speed milling Inconel 718 under finishing conditions. Int J Mach Tools Manuf 47(12):1839–1846
156. Sadat AB (1987) Surface characteristics of machined Inconel-718 nickel-base superalloy using natural and controlled contact length tools. Int J Mach Tools Manuf 27(3):333–342

157. Kishway HA, Elbestawi MA (1999) Effects of process parameters on material side flow during hard turning. Int J Mach Tools Manuf 39(7):1017–1030
158. Warnecke G, Bach P (1988) Mechanical and material influences on machined surface in precision turning of steel with ceramics. Transactions of the North American Research Conference 16: 209–216
159. Guo Y, Saldana C, Compton WD, Chandrasekar S (2011) Controlling deformation and microstructure on machined surfaces. Acta Mater 59(11):4538–4547
160. Wang QQ, Liu ZQ, Wang B, Mohsan AUH (2017) Stress-induced orientation relationship variation for phase transformation of α-Ti to β-Ti during high speed machining Ti-6Al-4V. Mater Sci Eng A 690:32–36
161. Hughes JI, Sharman ARC, Ridgway K (2005) The effect of cutting tool material and edge geometry on tool life and workpiece surface integrity. Proc Inst Mech Eng B J Eng Manuf 220(2):93–107
162. Sharman ARC, Hughes JI, Ridgway K (2008) Surface integrity and tool life when turning Inconel 718 using ultra-high pressure and flood coolant systems. Proc Inst Mech Eng B J Eng Manuf 222(6):653–664
163. Axinte DA, Andrews P, Li W, Gindy N, Withers PJ (2006) Turning of advanced Ni based alloys obtained via powder metallurgy route. CIRP Ann Manuf Technol 55(1):117–120
164. Ibrahim GA, Che-Haron CH, Ghani JA (2009) Surface integrity of Ti-6Al-4V ELI when machined using coated carbide tools under dry cutting condition. Int J Mech Mater Eng 4(2):191–196
165. Zhou JM, Bushlya V, Peng RL, Johansson S, Avdovic P, Ståhl JE (2011) Effects of tool wear on subsurface deformation of nickel-based superalloy. Procedia Eng 19:407–413
166. Arunachalam R, Mannan MA (2000) Machinability of nickel-based high temperature alloys. Mach Sci Technol 4(1):127–168
167. M'Saoubi R, Ryde L (2005) Application of the EBSD technique for the characterisation of deformation zones in metal cutting. Mater Sci Eng A 405(1):339–349
168. Imran M, Mativenga PT, Gholinia A, Withers PJ (2015) Assessment of surface integrity of Ni superalloy after electrical-discharge, laser and mechanical micro-drilling processes. Int J Adv Manuf Technol 79:1303–1311
169. Agmell M, Ahadi A, Zhou JM, Peng RL, Bushlya V, Ståhl JE (2017) Modeling subsurface deformation induced by machining of Inconel 718. Mach Sci Technol 21(1):103–120
170. Nouari M, Makich H (2014) On the physics of machining titanium alloys: interactions between cutting parameters, microstructure and tool wear. Metals 4(3):335–358
171. Wang WF, Wang MC, Zhang J, Sun FJ, Huang DW (2008) Research on the microstructure and wear resistance of titanium alloy structural members repaired by laser cladding. Opt Laser Eng 46(11):810–816
172. Abdel-Hady M, Hinoshita K, Morinaga M (2006) General approach to phase stability and elastic properties of β- type Ti-alloys using electronic parameters. Scripta Mater 55(5):477–480
173. Soo SL, Khan SA, Aspinwall DK, Harden P, Mantle AL, Kappmeyer G, Pearson D, M'Saoubi R (2016) High speed turning of Inconel 718 using PVD-coated PCBN tools. CIRP Ann Manuf Technol 65(1):89–92
174. Chen L, El-Wardany TI, Harris WC (2004) Modeling the effects of flank wear land and chip formation on residual stresses. CIRP Ann Manuf Technol 53(1):95–98
175. Peng RL, Zhou J, Johansson S, Billenius A, Bushlya V, Ståhl JE (2013) Surface integrity and the influence of tool wear in high speed machining of Inconel 718. Proceedings of the 13th International Conference on Fracture, Beijing, China, June 16-21
176. Sadat AB, Reddy MY (1992) Surface integrity of Inconel 718 nickel-base superalloy using controlled and natural contact length tools Part 1: Lubricated. Exp Mech 32(3):282–288